MESOSTRUCTURE ASSEMBLY IN TWO DIMENSIONS: SYNTHESIS, CHARACTERIZATION AND CATALYTIC APPLICATIONS OF ACIDIC POROUS CLAY HETEROSTRUCTURES

Dissertation for the Degree of Ph. D.
MICHIGAN STATE UNIVERSITY
MIHAI POLVEREJAN
2001

7007

This is to certify that the

dissertation entitled

Mesostructure Assembly in Two Dimensions: Synthesis, Characterization and Catalytic Applications of Acidic Porous Clay Heterostructures

presented by

Mihai Polverejan

has been accepted towards fulfillment of the requirements for

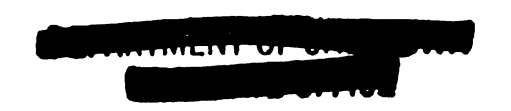
Ph.D. degree in Chemistry

Date June 8, 2001

MSU is an Affirmative Action/Equal Opportunity Institution

0-12771

MCMHS f. Sennavaea



PLACE IN RETURN BOX to remove this checkout from your record. TO AVOID FINES return on or before date due. MAY BE RECALLED with earlier due date if requested.

DATE DUE	DATE DUE	DATE DUE

6/01 c:/CIRC/DateDue.p65-p.15

MESOSTRUCTURE ASSEMBLY IN TWO DIMENSIONS: SYNTHESIS, CHARACTERIZATION AND CATALYTIC APPLICATIONS OF ACIDIC POROUS CLAY HETEROSTRUCTURES

Ву

Mihai Polverejan

A DISSERTATION

Submitted to

Michigan State University
in partial fulfillment of the requirements
for the degree of

DOCTOR OF PHILOSOPHY

Department of Chemistry

2001

ABSTRACT

MESOSTRUCTURE ASSEMBLY IN TWO DIMENSIONS: SYNTHESIS,
CHARACTERIZATION AND CATALYTIC APPLICATIONS OF ACIDIC POROUS
CLAY HETEROSTRUCTURES

By

Mihai Polverejan

Environmental concerns have raised a great deal of interest in the substitution of traditional acid catalysts such as aluminum chloride, sulfuric and hydrofluoric acids with solid-state alternatives, particularly microporous pillared clays and mesoporous molecular sieves. The recently reported new class of solid porous materials known as porous clay heterostructures (denoted PCH) shows promising acidic properties for catalytic organic conversions. Presented here is a comprehensive study on the synthesis, characterization and catalytic activity of a new porous clay heterostructures derived from synthetic saponite.

These mesostructured intercalates have been prepared through the surfactant - directed assembly of mesoporous silica within the galleries of the layered aluminosilicate. The removal of the intragallery mixture of neutral alkyl amine and quaternary ammonium ion surfactant (Q⁺) by calcination afforded PCH intercalates with basal spacings of 33 - 35 Å, BET specific surface areas of 800 - 920 m² g⁻¹, and pore volumes of 0.38 - 0.44 cm³ g⁻¹. The framework pore

sizes were in the super - micropore to small mesopore region ~15 - 25 Å. Temperature - programmed desorption of chemisorbed cyclohexylamine (CHA) indicated the presence of both weak and strong acid sites, corresponding to desorption temperatures near 220 and 410 °C, respectively. The total acidity (0.64 - 0.77 mmole CHA g⁻¹) increased with the saponite layer charge density, indicating that the acidity is correlated with the number of protons balancing the clay layer charge after calcination. Grafting aluminum into the gallery silica by a post-synthesis treatment can significantly enhance the acidic character of the saponite derivatives. The high acidity, structural stability to 750 °C, and supermicroporous to small mesoporous pore structure were verified by employing these PCH materials as catalysts for Friedel-Crafts alkylation and cumene cracking reactions.

To my wife and parents, for all of their love and support!

ACKNOWLEDGMENTS

I would like to thank my advisor, Dr. Thomas J. Pinnavaia for all of his patient guidance and support during my graduate studies. The freedom he has given me in my research to investigate different areas is greatly appreciated and I am also thankful for his advice on the non-chemistry related issues.

I want to express my thanks to current, and former Pinnavaia group members for their friendship and support. Special thanks to Dr. Thomas R. Pauly and Dr. Yu Liu for a fruitful collaboration.

I am grateful to my friend Emil Blaj for his assistance with various analyses.

To my family, I extend my love and thanks for being so supportive. My parents, Serban and Daniela Polverejan, my sister Dana and my brother in-law George Sampaleanu have continually offered encouragement and support.

My deepest gratitude goes to my wife Elena, for all the love and understanding she has given me over the years.

TABLE OF CONTENTS

LIST	Γ OF TA	BLES
LIST	OF FIG	GURES
ABB	REVIAT	TIONS
1.	Chap	ter 1: Introduction
	1.1.	Classification of Porous Materials
	1.2.	Lamellar Solids
	1.3.	Mobil's Ordered Mesoporous M41S Materials 1
	1.4.	Porous Clay Heterostructures
	1.5.	Research Objectives
	1.6.	References
2.		ter 2: Hydrothermal Synthesis and
		acterization of Saponite, a Trioctahedral Smectite
	Clay	Abstract
	2.2.	Introduction
	2.3.	Experimental5
		2.3.1. Saponite Synthesis
		2.3.2. Physical Measurements
	2.4.	Results and Discussion
	2.5.	Conclusion
	2.6.	References
3.	Chara Porou	ter 3: Mesostructured Clay Catalysts: Synthesis, acterization and Catalytic Activity of a New us Clay Heterostructure (SAP-PCH) Derived from actic Saponite
	3.1.	Abstract 7
	3.2.	Introduction
	3.3.	Experimental
		3.3.1. PCH Synthesis
		3.3.2. Catalytic Alkylation of 2,4-DBP with Cinnamyl Alcohol 7

		3.3.3. Cumene Cracking Reaction
		3.3.4. Physical Measurements
	3.4.	Results and Discussion
	3.5.	Conclusion
	3.6.	References
4.	Poroi Synth	ter 4: Post-Synthesis Grafting of Aluminum into us Clay Heterostructures (PCH) Derived from a netic Saponite
	4.1.	Abstract
	4.2.	Introduction
	4.3.	Experimental
		4.3.1. AI-PCH Synthesis
		4.3.2. Cumene Cracking Reaction
		4.3.3. Physical Measurements
	4.4.	Results and Discussion
	4.5.	Conclusion
	4.6.	References
	Hydro	ter 5: Covalent Grafting of Titanium on the oxyl Groups Lining the Pore Walls of SAP-
	5.1.	Abstract
	5.2.	Introduction
	5.3.	Experimental
		5.3.1. Ti-PCH Synthesis
		5.3.2. Catalytic oxidation of Cyclohexene with TBHP
		5.3.3. Physical Measurements
	5.4.	Results and Discussion
	5.5.	Conclusion
	5.6.	References
•	Meso	ter 6: Assembly of a Hexagonal Aluminosilicate structure (MSU-C) from Restructured Synthetic nite Clay
	62	Introduction

6.3.	Experimental	147
	6.3.1. MSU-C Synthesis	147
	6.3.2. Physical Measurements	148
6.4.	Results and Discussion	149
6.5.	Conclusion	159
6.6.	References	160

LIST OF TABLES

Table 2.1	Idealized structural formulas for some general 2:1 layered silicates	50
Table 2.2	Si/Al ratios, cation exchange capacities and unit cell formulas for synthetic saponite clays	59
Table 3.1	Properties of Q ⁺ and PCH intercalates of synthetic saponites and fluorohectotrite	85
Table 3.2	Alkylation of 2,4-di-tert-butylphenol with cinnamyl alcohol in the presence of various solid acid catalysts	97
Table 3.3	Cumene cracking activity of different mesoporous materials	98
Table 4.1	Properties of the PCH intercalate and Al-PCH derivatives	112
Table 4.2	Cumene cracking activity of Al-PCH's, parent SAP-PCH and aluminated mesostructures	121
Table 5.1	Properties of the PCH intercalate and Ti-PCH derivatives	133
Table 5.2	Oxidation of cyclohexene with TBHP in the presence of Ti-PCH and Ti-MCM-41	138
Table 6.1	BET surface area of acid hydrolyzed saponite	151

LIST OF FIGURES

Figure 1.1	A) Three-dimmensional channel system of the ZSM-5 zeolite structure consisting of two types of channels; sinusoidal and straight channels. B) "Stick "model of the structure of ZSM-5 zeolite; a perspective view down the straight channels	3
Figure 1.2	Schematic illustration of the pillaring process	8
Figure 1.3	The ideal smectite structure. The clay layer consists of an octahedral sheet, which is sandwiched through covalent bond formation between two tetrahedral sheets. Negative charge develops on the clay layer when ions of lower valency are substituted into the clay structure. Electrical neutrality is maintained by cationic interlayer M ⁿ⁺ species	9
Figure 1.4	The approach to mesoporosity via pillaring of layered solids: A) In most pillared solids, the interlayer regions contain only micropores. B) Mesoporosity is usually connected with a disordered arrangement of layered aggregates (tactoids)	11
Figure 1.5	Approaches to mesoporosity via the pillaring of layered solids. A) Attempts to use large elongated pillars to create interlayer mesoporosity may fail because the pillars are inclined with respect to layers. B) Post-intercalating organic compounds that can be removed upon calcination can prevent this failure. Stable links between pillars and layers are formed. C) Another possibility is the intercalation of pillars with end groups that act as bases for separating the pillars.	12
Figure 1.6	Mechanism of silicate induced ordering of hexagonally ordered surfactant-silicate structures. MCM-41 with an accessible pore volume is obtained after calcination	17
Figure 1.7	TEM image of calcined MCM-41 silica molecular sieve with 3.3 nm diameter	19
Figure 1.8	Powder X-ray diffraction patterns of M41S silicas. (A) calcined hexagonal MCM-41, (B) calcined cubic MCM-48 and (C) as made lamellar MCM-50	20

Figure 1.9	N ₂ adsorption-desorption isotherm of calcined MCM-41 molecular sieve. Inset: Horvath-Kawazoe pore size distribution curve plotted as normalized volume of N ₂ vs. pore diameter	22
Figure 1.10	Schematics of Porous Clay Heterostructure formation	27
Figure 1.11	N_2 adsorption-desorption isotherm for porous clay heterostructure prepared by gallery templated synthesis using fluorohectorite as layered host and A) decylamine or B) octylamine as co-surfactants. Inset: Horvath-Kawazoe pore size distribution curves plotted as normalized volume of N_2 vs. pore diameter	29
Figure 2.1	Idealized structure of saponite	53
Figure 2.2	XRD patterns of synthetic saponites	61
Figure 2.3	Dependence of the (060) spacing on the aluminum content of the tetrahedral layer of synthetic saponites	62
Figure 2.4	²⁹ Si MAS NMR spectra of synthetic saponites. The spectral components of the SAP-1.2 pattern (curves A, B and C) were obtained by deconvolution of the observed spectrum. Curve D represents the sum of the components	64
Figure 2.5	²⁷ Al MAS-NMR spectrum of synthetic saponite SAP-1.2	65
Figure 2.6	Representative TEM image of saponite SAP-1.5	66

Figure 3.1	Proposed mechanism for the formation of a porous clay heterostructures (PCH) by gallery assembly: (A) the initial amine-solvated bilayer structure with a thickness equivalent to the length of the quaternary cation (filled head groups) and the neutral amine (open head groups) surfactants; (B) the templated heterostructure in which a 2D hydrated silica is organized around micellar assemblies of Q+ and neutral amine; (C) the calcined PCH with a 2D framework of porous silica intercalated between the clay layers	76
Figure 3.2	Catalytic Alkylation of 2,4-Di-tert-butylphenol (2,4-DBP) with Cinnamyl Alcohol (CA)	80
Figure 3.3	Schematic illustration of the main steps involved in the porous clay heterostructures synthesis	84
Figure 3.4	XRD profiles for a) as-synthesized and b) calcined SAP-PCH materials	86
Figure 3.5	Various orientations of alkylammonium ions in the galleries of layered silicates with different charge densities	87
Figure 3.6	N_2 adsorption/desorption isotherms for porous clay heterostructures derived from synthetic saponites. The isotherms for SAP1.5 and SAP1.7-PCH are vertically displaced by 150 and 300 cm 3 g $^{-1}$, respectively. Insert: Horvath-Kawazoe pore size distribution curve. dW/dR is the derivative of the normalized adsorbate (N_2) volume adsorbed with respect to the pore diameter of the adsorbent in units of cm 3 g $^{-1}$ Å $^{-1}$.	89
Figure 3.7	Representative TEM image of a calcined SAP1.5-PCH	90
Figure 3.8	TEM of a thin-sectioned SAP1.5-PCH	91
Figure 3.9	Profiles for the thermal desorption of cyclohexylamine from SAP-PCH samples. dW/dT is the differential weight with respect to temperature in units of g/°C	94
Figure 4.1	XRD patterns for calcined PCH and the calcined Al-SAP-PCH derivatives.	113

Figure 4.2	Nitrogen adsorption/desorption isotherms for AI-PCH intercalates formed by using NaAlO ₂ and AlCl ₃ as aluminating agents. The isotherms are offset by 100 cc/g for clarity. Inset shows the BJH pore size distribution	114
Figure 4.3	²⁷ Al MAS NMR spectra for the calcined Al-PCH1-20 and Al-PCH1-10 samples, prepared by post-synthesis grafting with AlCl ₃	117
Figure 4.4	²⁷ Al MAS NMR spectra for the calcined Al-PCH2-10 and Al-PCH2-5 samples, prepared by post-synthesis grafting with NaAlO ₂	118
Figure 4.5	TPD Profiles for the desorption of cyclohexylamine from the parent PCH and AI-PCH derivatives	119
Figure 5.1	Reaction scheme for the condensed phase oxidation of cyclohexene with <i>tert</i> -butylhydroperoxide, catalyzed by Ti-PCH	130
Figure 5.2	XRD patterns for the calcined PCH and Ti grafted samples	134
Figure 5.3	Nitrogen adsorption/desorption isotherms for the calcined parent PCH and Ti-grafted compounds	135
Figure 5.4	UV-Vis spectra of the calcined Ti-containing materials	137
Figure 6.1	XRD patterns for the (A) parent and (B) acid hydrolyzed saponite (reaction time 2 h)	152
Figure 6.2	²⁷ AI MAS NMR spectra for the (A) starting saponite and (B) acid treated clay	153
Figure 6.3	XRD spectra for the (A) as-synthesized and (B) calcined MSU-C samples	155
Figure 6.4	Nitrogen adsorption-desorption isotherm for the calcined MSU-C material. Insert: Horvath-Kawazoe pore size distribution curve.	156

Figure 6.5	Representative TEM image of calcined MSU-C	158
i igui c v.v		

ABBREVIATIONS

2D -Two-dimensional.

2,4-DBP -2,4-di - *tert*- butylphenol.

BET Brunauer-Emmett-Teller.

CA -Cinnamyl Alcohol.

CHA -Cyclohexylamine.

cmc -critical micellar concentration.

-Cetyletrimethylammonium Bromide, C₁₆H₃₃N(CH₃)₃Br.

EtOH -Ethanol.

FH -Fluorohectorite.

HK -Horvath and Kawazoe pore size distribution model.

HMS -Hexagonal Mesoporous Silica.

IUPAC -International Union of Pure and Applied Chemistry.

M⁺ -Metal Cation.

MAS NMR - Magic Angle Spinning Nuclear Magnetic Resonance.

M41S -Mobil family of Mesostructured silicas.

-Mobil Composition of Matter 41, hexagonal mesophase (member of M41S family).

MCM-48 -Mobil Composition of Matter 48, cubic mesophase (member of M41S family).

MCM-50 -Mobil Composition of Matter 50, lamellar mesophase (member of M41S family).

MSU-C -Hexagonal mesostructured aluminosilicate synthesized from restructured saponite.

mmol -Millimoles.

nm -Nanometer (10⁻⁹m).

PCH -Porous Clay Heterostructure.

P/Po -Relative Pressure, P = pressure, Po = Saturation Pressure.

ppm -Part per million.

Q⁺ -Alkylammonium ion.

Q³ -Incompletely condensed silica sites, SiO(OSi)₃.

SBA -Mesostructured silicas assembled under high acid, low pH

conditions with TEOS as the inorganic precursor.

S_{BET} -Specific surface area in m²/g obtained from the linear part of the

adsorption isotherm using the Brunauer, Emmett, Teller equation.

TBHP -tert-butylhydroperoxide.

TMAOH -Trimethylammoniumhydroxide.

TEM -Transmission Electron Microscopy.

TEOS -Tetraethylorthosilicate.

TPD -Thermal Programmed Desorption.

XRD -X-ray Diffraction.

X -Halogen ion.

ZSM-5 -Zeolite Synthesized by Mobil.

Chapter 1

Introduction

1.1 Classification of Porous Materials

In general, nanoporous materials are solids with an accessible open space in the 1-10nm range. In describing porous materials the IUPAC has defined 3 size domains: 1 micropores < 2nm, mesopores 2 - 50 nm and macropores > 50nm. Thus the nanoporous regime spans the traditional midmicropore to lower mesopore size range. Inorganic macroporus solids are well known as porous gels² or porous glasses;³ these substances generally possess relatively broad pore size distributions due to their amorphous structures. Their typical applications are in the field of adsorption processes, for example chromatography or catalyst supports.^{4,5} Meso and macropores are usually associated with materials that are finely divided or structurally disordered (amorphous). Therefore meso and macro porosity often are consequences of the texture of a material. Zeolites and their related compounds exemplify the microporous solids. Zeolites are aluminosilicates with a periodic threedimensional framework structure containing voids (Figure 1.1). Related

components posses similar structure but differ in chemical composition of the framework (aluminophosphates). Due to the periodicity of the structure of these crystalline solids they exhibit a very narrow pore size distribution. This is important for their size specific application in absorption, molecular sieving and shape selective catalysis. ⁶⁻⁸ The open framework structures are used as nanosized reaction vessels ⁹⁻¹¹ or as hosts for controlled construction of assemblies of metal and semiconductor clusters ^{12,13} of organic molecules ¹⁴⁻¹⁶ or for polymerization reactions leading possibly to molecular wires in the case of conducting polymers. ¹⁷ Exciting applications have been proposed for these materials such as in nonlinear optics ¹⁸, as devices in electronic, optical computing and image processing ¹⁹ or as pigments.

The outstanding properties of zeolites and related compounds have made these materials one of the most important research subjects in solid-state chemistry for the last two decades. 20-22 The major drawback for their use is their limited pore size, which excludes larger molecular entities from the size specific processes occurring in the voids of these materials. Since the first applications of zeolites have been established, an urgent need has been developed for solids with well define pore sizes larger than the 7Å diameter window occurring in X/Y or ZSM zeolites. Typical extensions of current uses of zeolites include the catalytic cracking of heavy oil fractions. Aluminosilicate zeolite Y is currently being used with an enormous impact in the oil-refining industry as a cracking catalyst for the "middle distillates" in order to convert these to

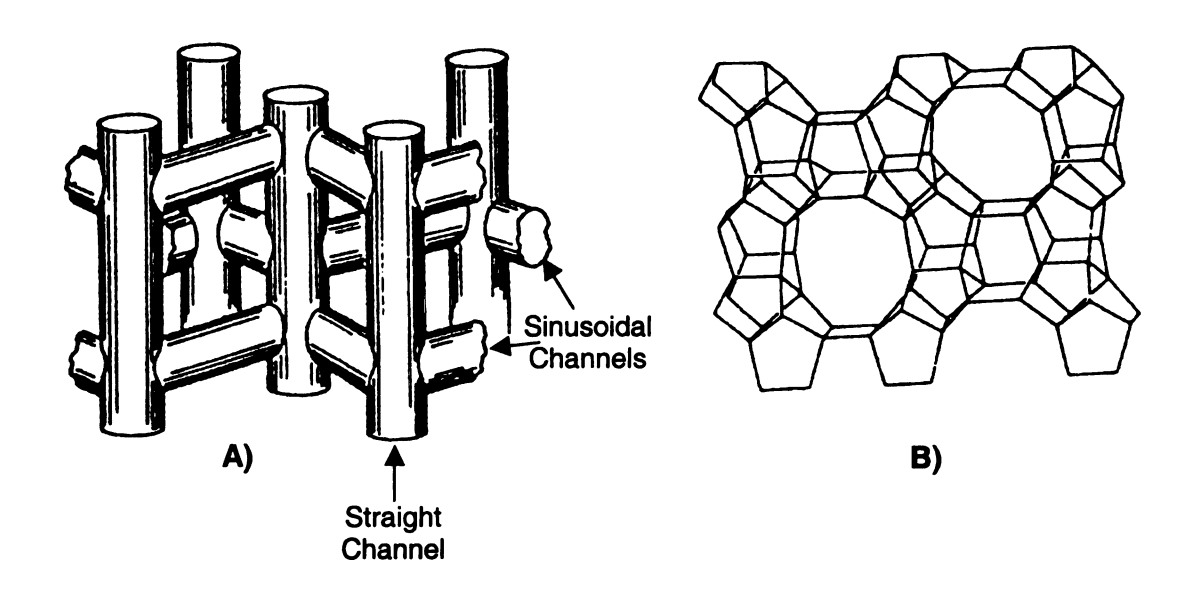


Figure 1.1: A) Three-dimmensional channel system of the ZSM-5 zeolite structure consisting of two types of channels; sinusoidal and straight channels. B) "Stick "model of the structure of ZSM-5 zeolite; a perspective view down the straight channels.

gasoline.²³⁻²⁶ However their restricted pore size excludes the larger hydrocarbon molecules from highly selective intra-pore cracking processes.

Zeolite-like compounds with a pure silicate framework (zeosils), exhibit a high efficiency in selectively sorbing organic hydrophobic pollutants from wastewaters. Increased pore size might extend the use of pure silicate frameworks to larger molecules, for example to the adsorption of toxic polychlorinated biphenyl's from chemical products or of traces of herbicide and pesticide molecules from drinking water.²⁷

Metal porphyrin complexes have been incorporated into zeolite void structures and molecular microstructures consisting of several redox active organic and inorganic species have been generated on zeolite host systems¹⁰ providing immobilized enzyme mimics²⁸ or models of biochemical electron transfer chains.^{10,29} Again, larger pores would allow a much better fine-tuning of such structures.

The fact that most of the imagined uses of mesoporous solids are extensions of applications of zeolites means that the mesoporous regime of most interest is located at the lower end of the IUPAC definition.

Three different approaches have been taken to prepare materials with larger pores. First is the controlled intercalation of spacers between the layers of lamellar solids.^{30,31} Then, in a method disclosed by Mobil researchers³², surfactant liquid crystals were used to direct the assembly of an inorganic precursor. Finally, a new class of materials denoted porous clay heterostructures (PCH's)³³ was made by using intercalate surfactants for the templated synthesis

of nanostructures within the interlayer spaces of clays. Using these methods, materials with pores covering the entire range from microporous to mesoporous can be synthesized.

1.2 Lamellar solids

Solids with layered structures possess basal planes of atoms that are tightly bonded within the planes but relatively weakly bonded in the direction perpendicular to the planes. The asymmetric bonding interactions translate into greatly different physical properties for the material in the in-plane and out-ofplane directions. The weakly interacting region between the stacked units is usually referred to as the "interlayer" or "gallery" region. When the layers are electrically neutral, as in graphite or FeOCI, the galleries are empty and the basal planes of the adjacent layers are in van der Waals contact. Neutral guest molecules often can be incorporated between the host layers to form regularly intercalated derivatives. The incorporation of neutral species into the van der Waals gap typically is accompanied by electron-transfer reaction between the molecular guest and the layered host.³⁴ The free energy change associated with the electron transfer step provides much of the driving force for the intercalation reaction. In several classes of lamellar solids, the layered units carry a net electrical charge. 35 These include smectite clays, layered double hydroxides, and Group 4 metal phosphates. To achieve an electrically neutral structure, counterions, usually solvated by water or other polar molecules, occupy the

gallery region between the layers. Thus, ionic lamellar solids qualitatively resemble the conventional intercalation compounds formed by electron-transfer reactions between neutral guest and layered host precursors. The difference, however, is that in ionic lamellar solids, charge separation between gallery ions and the layers is complete, whereas in conventional intercalates the extent of charge transfer between guest and layered host is seldom complete. Consequently, ionic lamellar compounds can justifiably be described as intercalation compounds, although in practice they are not formed by electrontransfer reactions. Instead they simply crystallize, complete charge separation between the gallery species and the host layers being a distinguishing feature of their structure. Owing to their nanoscale periodicity, ionic lamellar solids give rise to very large intracrystalline surface areas of several hundred square meters per gram or more. However, in most cases the gallery surface area is accessible only to water and other small polar molecules that are capable of solvating the gallery counterions and the charged layers surfaces. Removing the solvating molecules by outgassing at elevated temperatures results in the recollapse of the galleries, especially if the intercalated counterions are small relative to interstices occupied by the ions on the gallery surfaces. If the counterions are relatively large, they can function as molecular props or "pillars" and thereby prevent the galleries from collapsing completely when the solvating medium is removed (Figure 1.2). Ideally, one would like to tailor the gallery structure on a length scale that would allow the accommodation of organic and inorganic molecules for molecular assembly and, perhaps, catalytic chemical conversions. Pillaring

reactions of a lamellar host are an important route to achieving these desired structural modifications.³⁶ A material is considered pillared when the gallery species are sufficiently robust to prevent gallery collapse upon dehydration and laterally spaced to allow interpillar access by molecules at least as large as nitrogen. There are currently three main types of layered material that are used for pillaring, namely smectite clays, layered double hydroxides, and phosphonates and phosphonates of tetravalent metals.

Clays are naturally occurring three-layer sheet silicates. The sheets are formed of two layers with tetrahedrally coordinated atoms surrounding a layer with octahedrally coordinated atoms. The whole structure carries a net negative charge resulting from substitutions in either the tetrahedral (Al⁺³, Fe⁺³ for Si⁺⁴) or the octahedral (Fe⁺², Mg⁺² for Al⁺³, Li⁺ for Mg⁺²) layer. This negative charge is compensated by interlayer cations, which in natural smectite clays are alkali or alkali earth ions (Figure 1.3). In the case of smectite clays, the net negative charge of the layer is rather small; the clay can then easily swell in water. After swelling, the interlayer cations may be exchanged for larger oligomeric cations, for example the Keggin ion $[Al_{13}O_4(OH)_{24}(H_2O)_{12}^{+7}$ ("Al₁₃")^{37,38} or the zirconyl cation [Zr(OH)₂(H₂O)₄]₄+8.39,40 These cations are present in solutions of the metal ions under appropriate conditions of pH, concentration and temperature. Subsequent calcination of the exchanged clay at elevated temperatures, e.g. 500°C, dehydrates the pillars and establishes stable links between them and the layers. Because the ion exchange capacity, i.e. the number of cations necessary

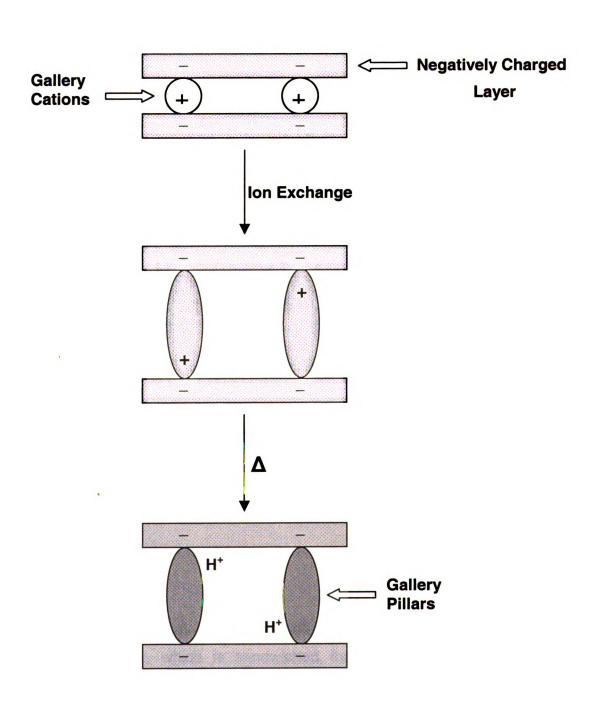


Figure 1.2: Schematic illustration of the pillaring process.

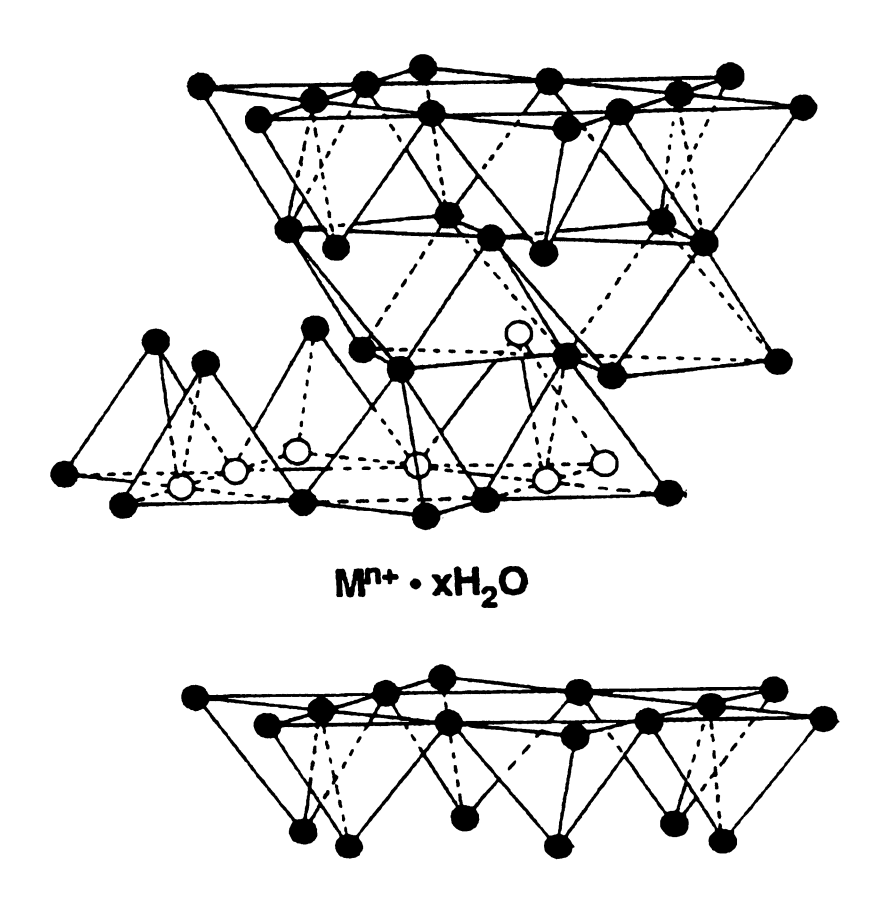
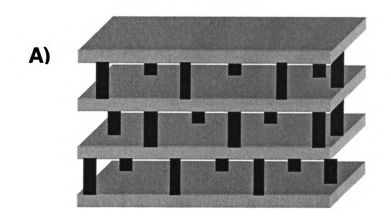


Figure 1.3: The ideal smectite structure. The clay layer consists of an octahedral sheet, which is sandwiched through covalent bond formation between two tetrahedral sheets. Negative charge develops on the clay layer when ions of lower valency are substituted into the clay structure. Electrical neutrality is maintained by cationic interlayer Mⁿ⁺ species.

for charge compensation, is small, a porous material with space left between pillars is obtained (see Figure 1.4 A).

Pore size distributions derived from sorption data of materials prepared in this way shows that the majority of pores are in the microporous range <10Å, as may be expected due to the rather small pillars. However, these compounds also exhibit mesopores with a rather broad size distribution between 20 and 200Å. The mesoporosity in these compounds may be traced back to a disordered arrangement of stacked layers as depicted schematically in figure 1.4 B. During swelling and ion exchange the clay delaminates to form small-layered packages or single layers. Upon drying after the pillaring reaction, these layered packages arrange themselves as shown, leaving open spaces between them. Even non-pillared clays are capable of forming such textural mesopores. Another possibility for the formation of mesopores arises from the bending of the layers. Both types of mesoporosity, however, are generated in an uncontrolled process and there is no simple way of controlling the pore shapes or sharpening the resulting pore size distribution.

Controlled interlayer mesoporosity through pillaring has been tackled by the use of larger pillars.⁴¹ Enlarged interlayer distances were indeed observed in the pillared clays. However, sol particles are usually spherical (or nearly so), so that, as they enlarge the height of the interlayer galleries, they also fill up the lateral interlayer space. Large, elongated ("slim") pillars tend to incline with respect to the layer surfaces (Figure 1.5 A). It may be possible to overcome this



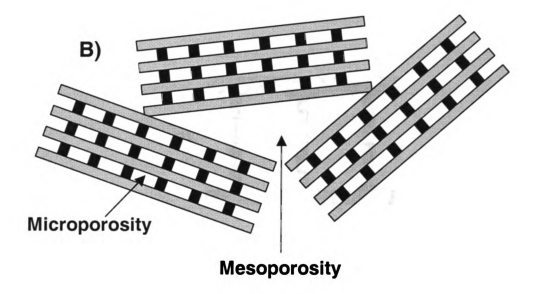


Figure 1.4: The approach to mesoporosity via pillaring of layered solids: A) In most pillared solids, the interlayer regions contain only micropores. B) Mesoporosity is usually connected with a disordered arrangement of layered aggregates (tactoids).

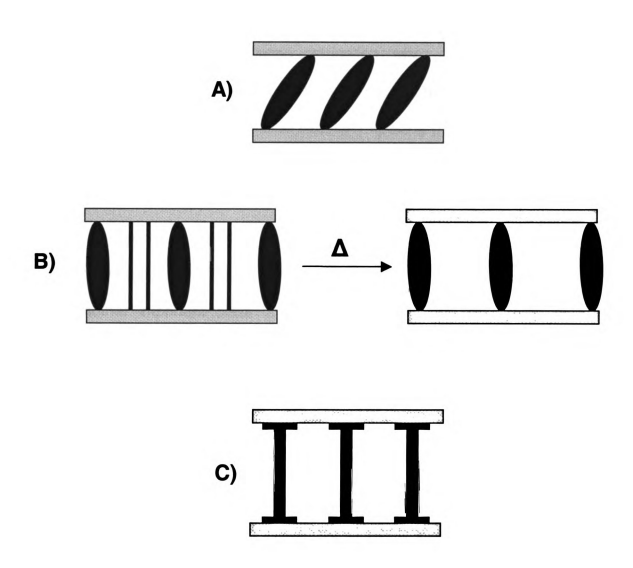


Figure 1.5: Approaches to mesoporosity via the pillaring of layered solids. A) Attempts to use large elongated pillars to create interlayer mesoporosity may fail because the pillars are inclined with respect to layers. B) Post-intercalating organic compounds that can be removed upon calcination can prevent this failure. Stable links between pillars and layers are formed. C) Another possibility is the intercalation of pillars with end groups that act as bases for separating the pillars.

problem by the post-intercalation of suitable organic molecules that might serve to keep the pillars upright. During calcination, when stable links are being established between the layers and the pillars, the organic burns off, leaving behind a pillared solid with increased interlayer spacing (Figure 1.5 B). Another way to achieve interlayer mesoporosity requires elaborate control of the shape of pillar, which is equipped with large end groups that function as "bases" so that the pillar cannot adopt an inclined position (Figure 1.5 C). So far, this approach seems to be feasible only for zirconium phosphonates. 42,43

Another important class of layered solids consists of layered double hydroxide (LDHs). The structure of these compounds is based on that of In brucite, magnesium ions occupy the octahedral sites Mg(OH)₂, brucite. between each second layer of close packing of hydroxide ions, thus giving rise to layer sequence OH-Mg-OH-OH-Mg-OH in the direction perpendicular to the layers. Mg(OH)₂ layers are neutral but substituting some of the divalent Mg⁺² ions by trivalent ions, e.g. Al+3, gives rise to positively charged layers. The interlayer gaps are filled by charge compensating anions (often carbonate and/or A typical LDH is the mineral hydrotalcite, hydroxide) and water. $[Mg_6Al_2(OH)_{16}]CO_3.4H_2O.$ LDH can be prepared with many different combinations of di and trivalent cations, e.g., Fe⁺², Ni²⁺, Zn⁺², Cr⁺³, Fe⁺³, and the ratio of divalent to trivalent metal ions can vary in a broad compositional range. The most important property of LDHs is the fact that they are anion exchangers, and these compounds have been termed anionic clays.44 Most of the inorganic ion exchange active compounds such as zeolites, clays and others are cation

exchangers⁴⁵, and thus LDHs play an outstanding role in that regime. Besides that, they have (potential) applications in catalysis⁴⁶, as sorbents and as pharmaceuticals, e.g. as antacids. Although the possibility of pillaring LDHs has been demonstrated^{47,48}, this chemistry is still in its infancy. The fact that among the oligomeric oxo/hydroxo ions many more anions than cations are known makes the extension of the pillaring approach from clays to LDHs very promising. The thermal stability of the hydroxides, however, is reduced in comparison to that of aluminosilicate clays. This shows up, for example, in the fact that calcining an LDH under conditions were clays are stable leads to an amorphous solid. Astonishingly enough, the double hydroxide layer is restored from their amorphous oxide after rehydration.

The third important class of pillared layered solids is based on the expansion of the interlayer space of the phosphates Me(HPO)₂..nH₂O of tetravalent metals (Me) such as Ti, Zr and Sn.^{17,49,50} In these compounds the oxygen atoms of the phosphate ions octahedrally coordinate the metal ions. The protons of the [HPO₄]²⁻ group project into the interlayer region, which is filled with water. Typical substances capable of intercalating into the acidic interlayer regions of the layered phosphates are organic amines. Pillaring agents such as the Keggin ion Al₁₃ do not intercalate directly but enter the gaps only when the layers have been spread apart by pre-intercalation with amines.^{51,52} This procedure leads to porous materials with a 20-30Å range.

Another approach to pillaring dense layered metal oxides and silicates converting them into high surface area molecular sieves with large interlayer

separations was developed by Landis et al.⁵³ This procedure is applicable to a wide variety of layered phases and allows for the engineering of microporous materials with diverse composition and physical properties. The pillaring procedure developed for smectite clays is not generally applicable to the wide variety of laminar metal oxides that do not spontaneously delaminate in water. It has been found that pillaring could be facilitated by utilizing a preswelling step in which the interlayer is exposed to organoammonium ions. According to procedures developed earlier, layered metal oxides⁵⁴ and silicates⁵⁵ have been intercalated with an aqueous solution of long-chain organoammonium salt or amine. An organic pillar precursor such as tetraethylorthosilicate (TEOS) is then absorbed into the organophilic interlayer region, where it was converted to a metal oxide pillar. Typically, the organoammonium ion exchanged product was stirred with excess TEOS for 1 - 3 days at 25 - 80 °C, filtered and dried. The final microporous material is obtained by calcination for several hours in air at 540 °C. The water, the preswelling organoammonium ion and the organic byproduct from TEOS hydrolysis are removed, affording the silica-pillared product. This procedure has allowed preparation of porous materials from a wide variety of layered oxides including alkali titanates, alkali metal-substituted titanates⁵⁶ A_x[MTi]₂O₄ and layered silicates such as magadiite Na₂Si₇O₁₅ and kenyaite K₂Si₁₄O₂₉.

The ability to controllably modify chemical composition as well as pore size provides the flexibility to tailor catalysts for specialized end uses. The catalytic potential of these materials is actively being explored.⁵⁷⁻⁵⁹

1.3 Mobil's Ordered Mesoporous M41S Materials

A giant stride forward into the ultra-large pore size range of 15-100Å has been recently disclosed^{32,60,61} by Mobil researchers in the patent and open literature, with the creative use of surfactant liquid crystal templates. These consist of hexagonal or cubic close packed aggregates of cylindrically shaped micelles, being composed of surfactant molecules containing hydrophobic alkane chains, hydrophilic hydroxyl and/or halide anions.^{32,62} These micelles effectively serve as "massive templates" for the creation of ultra-large cylindrically shaped pore⁶³, zeolite and molecular sieve-like structures (Figure 1.6). By judiciously selecting the alkyl chain lengths of the surfactant, the solution chemistry, and the use of auxiliary organic molecule fillers, the effective diameter of the cylindrical micellar aggregates can be adjusted to yield ultra-large pore zeolite like structure with diameters in the range of 15-100Å.

A typical Mobil preparation of MCM-41³² involves an aqueous solution of cationic surfactant, such as cetyltrimethylammonium chloride, partially exchanged for OH-(C₁₆H₃₃(CH₃NOH/C1) over an ion-exchanged resin. The surfactant concentration of this solution was approximately 25 wt%, much larger than the critical micelle concentration (cmc) necessary for the formation of rod-like micelles (~11-25 wt%).

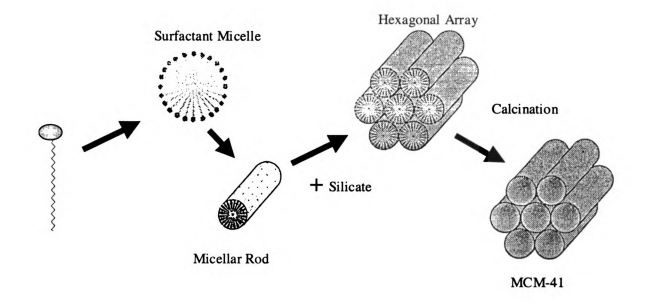


Figure 1.6: Mechanism of silicate induced ordering of hexagonally ordered surfactant-silicate structures. MCM-41 with an accessible pore volume is obtained after calcination.

The sources of silica varied from sodium silicate, amorphous fumed silica, colloidal silica to tetraethylorthosilicate (TEOS). In some cases aluminum substituted analogs were prepared by using alumina sources selected from the group of sodium aluminate, aluminum sulfate and pseudoboehmite. Following is a typical reaction mixture composition for the preparation of MCM-41 (expressed in moles):

1.0 SiO₂: 0.03 Al₂O₃: 0.007 Na₂O: 0.183 (CTMA)₂O: 0.156 (TMA)₂O: 23.5 H₂O

The addition of tetramethylammonium hydroxide (TMAOH) was most likely dictated by the need for a base capable of dissolving the amorphous silica source. The preparation procedure consists of mixing the inorganic precursors with the template solution and autoclaving the mixture at temperatures between 100 to 150°C for a period of time from 4 to 144 h. The crystalline product is recovered by filtration, air-dried and heated in a N_2 atmosphere at 550°C for 1 h followed by calcination in air at the same temperature for 6 h. Transmission electron microscopy shows the regular hexagonal array of uniform channels characteristic of MCM-41. A representative electron diffraction pattern, with MCM-41 in the same orientation confirms the periodicity of the structure (Figure 1.7). For the sample described above, an interplanar spacing $d_{100} = 40$ Å has been observed.

MCM-41 identifies a subclass of the mesoporous silica that contains onedimensional cylindrical pores packed into a hexagonal array. Cubic MCM-48 and lamellar MCM-50 mesophases have also been identified and are consistent with liquid crystal phases known to exist in pure surfactant/water mixtures.

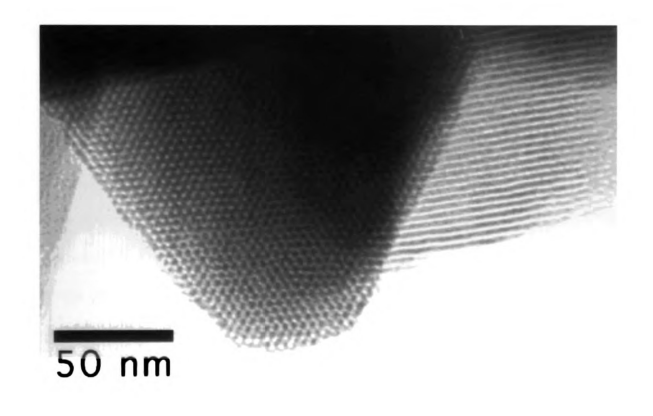


Figure 1.7: TEM image of calcined MCM-41 silica molecular sieve with 3.3 nm diameter.

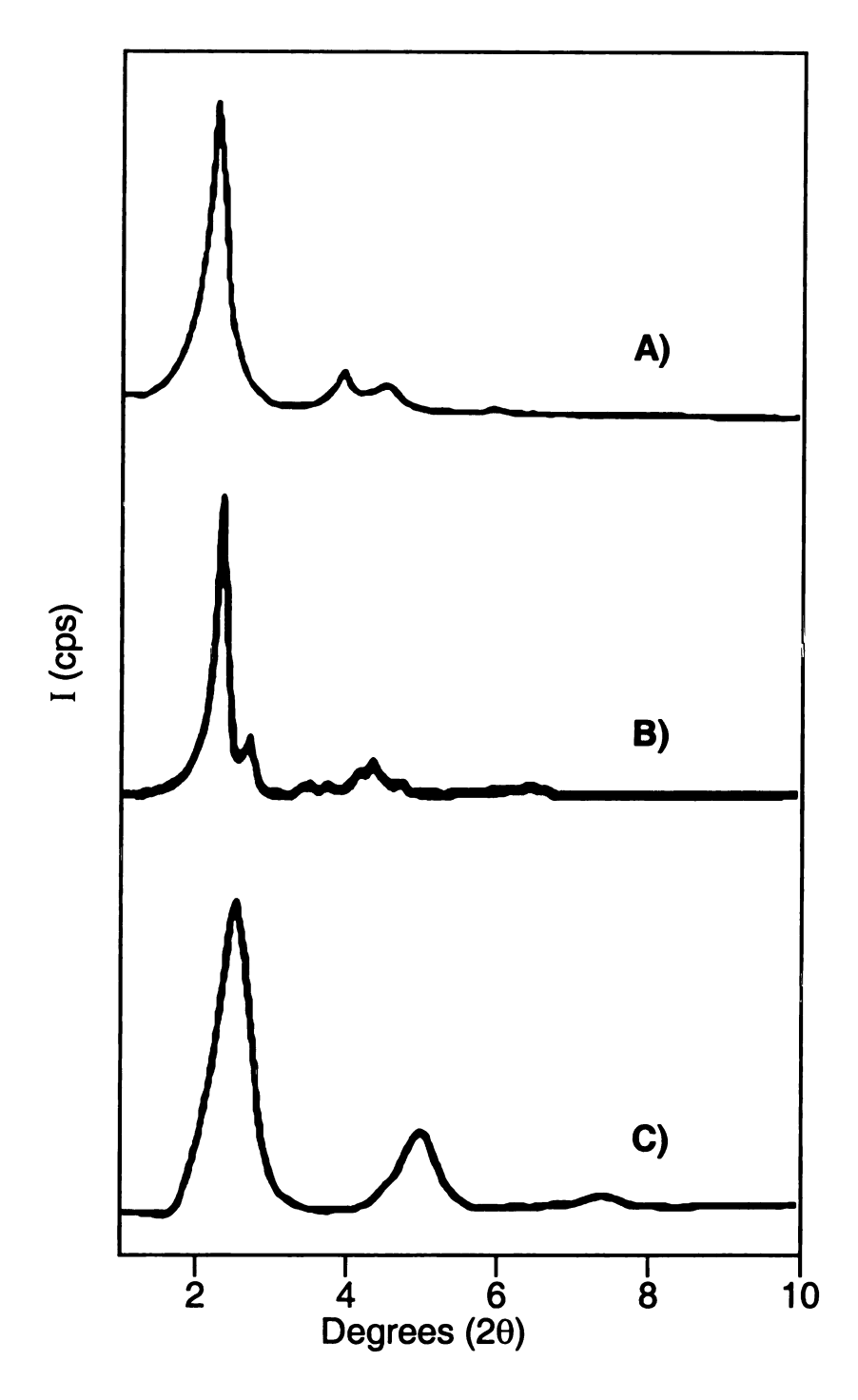


Figure 1.8: Powder X-ray diffraction patterns of M41S silicas. (A) calcined hexagonal MCM-41, (B) calcined cubic MCM-48 and (C) as made lamellar MCM-50.

Characterization of the mesophases formed in M41S silicas is conclusively done with powder X-ray diffraction. Their powder X-ray diffraction patterns show at least three diffraction peaks (d₁₀₀, d₁₁₀ and d₂₀₀) that can be indexed to the hexagonal unit cell with a unit cell parameter $a_0 = 2d_{100}*3^{-1/2}$ (Figure 1.8 A). MCM-48 and MCM-50 also show X-ray diffraction patterns characteristic of the long-range symmetry of the mesophase (Figures 1.8 B and C). Generally, both electron and X-ray diffraction pattern shows only a few low order members of the The BET surface area⁶⁴ of these hk0 subset of hexagonal reflections. compounds is >1000 m² g⁻¹ with exceptionally high sorption capacities.³² The range of pore volumes for MCM-41 samples is 0.7-1.2 cm³ gm⁻¹. Figure 1.9 shows the N₂ adsorption isotherms and pore size distribution for this material. Pore size distributions are calculated from the adsorption branch of the isotherm using various models. Originally Mobil modeled their pore sizes using the model of Horvath and Kawazoe. This model (Figure 1.9 inset) has been shown to accurately determine the average pore diameter of cylindrical mesopores of less than 5.0 nm in diameter even though it was originally proposed as a model for microporous materials with slit-like pore geometries. 65 The morphology of MCM-41 depends on the synthesis conditions, but it is possible to obtain relatively large (2µm) hexagonal prisms of MCM-41. The nature of the ordering in the walls of MCM-41 - that is, the degree to which the atoms are precisely ordered is not fully understood. The C/N molar ratio for as-synthesized C₁₆-based MCM-41 is 19, which is consistent with the surfactant remaining intact.

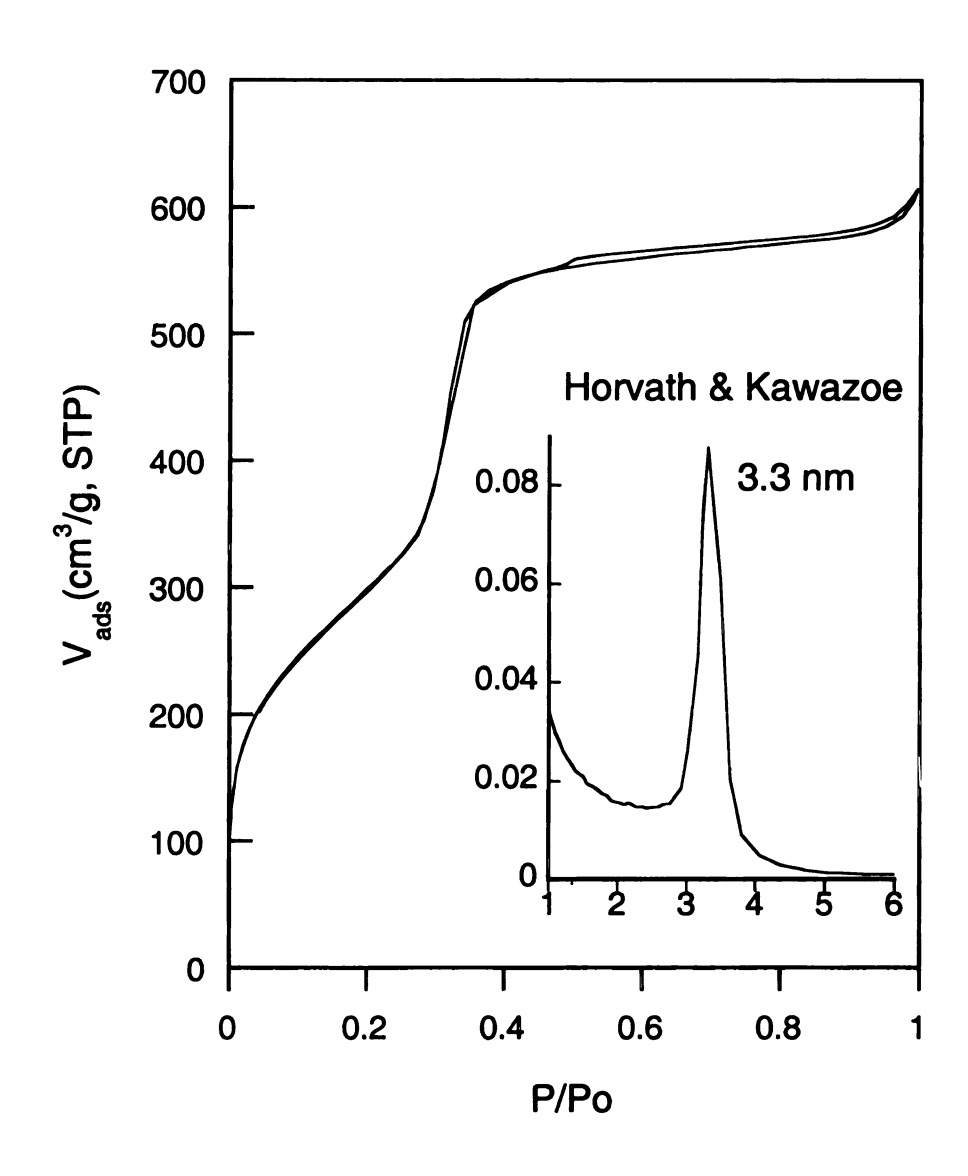


Figure 1.9: N_2 adsorption-desorption isotherm of calcined MCM-41 molecular sieve. Inset: Horvath-Kawazoe pore size distribution curve plotted as normalized volume of N_2 vs. pore diameter.

Along with the change of the surfactant chain length, another way of altering the pore diameter of MCM-41 is to add auxiliary hydrocarbons such as alkylated benzene (for example 1, 3, 5 trimethylbenzene), to the synthesis mixture.⁶⁰ The incremental addition of 1, 3, 5 trimethylbenzene results in the concomitant increase of d₁₀₀ and the pore diameter. Hexagonal phases with pore diameter up to 100Å have been characterized.

The observed dependence on alkyl chain length and the influence of auxiliary organic molecules on the resultant inorganic product are also consistent with two phenomena observed for liquid crystals. The diameter of the hexagonal liquid crystal phases prepared with ionic surfactants depends on the alkyl chain lengths of the surfactant. Organic species may be solubilized inside the hydrophobic regions of micelles, causing an increase in micelle diameter. Reagents soluble in micellar solutions can increase the porosity of amorphous adsorbents. These similarities suggest that these mesoporous molecular sieves are formed by a liquid-crystal templating mechanism.³² In this mechanism, inorganic material occupies the continuous solvent (water) region to create inorganic walls between the surfactant cylinders. It may be that encapsulation occurs because anionic silicate species enter the solvent region to balance the cationic hydrophilic surfaces of the micelles. Alternatively, it may be the introduction of the silicate species themselves that mediates the ordering. Once an ordered array is established, subsequent thermal processing is used to remove the organic material and produce a stable molecular sieve. Stucky and coworkers⁶⁶ elaborated on the mechanism put forth by Mobil for the formation of

MCM-41 and identified three important processes. One, there exists multidentate binding between silicate oligomers and the cationic surfactant head groups resulting in two, the favored polymerization of the silicate species at the Three, as the polymerization proceeds, charge density micelle interface. matching occurs between inorganic and organic phases resulting in interfacial surface curvature dependent on the organic to silica ratio. Initially, when the silica reacts with the cationic micelle, the interface of the micelle decreases in its surface curvature due to the shielding effect that the silica imparts to the surfactant head group and due to the decrease in repulsive forces between head groups at the interface. As condensation and polymerization of the silica matrix occur, the charge density of the silica species decreases. As a result, the repulsive forces between the head groups increase which coupled with an increase in size of the oligomeric silica species interacting with the surfactant, results in an interface with increasing surface curvature. The final mesophase formed is directly dependent on the ratio of silica to surfactant. Further work by Davis⁶⁷ showed that during the formation of MCM-41, the assembly mechanism did not include the formation of the liquid crystal phase prior to addition of the silicate, thereby discounting the first of the two routes Mobil initially offered as a potential mechanism. The liquid crystal pathway, however, has been successfully used to form numerous mesostructured materials, including mesostructured platinum metal. 68,69

From the standpoint of a range of basic scientific issues and technological applications, this discovery of ultra large-pore silicates, aluminosilicates and

aluminophosphates must be considered a landmark in the history of the synthesis of zeolite and molecular sieve type materials. Presumably one can tune the pore sizes and even dimensionality further by the appropriate choice of "secondary" chemistry involving the aluminum sites and/or the surface hydroxyl groups on the inside of the walls or the cylindrical channels, following removal of the micellar template. These ultra large-pore materials have tremendous potential for very large molecule size and shape selective catalysis, gas adsorption and separation, as well as advanced materials for future nanoscale device applications.

The 6-13 Å pore size barrier of known zeolite and molecular sieve type materials has been dramatically broken by the discovery of the ultra large-pore size materials. The 6 to hundreds of Å (mesostructured cellular foams^{70,71}) range of window and channel spaces now available expands the kinds of host-guest inclusion chemistry accessible to the nanochemist. This provides an unprecedented opportunity to make interesting and significant contributions to the world of organized nanomaterials for various kinds of nanoscale device applications. The future of the field of nanochemistry, based on these kinds of ultra-large pore materials, looks very bright.

Many results in this research area have been reported, such as various synthesis and formation mechanisms for the M41S family (MCM-41, MCM-48, MCM-50)^{32,66,67,72-85}. Other examples include the synthesis of silica and alumina mesoporous materials with non-ionic surfactants^{86,87}, of high aluminum MCM-41⁸⁸⁻⁹⁰, of mesoporous materials by using layered silicates⁷² and of various metal

substituted (Ti, V, B, Mn, Fe) MCM-41 or MCM-48.^{82,84,85,91-107} A generalized synthesis method has been developed for a wide range of transition and main group element oxide mesostructured materials with cationic and anionic surfactants, by using acidic and basic media (SBA -1, 2, 3)^{66,108,109}, with low surfactant concentration and low reaction temperatures.

1.4 Porous Clay Heterostructures

Recently³³, a new route to mesoporous molecular sieves was reported through the use of intercalated surfactants for the templated synthesis of structures within the interlayer spaces (galleries) of clays. The designated material was called a porous clay heterostructure (PCH). The approach to designing porous clay heterostructures is based on the use of intercalated quaternary ammonium cations and neutral amines as co-surfactants to direct the interlamellar hydrolysis and condensation polymerization of neutral inorganic precursor (for example tetraethylorthosilicate, TEOS) in the two - dimensional galleries of 2:1 mica - type layered silicate with high charge density, such as in fluorohectorite, rectorite, and vermiculite. The idea was to replace the inorganic ions of a clay like fluorohectorite with surfactant alkylammonium ions and then to further swell the gallery by co-intercalating a co-surfactant (a neutral amine) forming lipid by-layer arrangement inside the gallery. TEOS was then added to have the gallery restructured to a micellar structure. The gallery pores are a consequence of the supermolecular assembly and not a consequence of a

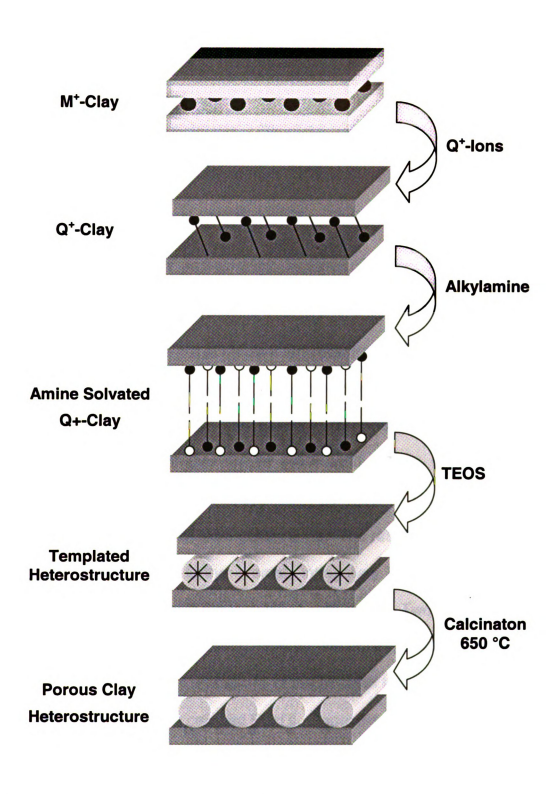


Figure 1.10: Schematics of Porous Clay Heterostructure formation.

pillaring process. Removal of the surfactant by calcination generates porous products (Figure 1.10).

In a typical PCH synthesis, Li⁺fluorohectorite (Li⁺FH) was converted to a quaternary ammonium exchanged form (Q+FH) by ion exchange with a two fold excess of aqueous [C₁₆H₃₃N(CH₃)₃]⁺Cl⁻. The intercalate was then washed free of excess surfactant, and air-dried. Mixtures of the hydrated Q+-FH (~7 H2O per O₂₀F₄ unit cell), neutral amines and TEOS at different stoichiometric ratios were allowed to react for 4 h at ambient temperature. Under these stoichiometric conditions the galleries are swollen by the co-templating amine and are readily accessible to TEOS. Also, the extra gallery water concentration is low, as judged by the water content of the amines (~0.4 wt%). Thus the base catalyzed hydrolysis of TEOS is much faster in the clay galleries than in solution, minimizing the formation of extra gallery silica. The resulting intercalates were centrifuged, dried in air to further promote intragallery TEOS hydrolysis and then calcined at 600°C to remove the templating surfactants. Two or more orders of (001) X-ray reflections, indicating layered structures, were observed for all products. Furthermore, the crystallinity of the air-dried templated heterostructures was better than that of the calcined PCH's. Depending on the chain length of the exchange cation and neutral amine co-template, the gallery height could be varied from 14.9Å (hexylamine) to 24.0Å (dodecylamine). Nitrogen BET surface areas for PCH materials synthesized using different Q+ and neutral amine cosurfactants ranged from 470-850 m²/g. A typical nitrogen isotherm of these

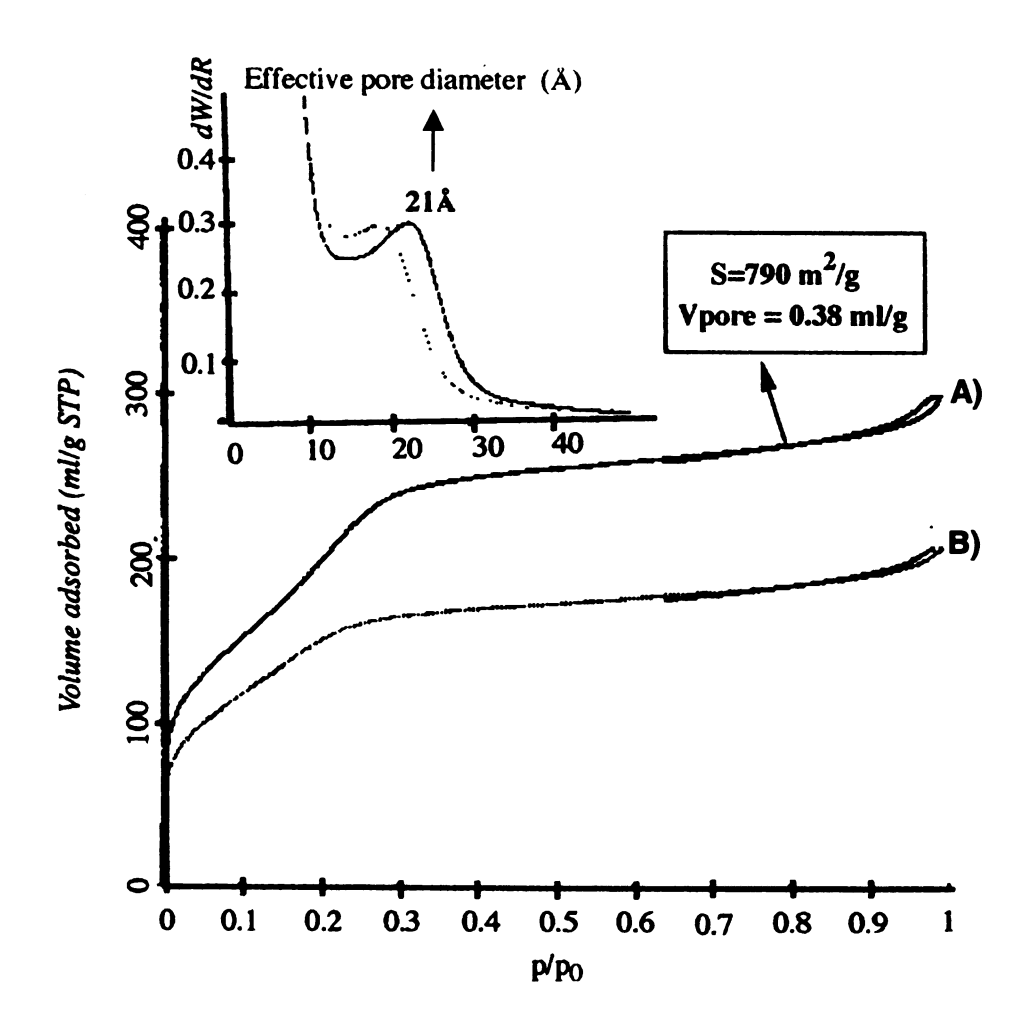


Figure 1.11: N_2 adsorption-desorption isotherm for porous clay heterostructure prepared by gallery templated synthesis using fluorohectorite as layered host and A) decylamine or B) octylamine as co-surfactants. Inset: Horvath-Kawazoe pore size distribution curves plotted as normalized volume of N_2 vs. pore diameter.

materials shows at a low partial pressure a beginning of a step, which fitted to the H-K model gives an average pore size of about 21 Å (Figure 1.11). The length of the carbon chain in the surfactant or co-surfactant is strictly correlated with the final pore dimension and it can vary from 15 to 22 Å. What we have here is a porous material with a pore size intermediate between what we call a supermicroporous (bigger than 10 Å) and small mesoporous (lower than 25 Å). The gallery height for the air-dried samples increases with chain length of the alkylamine. On calcination of the samples at 650°C there is a slight contraction in the gallery height due to the loss of intragallery water, loss of the template and dehydroxylation of the silica mesostructure. The relationship between PCH pore size distribution, chain lengths of the templating surfactants and the reaction stoichiometry support a templating mechanism analogous to structure-directed M41S mesostructure syntheses.

Because of the complementary chemical functionality of the layered and gallery-templated components and stable pore size distributions in the supermicropore to small mesopore range (14-25 Å), porous clay heterostructures formed by gallery-templated reactions of layered silicate clays offer new opportunities for the rational design of heterogeneous catalyst systems. Also, PCH materials bridge a potentially important pore size region between microporous zeolites and pillared clays, and M41S mesostructures. Heavy crude oils, biological molecules and other large macromolecular species can be accommodated in PCH galleries for shape selective processing or catalysis. These materials may also find important applications in molecular separations,

particularly biological molecules and pre-polymers and oligomers in the super micropore to small mesopore range.

Therefore, the porous clay heterostructure syntheses set forth here represents a novel strategy for obtaining nanoporous molecular sieves. In some respects PCH synthesis is similar to conventional pillaring reactions of lamellar solids. But, whereas pillared clays are formed by the insertion of dense nanoscale aggregates into the galleries of the layered host, the new intragallery templating process involves *in situ* assembly of surfactant-inorganic precursor nanostructures, the morphology of which is determined by the collective energetics of the inorganic and organic species as they assemble together.

1.5 Research Objectives

Many of the same ionic surfactants used for the assembly of mesostructured molecular sieve catalysts^{32,91,110} and related bulk phases¹¹¹ can be intercalated in a variety of layered host structures.⁷³ Previous studies recently demonstrated that some of these mesostructure - forming surfactants retain their structure directing properties when intercalated in the galleries of smectite clays. In a manner quite analogous to bulk mesostructure formation, the intercalated surfactants direct the assembly of an open framework metal oxide (silica) structure within the constrained gallery regions of the layered host.³³ The resulting porous intercalates are referred to as porous clay heterostructures (PCH).

Due to its high charge density and homogenous layer charge distribution synthetic fluorohectorite is one of the few available layered hosts suitable for PCH formation. However, even this clay proved to have some disadvantages. Synthetic fluorohectorite is obtained from molten fluxes and is unstable with respect to calcination (partial defluorination) at 350 °C. Most of the known synthetic clays have a low layer charge density, a feature that makes them unsuitable for supramolecular assembly of surfactants in the gallery. Natural clays posses a very heterogeneous layer charge distribution, which is also undesirable for intra-gallery assembly. Consequently, more readily accessible synthetic smectite clays with high layer charge density are needed to fully develop the chemistry of PCH materials.

The first objective of my research is the synthesis of new clays for future use as layered hosts in the PCH synthesis. The intragallery space of organoclays depends on the smectite clays layer charge density and on the structure of the surfactant onium ion.³⁵ The orientation of the onium ion is strongly dependent on the charge density, high d-spacing organoclays being formed for smectites with high layer charge density. Since the intragallery orientation of the surfactant is a major factor, a successful PCH synthesis can be achieved only by employing a high charge density smectite as a starting reactant. Therefore, a new approach to high and uniform charge density smectite synthesis is needed.

In order to obtain a more suitable PCH precursor this approach must fulfill certain requirements. The new clay should be readily available and made with affordable reagents at relatively low temperatures under hydrothermal conditions.

Also, this new material must possess intrinsic acidity, feature very desirable for a future catalyst.

Synthetic saponites are the clays that seem to meet these needs. They can be made within a short period of time (20 hours), using available reagents (AI(OH)₃, SiO₂, NH₄OH etc.) at low temperatures. Their acidity is determined by the AI-Si substitution in the tetrahedral layer. They have already been successfully used as catalysts in few reactions such as cracking of n-dodecane and benzene alkylation with propylene.

Another objective is the synthesis, characterization and catalytic activity of the new saponite mesostructured derivatives. PCH materials offer new opportunities for the rational design of heterogeneous catalyst systems, because the pore size distributions are in the supermicropore to small mesopore range (14-25 Å) and chemical functionality (e.g., acidity) can be introduced by adjusting the composition of the layered silicate host. The approach to designing PCH materials is based on the use of intercalated quaternary ammonium cations and neutral amines as co-surfactants to direct the interlamellar hydrolysis and condensation polymerization of neutral inorganic precursor (for example, tetraethylorthosilicate, TEOS) within the galleries of an ionic lamellar solid.

In alumina - pillared form saponite is an effective solid acid catalyst, ^{112,113} but its catalytic utility is limited in part by a pore structure in the micropore domain. The PCH form of saponite should be much more accessible for large molecule catalysis. Accordingly, Friedel-Crafts alkylation of bulky 2, 4-di-tert-butylphenol (DBP) (molecular size (Å): 9.5×6.1×4.4) with cinnamyl alcohol to

produce 6,8-di-tert-butyl-2, 3-dihydro[4H] benzopyran (molecular size (Å): 13.5×7.9× 4.9) will be used as a probe reaction to test the mesoporosity of our SAP-PCH. This large substrate reaction also was selected in part because only mesoporous molecular sieves are known to provide the accessible acid sites for catalysis. Conventional zeolites and pillared clays are poor catalysts for this reaction because the reagents cannot readily access the small micropores.

In order to test the Bronsted acidity of our new materials they will be used as catalysts for the cumene cracking reaction. The acidic character of the saponite derivatives can be further enhanced by a post synthesis treatment in a manner quite analogous to the alumination of MCM-41. 115-117

1.6 References

- (1) Sing, K. S. W.; Everet, D. H.; Haul, R. A. W.; Moscou, L.; Pierotti, R. A.; Rouquerol, J.; Siemieniewska, T. *Pure Applied Chemistry* **1985**, *57*, 603.
- (2) Janowsky, F.; Heyer, W. *Porose Glaser*, VEB Deutcher Verlag fur Grundstoffindustrie: Leipzig, 1982.
- (3) Iler, R. K. *The Chemistry of Silica: Solubility, Polymerization, Colloid and Surface Properties and Biochemistry*, Wiley: New York, 1979.
- (4) Davis, M. E. Chemical Industries 1992, 137.
- (5) Satterfield, C. N. Heterogeneous Catalysis in Industrial Practice. 2nd Ed; McGraw-Hill: New York, 1991.
- (6) van Bekkum, H.; Flanigen, E. M.; Jansen, J. C. *Introduction to Zeolites, Science and Practice*; Elsevier: Amsterdam, 1991; Vol. 58.
- (7) Christophliemk, P.; Gerike, P.; Potokar, M. *Detergents*; Springer: Berlin, 1992.
- (8) Holderich, W. F.; Hesse, F.; Naumann, F. *Angewante Chemie International Edition* **1988**, *100*, 232.
- (9) Herron, N. *Inclusion Compounds*; Oxford University Press: Oxford, 1991; Vol. 5.
- (10) Ozin, G. A.; Gil, C. Chemical Reviews 1989, 89, 1749-1764.
- (11) Ozin, G. A.; Ozkar, S.; Pastore, H. O.; Poe, A. J.; Vichi, E. J. S. *ACS Symposium Series* **1992**, *499*, 314-332.
- (12) Ozin, G. A. Advanced Materials 1992, 4, 612-649.
- (13) Bein, T. ACS Symposium Series 1992, 499, 1-7.

- (14) Cox, S. D.; Gier, T. E.; Stucky, G. D. *Chem. Mat.* **1990**, *2*, 609-619.
- (15) Hoppe, R.; Schultz-Ekloff, G.; Whorle, D.; Ehrl, M.; Brauchle, C. *Zeolite Chemistry and Catalysis*; Elsevier: Amsterdam, 1991; Vol. 73.
- (16) Werner, L.; Caro, J.; Finger, G.; Kornatowski, J. *Zeolites* **1992**, *12*, 658-663.
- (17) Enzel, P.; Bein, T. *Journal of Physical Chemistry* **1989**, *93*, 6270-6272.
- (18) Stucky, G. D. *Materials Research Society Symposium Proceedings* **1991**, *206*, 507.
- (19) Stein, A.; Ozin, G. A.; Stucky, G. D. Journal of Society of Photographic Science and Technology of Japan 1990, 53, 322.
- (20) Corma, A. *Proceedings. VIIIth International Zeolite Conference*; Elsivier: Amsterdam, 1989; Vol. 49.
- (21) Corma, A.; Martinez, A. Advanced Materials 1995, 7, 137-144.
- (22) Roland, E. Stud. Surf. Sci. Catal. 1989, 46, 645.
- (23) Corma, A.; Fornes, V.; Mocholi, F. A.; Monton, J. B.; Rey, F. *Acs Symposium Series* **1991**, *452*, 12-26.
- (24) Corma, A.; Llopis, F.; Monton, J. B. J. Catal. 1993, 140, 384-394.
- (25) Guerzoni, F. N.; Abbot, J. Appl. Catal. A-Gen. 1995, 127, 41-50.
- (26) Otterstedt, J. E.; Zhu, Y. M.; Sterte, J. *Applied Catalysis* **1991**, *70*, 43-52.
- (27) Behrens, P.; Panz, C.; Hufnagel, V.; Lindlar, B.; Freyhardt, C. C.; van de Goor, G. Solid State Ionics 1997, 101, 229-234.
- (28) Herron, N. CHEMTECH. 1989, 542.

- (29) Li, Z.; Wang, C. M.; Mallouk, T. E. *Journal of Physical Chemistry* **1988**, *92*, 2592.
- (30) Ohtsuka, K. Chem. Mat. 1997, 9, 2039-2050.
- (31) Corma, A. Chemical Reviews 1997, 97, 2373-2419.
- (32) Beck, J. S.; Vartuli, J. C.; Roth, W. J.; Leonowicz, M. E.; Kresge, C. T.; Schmitt, K. D.; Chu, C. T. W.; Olson, D. H.; Sheppard, E. W.; McCullen, S. B.; Higgins, J. B.; Schlenker, J. L. *J. Am. Chem. Soc.* **1992**, *114*, 10834-10843.
- (33) Galarneau, A.; Barodawalla, A.; Pinnavaia, T. J. *Nature* **1995**, *374*, 529-531.
- (34) Whittingham, M. S. Intercalation Chemistry New York, 1982.
- (35) Lagaly, G. Solid State Ion. 1986, 22, 43-51.
- (36) Pinnavaia, T. J. In *Materials Chemistry*, 1995; Vol. 245, pp 283-300.
- (37) Pires, J.; deCarvalho, M. B.; Carvalho, A. P. Zeolites 1997, 19, 107-113.
- (38) Fetter, G.; Heredia, G.; Velazquez, L. A.; Maubert, A. M.; Bosch, P. *Appl. Catal. A-Gen.* **1997**, *162*, 41-45.
- (39) Farfantorres, E. M.; Sham, E.; Grange, P. *Catalysis Today* **1992**, *15*, 515-526.
- (40) Pereira, P. R.; Pires, J.; de Carvalho, M. B. *Langmuir* **1998**, *14*, 4584-4588.
- (41) Behrens, P. *Advanced Materials* **1993**, *5*, 127-132.
- (42) Alberti, G.; Murcia-Mascaros, S.; Vivani, R. *Mater. Chem. Phys.* **1993**, *35*, 187-192.

- (43) Alberti, G.; Murcia Mascaros, S.; Vivani, R. *Mater. Sci. Forum* **1994**, *152-153*, 87-98.
- (44) Iqbal, Z.; Baughman, R. H.; Ramakrishna, B. L.; Khare, S.; Murthy, N. S.; Bornemann, H. J.; Morris, D. E. *Science* **1991**, *254*, 826-829.
- (45) lijima, S. Journal of Crystal Growth 1980, 50, 675-683.
- (46) Gardner, E.; Pinnavaia, T. J. Appl. Catal. A-Gen. 1998, 167, 65-74.
- (47) Yun, S. K.; Constantino, V. R. L.; Pinnavaia, T. J. *Clays and Clay Minerals* **1995**, *43*, 503-510.
- (48) Serwicka, E. M.; Nowak, P.; Bahranowski, K.; Jones, W.; Kooli, F. *J. Mater. Chem.* **1997**, *7*, 1937-1939.
- (49) Alberti, G.; Constantino, U.; Marmottini, F.; Vivani, R.; Zapelli, P. *Microporous and Mesoporous Materials* **1998**, *21*, 297-304.
- (50) Ebbesen, T. W.; Ajayan, P. M. *Nature* **1992**, *358*, 220-222.
- (51) Bogomolov, V. N.; Kholodkevich, S. V.; Romanov, S. G.; Agroskin, L. S. Solid State Communications 1983, 47, 181-182.
- (52) Terasaki, O.; Yamazaki, K.; Thomas, J. M.; Ohsuna, T.; Watanabe, D.; Sanders, J. V.; Barry, J. C. *Nature* **1987**, *330*, 58-60.
- (53) Landis, M. E.; Aufdembrink, B. A.; Chu, P.; Johnson, I. D.; Kirker, G. W.; Rubin, M. K. J. Am. Chem. Soc. 1991, 113, 3189-3190.
- (54) Weiss, A. *Angewante Chemie* **1960**, 413.
- (55) Beneke, K.; Lagaly, G. American Mineralogist 1983, 68, 818-826.
- (56) Groult, D.; Mercey, C.; Raveau, B. *Journal of Solid State Chemistry* **1980**, *32*, 289-296.

- (57) Long, R. Q.; Yang, R. T. J. Catal. 2000, 196, 73-85.
- (58) Gonzalez, F.; Pesquera, C.; Benito, I.; Herrero, E.; Poncio, C.; Casuscelli, S. Appl. Catal. A-Gen. 1999, 181, 71-76.
- (59) Sugunan, S.; Nisha, K.; Rekha, R.; Rahna, K. S.; Suja, H.; Deepa, C. S. Indian Journal of Chemistry Section a-Inorganic Bio-Inorganic Physical Theoretical & Analytical Chemistry 2000, 39, 765-768.
- (60) Beck, J. S. US Patent 1991, 5.057.296.
- (61) Beck, J. S.; Chu, C. T. W.; Johnson, I. D.; Kresge, C. T. *WO Patent* **1991**, *91/11390*.
- (62) Kresge, C. T.; Leonowicz, M. E.; Roth, W. J.; Vartuli, J. C.; Beck, J. S. *Nature* **1992**, *359*, 710-712.
- (63) Luzzati, V. Biological Membranes; Ed. Academic: New York, 1968.
- (64) Gregg, S. J.; Sing, K. S. W. Adsorption, Surface Area and Porosity. 2nd Ed London, 1982.
- (65) Horwath, G.; Kawazoe, K. J. Journal of Chemical Engineering of Japan 1983, 16, 470.
- (66) Monnier, A.; Schuth, F.; Huo, Q.; Kumar, D.; Margolese, D.; Maxwell, R. S.; Stucky, G. D.; Krishnamurty, M.; Petroff, P.; Firouzi, A.; Janicke, M.; Chmelka, B. F. *Science* **1993**, *261*, 1299-1303.
- (67) Chen, C. Y.; Burkett, S. L.; Li, H. X.; Davis, M. E. *Microporous Materials* 1993, 2, 17.
- (68) Shin, H. J.; Ko, C. H.; Ryoo, R. *J. Mater. Chem.* **2001**, *11*, 260-261.

- (69) Shin, H. J.; Ryoo, R.; Liu, Z.; Terasaki, O. *J. Am. Chem. Soc.* **2001**, *123*, 1246-1247.
- (70) Schmidt-Winkel, P.; Lukens, W. W.; Yang, P. D.; Margolese, D. I.; Lettow,J. S.; Ying, J. Y.; Stucky, G. D. *Chem. Mat.* 2000, *12*, 686-696.
- (71) Lettow, J. S.; Han, Y. J.; Schmidt-Winkel, P.; Yang, P. D.; Zhao, D. Y.; Stucky, G. D.; Ying, J. Y. *Langmuir* **2000**, *16*, 8291-8295.
- (72) Vartuli, J. C.; Kresge, C. T.; Leonowicz, M. E.; Chu, A. S.; McCullen, S. B.;
 Johnsen, I. D.; Sheppard, E. W. Chem. Mat. 1994, 6, 2070-2077.
- (73) Huo, Q. S.; Margolese, D. I.; Ciesla, U.; Demuth, D. G.; Feng, P. Y.; Gier,
 T. E.; Sieger, P.; Firouzi, A.; Chmelka, B. F.; Schuth, F.; Stucky, G. D. Chem.
 Mat. 1994, 6, 1176-1191.
- (74) Huo, Q. S.; Margolese, D. I.; Ciesla, U.; Feng, P. Y.; Gier, T. E.; Sieger,P.; Leon, R.; Petroff, P. M.; Schuth, F.; Stucky, G. D. *Nature* 1994, 368, 317-321.
- (75) Firouzi, A.; Kumar, D.; Bull, L. M.; Besier, T.; Sieger, P.; Huo, Q.; Walker, S. A.; Zasadzinski, J. A.; Glinka, C.; Nicol, J.; Margolese, D.; Stucky, G. D.; Chmelka, B. F. *Science* **1995**, *267*, 1138-1143.
- (76) Tanev, P. T.; Pinnavaia, T. J. Supramolecular Science 1998, 5, 399-404.
- (77) Stucky, G. D.; Monnier, A.; Schuth, F.; Huo, Q.; Margolese, D.; Kumar, D.; Krishnamurty, M.; Petroff, P.; Firouzi, A.; Janicke, M.; Chmelka, B. F. *Molecular Crystals and Liquid Crystals Science and Technology Section a-Molecular Crystals and Liquid Crystals* 1994, 240, 187-200.
- (78) Chen, C. Y.; Burkett, S. L.; Li, H. X.; Davis, M. E. *Microporous Materials* 1993, 2, 27.

- (79) Cheng, C. F.; Luan, Z. H.; Klinowski, J. Langmuir 1995, 11, 2815-2819.
- (80) Jun, S.; Kim, J. M.; Ryoo, R.; Ahn, Y. S.; Han, M. H. *Microporous and Mesoporous Materials* **2000**, *41*, 119-127.
- (81) Kim, J. M.; Kwak, J. H.; Jun, S.; Ryoo, R. *Journal of Physical Chemistry* **1995**, *99*, 16742-16747.
- (82) Kruk, M.; Jaroniec, M.; Ryoo, R.; Joo, S. H. *Chem. Mat.* **2000**, *12*, 1414-1421.
- (83) Lin, H. P.; Hwang, J. H.; Mou, C. Y.; Tang, C. Y. *Journal of the Chinese Chemical Society* **2000**, *47*, 1077-1082.
- (84) Morey, M.; Davidson, A.; Stucky, G. *Microporous Materials* **1996**, *6*, 99-104.
- (85) Morey, M. S.; O'Brien, S.; Schwarz, S.; Stucky, G. D. *Chem. Mat.* **2000**, *12*, 898-911.
- (86) Bagshaw, S. A.; Prouzet, E.; Pinnavaia, T. J. *Science* **1995**, *269*, 1242-1244.
- (87) Attard, G. S.; Glyde, J. C.; Goltner, C. G. *Nature* **1995**, *378*, 366-368.
- (88) Luan, Z. H.; Cheng, C. F.; Zhou, W. Z.; Klinowski, J. *Journal of Physical Chemistry* **1995**, *99*, 1018-1024.
- (89) Janicke, M.; Kumar, D.; Stucky, G. D.; Chmelka, B. F. Zeolites and Related Microporus Materials: State of the Art, 1994.
- (90) Schmidt, R.; Akporiaye, D.; Stocker, M.; Ellestad, O. H. *Journal of the Chemical Society-Chemical Communications* **1994**, 1493-1494.

- (91) Corma, A.; Navarro, M. T.; Pariente, J. P. *Journal of the Chemical Society-Chemical Communications* **1994**, 147-148.
- (92) Reddy, K. M.; Moudrakovski, I.; Sayari, A. *Journal of the Chemical Society-Chemical Communications* **1994**, 1059-1060.
- (93) Reddy, K. M.; Moudrakovski, I.; Sayari, A. *Journal of the Chemical Society-Chemical Communications* **1994**, 1491-1492.
- (94) Sayari, A.; Moudrakovski, I.; Danumah, C.; Ratcliffe, C. I.; Ripmeester, J. A.; Preston, K. F. *Journal of Physical Chemistry* **1995**, *99*, 16373-16379.
- (95) Sayari, A.; Danumah, C.; Moudrakovski, I. L. *Chem. Mat.* **1995**, *7*, 813-815.
- (96) Yuan, Z. Y.; Liu, S. Q.; Chen, T. H.; Wang, J. Z.; Li, H. X. *Journal of the Chemical Society-Chemical Communications* **1995**, 973-974.
- (97) Morey, M.; Davidson, A.; Eckert, H.; Stucky, G. *Chem. Mat.* **1996**, *8*, 486-492.
- (98) Morey, M. S.; Bryan, J. D.; Schwarz, S.; Stucky, G. D. *Chem. Mat.* **2000**, *12*, 3435-3444.
- (99) Antonelli, D. M.; Ying, J. Y. Angewandte Chemie-International Edition in English 1995, 34, 2014-2017.
- (100) Caps, V.; Tsang, S. C. Catalysis Today 2000, 61, 19-27.
- (101) Chatterjee, M.; Iwasaki, T.; Hayashi, H.; Onodera, Y.; Ebina, T.; Nagase,T. Chem. Mat. 1999, 11, 1368-1375.
- (102) Kosslick, H.; Lischke, G.; Landmesser, H.; Parlitz, B.; Storek, W.; Fricke, R. *J. Catal.* **1998**, *176*, 102-114.

- (103) Oberhagemann, U.; Jeschke, M.; Papp, H. *Microporous and Mesoporous Materials* **1999**, *33*, 165-172.
- (104) Oye, G.; Sjoblom, J.; Stocker, M. *Journal of Dispersion Science and Technology* **2000**, *21*, 229-243.
- (105) Stockenhuber, M.; Hudson, M. J.; Joyner, R. W. Journal of Physical Chemistry B 2000, 104, 3370-3374.
- (106) Xu, J.; Luan, Z. H.; Hartmann, M.; Kevan, L. *Chem. Mat.* **1999**, *11*, 2928-2936.
- (107) Zhao, X. S.; Lu, G. Q.; Hu, X. Microporous and Mesoporous Materials 2000, 41, 37-47.
- (108) Ryoo, R.; Ko, C. H.; Kruk, M.; Antochshuk, V.; Jaroniec, M. Journal of Physical Chemistry B 2000, 104, 11465-11471.
- (109) Newalkar, B. L.; Komarneni, S.; Katsuki, H. *Physical Chemistry Chemical Physics* **2000**, *2*, 2389-2390.
- (110) Tanev, P. T.; Chibwe, M.; Pinnavaia, T. J. *Nature (London)* **1994**, *368*, 321-323.
- (111) Wu, C. G.; Bein, T. Science (Washington, D. C.) 1994, 264, 1757-1759.
- (112) Casal, B.; Merino, J.; Ruiz-Hitzky, E.; Gutierrez, E.; Alvarez, A. *Clay Miner.* **1997**, *32*, 41-54.
- (113) Booij, E.; Kloprogge, T.; Van Veen, J. A. R. *Clays Clay Miner.* **1996**, *44*, 774-782.
- (114) Armengol, E.; Cano, M. L.; Corma, A.; Garcia, H.; Navarro, M. T. *J. Chem. Soc., Chem. Commun.* **1995**, 519-520.

- (115) Luan, Z. H.; Hartmann, M.; Zhao, D. Y.; Zhou, W. Z.; Kevan, L. *Chem. Mat.* **1999**, *11*, 1621-1627.
- (116) Mokaya, R.; Jones, W. Chemical Communications 1997, 2185-2186.
- (117) Ryoo, R.; Jun, S.; Kim, J. M.; Kim, M. J. *Chemical Communications* **1997**, 2225-2226.

Chapter 2

Hydrothermal Synthesis and Characterization of Saponite, a Trioctahedral Smectite Clay

2.1 Abstract

A new method for the preparation of three saponite compositions is reported here. This clay is readily available and made with affordable reagents under hydrothermal conditions (175 °C) from sodium metasilicate, magnesium nitrate and sodium aluminate for periods of about 18 hours. The reaction stoichiometries were targeted at unit cell compositions of Na_x[Mg₆](Si_{8-x}Al_x)O₂₀(OH)₄·nH₂O with x = 1.2, 1.5, and 1.7. These charge densities were selected so that sufficient quaternary ammonium ions (denoted Q⁺) and a neutral alkyl amine co-surfactant could be subsequently incorporated into the galleries for PCH formation. The resulting reaction products were designated SAP-1.2, -1.5, -1.7, respectively.

2.2 Introduction

Clays are the most abundant minerals found at the earth's surface. Not surprisingly, one of the earliest applications of chemical processing was concerned with the manufacturing of pottery using clays ad the raw material. Clay minerals are (hydrous) layered silicates and usually have a particle size smaller than 2 micrometers. These phyllosilicates are assembled from two basic components, a tetrahedral and an octahedral sheet. The tetrahedral sheet is composed from SiO₄ tetrahedra, which are linked together in a hexagonal arrangement through sharing three basal oxygen atoms. The fourth apical oxygen atom is connected to the octahedral sheet. The octahedral sheet is built from edge sharing octahedral in a structure similar to brucite Mg(OH)₂ or gibbsite Al(OH)₃. Condensation of the two sheet types defines a plane that contains all apical oxygen atoms from SiO₄ tetrahedra and one unconnected octahedral OH⁻ group (see Figure 1.3, Chapter 1). One hydroxyl group is positioned in a cavity formed by a hexagonal-like opening in the tetrahedral sheet.

From the structural point of view, clay minerals are divided in two classes, namely 1:1 and 2:1 types. Kaolinite, [Al₄](Si₄)O₁₀(OH)₈ the most representative 1:1 layered silicate has a layered structure that joins one tetrahedra and one octahedral sheet. This is the major component of china clay. The octahedral sheet of kaolinite is classified as dioctahedral because only two out of three octahedral sites are filled with aluminum ions. Other examples of 1:1 structures are the serpentine group minerals, which have a similar sheet arrangement as

kaolinite, but their chemical composition is different. In the serpentines [Mg₆](Si₄)O₁₀(OH)₈, all octahedral layer sites are occupied by magnesium ions.

A 2:1 assembly is formed when two tetrahedral sheets are condensed on an octahedral sheet. Pyrophyllite [Al₄](Si₈)O₂₀(OH)₄, and talc [Mg₆](Si₈)O₂₀(OH)₄ are the most common di- and trioctahedral forms of 2:1 layered silicates. The individual layers of these clays are bonded together by weak van der Waals forces that are operating between layers themselves. Thus, stacks of layers are agglomerated into particles. The weak cohesion between the layers is responsible for the soft nature of these clays.

Negative charge develops on the 2:1 silicate layers when lower valency ions are substituted into the clay structure. Positively charged interlayer ions compensate this excess anionic layer charge in order to maintain electrical neutrality. These interlayer (gallery) cations may be hydrated, inducing interlayer expansion, and swelling of the clay.^{2,3} Hence, interlayer access allows for the replacement of gallery cations by other cationic species through cation exchange processes.

2:1 layered silicates can be classified in four categories according to their layer charge. Table 2.1 summarizes the ideal chemical formulas for the most common 2:1 layered silicates. First category includes pyrophyllite and talc with a neutral layer followed by smectites with a moderate layer charge $(0.3 - 1.2 e^{-})$. Vermiculites in the third category possess a higher charge on the layer $(1.4 - 1.8 e^{-})$. Finally, micas in the fourth category own the highest layer charge $(2 e^{-})$ unit cell). Due to their layer charge range, smectites are capable of swelling in water

or in other polar solvents. In the smectite category we can also distinguish between clays according either to the source of the layer charge or to the occupancy in the octahedral sheet. Montmorillonite, Mx[Al4-xMgx](Si8)O20(OH)4 is a common dioctahedral smectite with a layer charge arising mainly from the octahedral sheet where octahedral aluminum cations are partially replaced by magnesium ions. Beidellite, M_V[Al₄](Si_{8-v}Al_v)O₂₀(OH)₄ is also a dioctahedral clay but the charge on the layer is primarily located on the tetrahedral sheets by the partial substitution of silicon by tetrahedral aluminum. An analogous trioctahedral smectite clay series ranges from octahedrally charged hectorite MxIMge. xLix](Si₈)O₂₀(OH)₄ to tetrahedrally charged saponite M_x[Mg₆](Si_{8-x}Al_x)O₂₀(OH)₄. Other smectite mineral clays belonging to one of these series may have octahedral substitutions by ions such as Fe^{2+, 3+}, V³⁺, Cr²⁺, Mn²⁺, Co²⁺, Ni²⁺, Cu²⁺, or Zn²⁺. Even octahedral vacancies can be a source of negative charge as is the case with stevensite. Tetrahedral charge sites arise mainly by substitution of Si⁴⁺ with Al³⁺ and rarely from substitution with cations like Fe³⁺ or B³⁺.

As previously described in Chapter 1, Section 1.4, the parent material for the porous clay heterostucture (PCH) synthesis is a smectic clay. These materials possess a combination of cation exchange, intercalation and swelling properties, which make them unique. Their capacity as cation exchangers is fundamental to their intercalation and swelling properties. This is the main feature that distinguishes smectic clays from mica and pyrophyllite-talc group of minerals, which have little or no ion exchange capacity. Due to the ability of the

minerals to imbibe a large variety of cations, an almost limitless number of intercalates are possible.

Neutral molecules like water can also be intercalated between the silicate layers of smectites. The intercalation process can be operated by several binding mechanisms. The reaction of the hydrated ion functioning as a Bronsted acid and the intercalant acting as a base constitutes one of the most common intercalation mechanisms. A large number of experiments have shown that hydrated cations are more acidic in the clay interlayers that in homogeneous aqueous solutions.^{4,5} The enhanced Bronsted acidity under intercalated conditions is due is part to the polarizing influence of the cation on the water molecule, in the spatially restricted galleries. The interlayer acidity is found to increase with increasing charge to radius ratio of the cation and with decreasing water content of the interlayer.

As discussed earlier, the most important step in the PCH synthesis is represented by the surfactant intercalation in the galleries of the layered host. Alkylammonium derivatives obtained by cation exchange are distinguished by a great diversity of interlayer structures. Packing density, type of aggregation and, therefore, the intragallery space, will depend on the charge density of the clay layer, the geometry of its surface and the degree of exchange. The alkylammonium ion in 2:1 clay minerals lie flat on the silicate surface in mono- or bi-layers or form paraffin-type arrangements with the chains radiating away from the surface. They can also adopt a pseudo trimolecular arrangement in low charge density clays where some chain ends are shifted above one another, so

Table 2.1. Idealized structural formulas for some general 2:1 layered silicates.

Mineral Group	Layer Charge (x)	Dioctahedral	Trioctahedral
Pyrophyllite Talc	-	[Al ₄](Si ₈)O ₂₀ (OH) ₄ Pyrophyllite	[Mg ₆](Si ₈)O ₂₀ (OH)₄ Talc
Smectite	0.3 –1.2 e ⁻	$M_x[Al_{4-x}Mg_x](Si_8)O_{20}(OH)_4$ $Montmorillonite$ $M_x[Al_4](Si_{8-x}Al_x)O_{20}(OH)_4$ $Beidellite$	$M_x[Mg_{8-x}Li_x](Si_8)O_{20}(OH)_4$ Hectorite $M_x[Mg_6](Si_{8-x}Al_x)O_{20}(OH)_4$ Saponite
Vermiculite	1.2 –1.8 e ⁻	M _{y-x} [Mg _{6-x} Al _y](Si _{8-y} Al _y)O ₂₀ (OH) ₄ Vermiculite	
Mica	2.0 e ⁻	K ₂ [Al ₄](Si ₈ Al ₂)O ₂₀ (OH) ₄ Muscovite	K₂[Mg ₆](Si ₆ Al₂)O₂₀(OH)₄ Phlogopite

that the spacing is determined by the thickness of three alkyl chains. The chains assume the required conformation by kinking. As opposed to pseudo trimolecular layers, the paraffin-type aggregation encountered in high charge density smectites allows a better fit of the alkyl groups to the layer surface oxygen atoms. As a result, high d-spacing organoclays are obtained only from smectites with high layer charge density.

Since the intragallery orientation of the surfactant is a major factor, a successful PCH synthesis can be achieved only by employing a high charge density smectite as a starting reactant. Therefore synthetic clays with uniform and high charge density are needed. Most of the known synthetic clays have a low layer charge density, a feature that makes them unsuitable for supramolecular assembly of surfactants in the gallery. The clay that was so far most suitable for supramolecular assembly is fluorohectorite.⁷

Fluorohectorite, can be easily synthesized from molten fluxes, but PCH derivatives based on fluorohectorite are thermally unstable and undergo defluorination above 350 °C.8 This problem was somewhat solved by using other clays like vermiculite or rectorite which have layer charges similar to fluorohectorite. Although vermiculite occurs abundantly in nature, this mineral is almost always contaminated with iron impurities that can compromise catalytic properties. Rectorite, although found abundantly in China, is not commercially available. Neither mineral is easily synthesized.

The crucial thing to obtain a supermolecular assembly was to be able to pack enough cationic surfactant and neutral co-surfactant in the clay gallery. In

other words the layer charge density is a main factor in this process. Actually, in order to achieve a supermolecular assembly, the layered host must have a charge of at least 1 e^- units per $O_{20}(OH)_4$ clay unit cell. Saponite is the clay that seems to meet these requirements.

Saponite is a 2:1 type trioctahedral phyllosilicate being a member of the smectite group of the clay minerals. The saponite structure (Figure 2.1) is composed of a central octahedral sheet with a brucite structure, in which oxygens replace four out of six OH- groups. These oxygens are connected to two tetrahedral sheets consisting of SiO₄ tetrahedra situated on both sides of the central octahedral sheet. A restricted amount of isomorphous substitution of Si⁴⁺ by Al³⁺ in the tetrahedral sheet results in a charge deficiency, compensated by exchangeable interlayer cations. The ideal structural formula of saponite is presented in Table 2.1 where M⁺ is the interlayer cation (Na⁺, K⁺) and x has a maximum value of 1.2.

Natural saponites are usually found in weathered volcanic rocks, although weathering of other Mg-containing rocks may also result in saponite formation. Although in natural systems the octahedral sheet is mainly occupied by Mg²⁺, some minor incorporation of Fe^{2+, 3+}, Al³⁺, Li⁺, Mn²⁺, Ti⁴⁺, Ni²⁺ is possible together with the isomorphous substitution of Si⁴⁺ by Fe³⁺ next to Al³⁺ in the tetrahedral sheet.

Because the chemical composition largely determines the acidic properties of the clay it is extremely important for catalytic applications of saponite that the composition of the clay material can be adjusted. In addition,

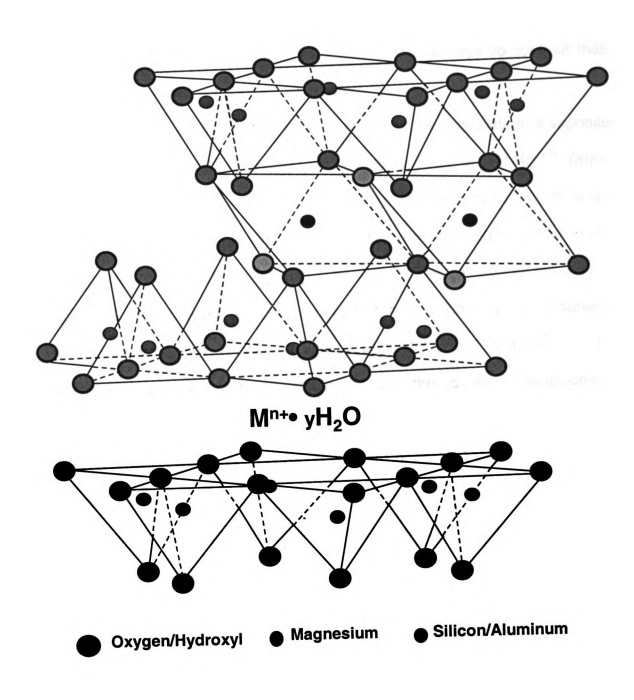


Figure 2.1: Idealized structure of saponite.

the saponite must be free of impurities, must contain a high specific area and pore volume that can be readily accessed from the bulk gas or liquid phase, and must be available in sufficient quantities. Since natural clays do not fulfill these requirements synthetic saponites are needed.

Most of the synthesis attempts are aimed at the preparation of saponites with the sites within the octahedral sheet entirely occupied by Ma²⁺. 9 Various groups have performed saponite synthesis at temperatures below 100 °C and at atmospheric pressures. 10-19 They were able to synthesize Mg-saponites in very diluted solutions containing AICl₃, MgCl₂ and Si(OH)₄ at 90 °C for 8 to 12 weeks. 14,15 They succeeded in the preparation of saponites with octahedral sheets containing various metals such as Mg²⁺, Ni²⁺, Co²⁺ and Fe²⁺. 12,13 The starting material was a co-precipitate prepared by the addition of stoichiometric amounts of sodium silicate and metal chloride salts (e. g., Mg, Al, Ni, Fe, Zn, Mn, Cu) to a solution with they appropriate amount of HCl. Aging the resulting coprecipitate for usually 3 weeks in water at temperatures between 23 - 100 °C led to the formation of saponite flakes with a low crystallinity. Later studies^{20,21} using this procedure applied hydrothermal conditions of 200 - 250 °C for 15 - 60 days resulting in well-crystallized saponites. Other reports 10 published a very similar gel preparation method by co-precipitating sodium silicate and sodium aluminate in HCl. Treatment of this gel in boiling solutions containing magnesium acetate for 45 days resulted in the formation of saponite.

Most of the preparation procedures for saponites described in the literature are performed by hydrothermally treating a homogeneous slurry

consisting of stoichiometric amounts of amorphous silica, aluminum either as an oxide or hydroxide or a salt, and magnesium (hydro)oxide/salt together with a component of the intended interlayer cation as a starting material. 18,20-34 All synthesis procedures were carried under hydrothermal conditions at temperatures ranging from 150 - 450 °C and pressures between the autogenous water pressure and 1500 bar. The reaction time was of the order of days to weeks. Urabe and co-workers 35,36 synthesized saponites with Ni²⁺ incorporated in the octahedral sheet using a Si – Al – Ni – Na gel as a starting material, at 285 °C for 3 days. Other studies reported the substitution of Si⁴⁺ by B³⁺ instead of Al³⁺ in the tetrahedral sheets. These boron saponites were prepared from mixtures containing the appropriate constituents. The synthesis conditions were 350 °C under autogenous water pressures or 1700 psi for 15 days.

This literature survey concerning the synthesis of saponites has demonstrated that the procedures according to the state of the art are very unfavorable for production on a large scale. The periods of time involved in the synthesis are mostly extremely long and performing the synthesis at high water pressure requires expensive equipment.

Here we show the development of a simple procedure for the preparation of saponites under mild hydrothermal conditions (< 200 °C) and short periods of time (<40 hours). For catalytic proposes it is extremely important that the textural as well as the chemical properties of the synthetic saponites can be controlled accurately within a broad range of chemical compositions. Therefore the Si/Al

ratio within the tetrahedral sheet has been varied between 3.5 and 5.7 in order to adjust the surface and interlayer properties of the saponites.

2.3 Experimental

2.3.1 Saponite Synthesis

A gel with a composition corresponding to saponite with the desired charge density was prepared from basic solutions of aluminum, silicate, and magnesium using a procedure analogous to the method described by Vogel¹⁹. The initial Si/Al molar ratio was in the range 3.5 to 5.7. The mixture was hydrothermally treated at 175 - 200 °C for 18 - 40 hours of synthesis time. The resulting solids were filtered, washed and dried overnight in air at 120 °C.

2.3.2 Physical Measurements

The cation exchange capacity (CEC) of the saponite was determined by first saturating the clay with the ammonium ions at the exchange sites. The ammonium saponite was then treated with 10M NaOH. The amount of released ammonia was measured using an ammonia selective electrode.

Elemental analyses were carried out by inductively coupled plasma emission spectroscopy at the University of Illinois Elemental Analysis Laboratory.

Powder X-ray diffraction patterns were obtained on a Rigaku Rotaflex diffractometer equipped with a rotating anode (CuK_{α} radiation) operated at 45 kV and 100 mA. The scattering and receiving slits were 1/6 and 0.3 degrees, respectively.

²⁹Si MAS (magic angle spinning) NMR spectra were obtained on a Varian VXR 400 MHz spectrometer at 79.5 MHz using a 7 mm zirconia rotor and a sample spinning frequency of 4 kHz. A pulse duration of 9 μ s and a delay time of 600 s allowed for a full relaxation of the Si nucleus. An external reference of talc (δ=-98.1 ppm relative to TMS) was used to determine the chemical shift values.

²⁷Al MAS (magic angle spinning) NMR spectra were obtained on a Varian VXR 400 MHz spectrometer at 104.26 MHz using a 7 mm zirconia rotor and a sample spinning frequency of 4 kHz. A pulse duration of 9 μs and a delay time of 2 seconds allowed for a full relaxation of the Al nucleus. An external reference of Al(NO₃)₃ (δ = 0 ppm) was used to determine the chemical shift values.

TEM images were obtained on a JEOL JEM-100CX II microscope with a CeB_6 filament and an accelerating voltage of 120 kV, a beam diameter of approximately 5 μm and an objective lens aperture of 20 μm . TEM samples were prepared by sonication of the powder in ethanol for 20 minutes and evaporating 1 drop onto a holey carbon film

2.4 Results and Discussion

As a member of the trioctahedral subgroup of 2:1 phyllosilicates, saponite contains primarily Mg²⁺ cations in each of the six octahedral positions of the O₂₀(OH)₄ unit cell, and a mixture of Si⁴⁺ and Al³⁺ ions in the eight tetrahedral positions of the cell. Consequently, the layer charge density is determined primarily by the Si/Al ratio in the tetrahedral sheet, and the layer charge is balanced by exchangeable cations in the gallery region between the 2:1 layers. Naturally occurring saponites usually have Fe²⁺, Fe³⁺, Mn²⁺, and other transition metal ions substituting for Mg²⁺, making them unattractive for catalytic applications.

The reaction stoichiometries were targeted at unit cell compositions of $Na_x[Mg_6](Si_{8-x}Al_x)O_{20}(OH)_4 \cdot nH_2O$ with x=1.2, 1.5, and 1.7. These charge densities were selected so that sufficient quaternary ammonium ions (denoted Q^+) and a neutral alkyl amine co-surfactant could be subsequently incorporated into the galleries for PCH formation. The resulting reaction products were designated SAP-1.2, -1.5, -1.7, respectively.

Table 2.2 provides the Si/Al ratios of the synthetic saponite products as determined by chemical analysis and ²⁹Si MAS NMR spectroscopy. Included in the table are the experimentally determined cation exchange capacities (CEC).

Table 2.2 also reports the corresponding unit cell formulas based on the chemical analyses. Figures 2.2 and 2.4 illustrate the X-ray diffraction patterns and ²⁹Si MAS NMR spectra, respectively, for the reaction products.

Table 2.2. Si/Al ratios, cation exchange capacities and unit cell formulas for synthetic saponite clays.

	Si / Al			CEC	Unit Cell Formulas ^b		
Sample	Calc.a	²⁹ Si-NMR	Element. Analysis	(meq/100g)			
SAP-1.2	5.67	6.43	6.62	90	Na _{1.11} Mg _{6.1} Al _{1.05} Si _{6.95} O ₂₀ (OH) ₄		
SAP-1.5	4.34	5.22	5.29	104	Na _{1.33} Mg _{6.05} Al _{1.26} Si _{6.77} O ₂₀ (OH) ₄		
SAP-1.7	3.57	4.28	4.50	112	Na _{1.48} Mg _{5.97} Al _{1.45} Si _{6.53} O ₂₀ (OH) ₄		

^aThe Si/Al ratio of the initial gel prior to hydrothermal crystallization.

^bThe unit cell formulas were found by elemental analysis.

All of the reaction products have a basal spacing of 12.5 Å and clearly exhibit the hkl reflections expected for a trioctahedral clay mineral (Figure 2.2). Also, as shown by the plot of the basal spacing for the 060 reflection in Figure 2.3, the b lattice parameter increases in proportion to the aluminum content in accord with Vegard's Law.²¹ This result verifies the incorporation of increasing amounts of aluminum into the layers with increasing aluminum content of the reaction gel. The ²⁹Si MAS-NMR spectra shown in Figure 2.4 also verify the structural composition of the saponite layers. Each sample exhibits two peaks at -95.8 and -90.5 ppm (Figure 2.4, curves C and B respectively) and a shoulder at -86.1 ppm (Figure 2.4, curve A), which are assigned, in accord with previous NMR assignments³⁸, to SiO₄ tetrahedra in Q³(0Al), Q³(1Al) and Q³(2Al), respectively. In this assignment scheme, the SiO₄ tetrahedra are linked to three adjacent tetrahedra containing one, two, or three aluminum centers. Increasing the amount of aluminum clearly results in an increase in the intensity of the Q³(1Al) resonance and, to a lesser extent that of the Q³(2AI) signal, as well. The deconvolution of the ²⁹Si MAS-NMR spectra allows for a quantitative assessment of the fraction of tetrahedral sites occupied by aluminum and, therefore, the determination of the Si/Al ratios through the relationship:38

Si/AI = 3/
$$\sum_{i=1}^{3} iI_{i}$$

where I is the normalized intensities of the SiO_4 centers linked to i adjacent AlO_4 centers (i = 1, 2, 3). The Si/Al ratios determined by NMR are in good agreement with those found through elemental analyses (Table 2.2).

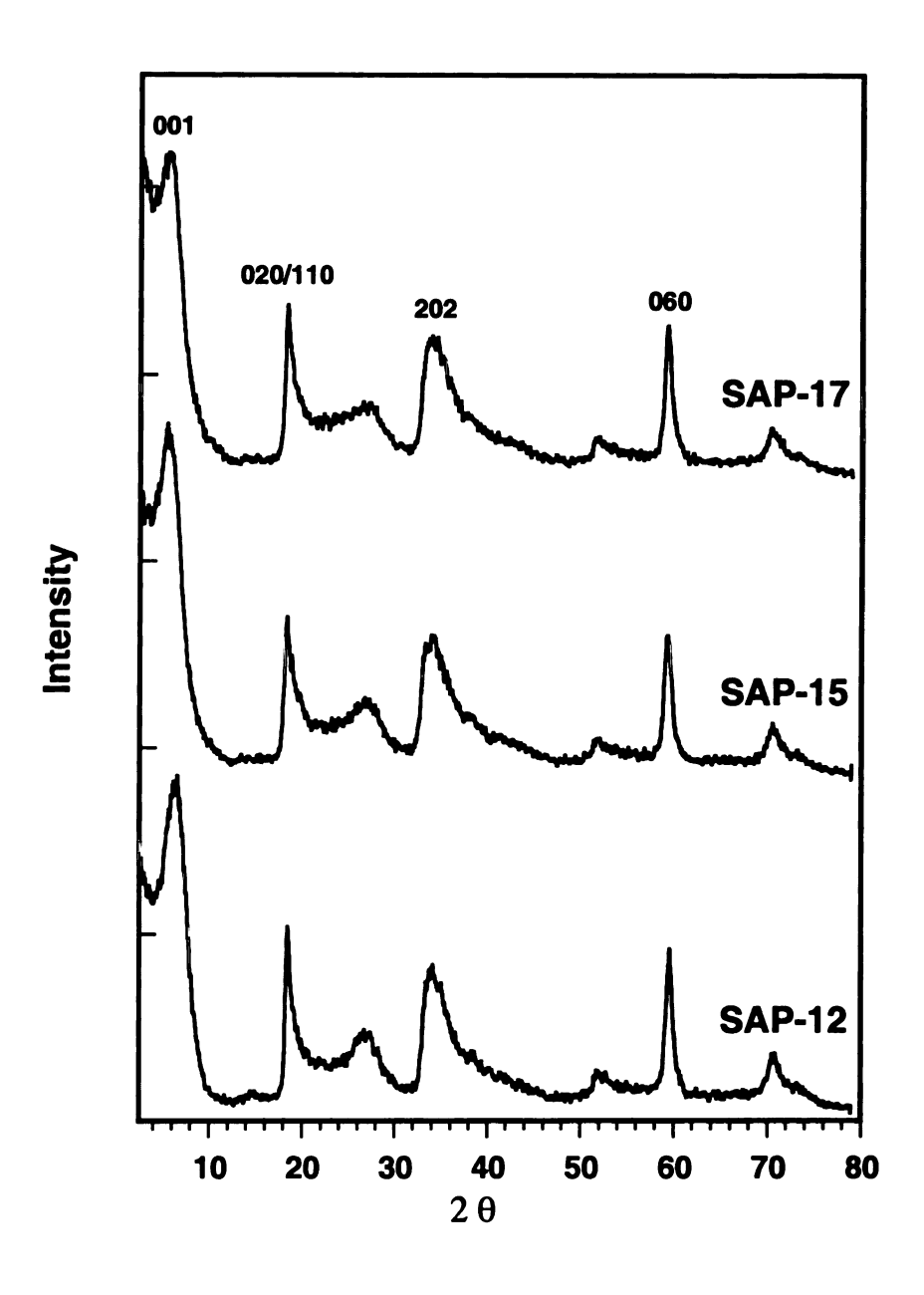


Figure 2.2: XRD patterns of synthetic saponites.

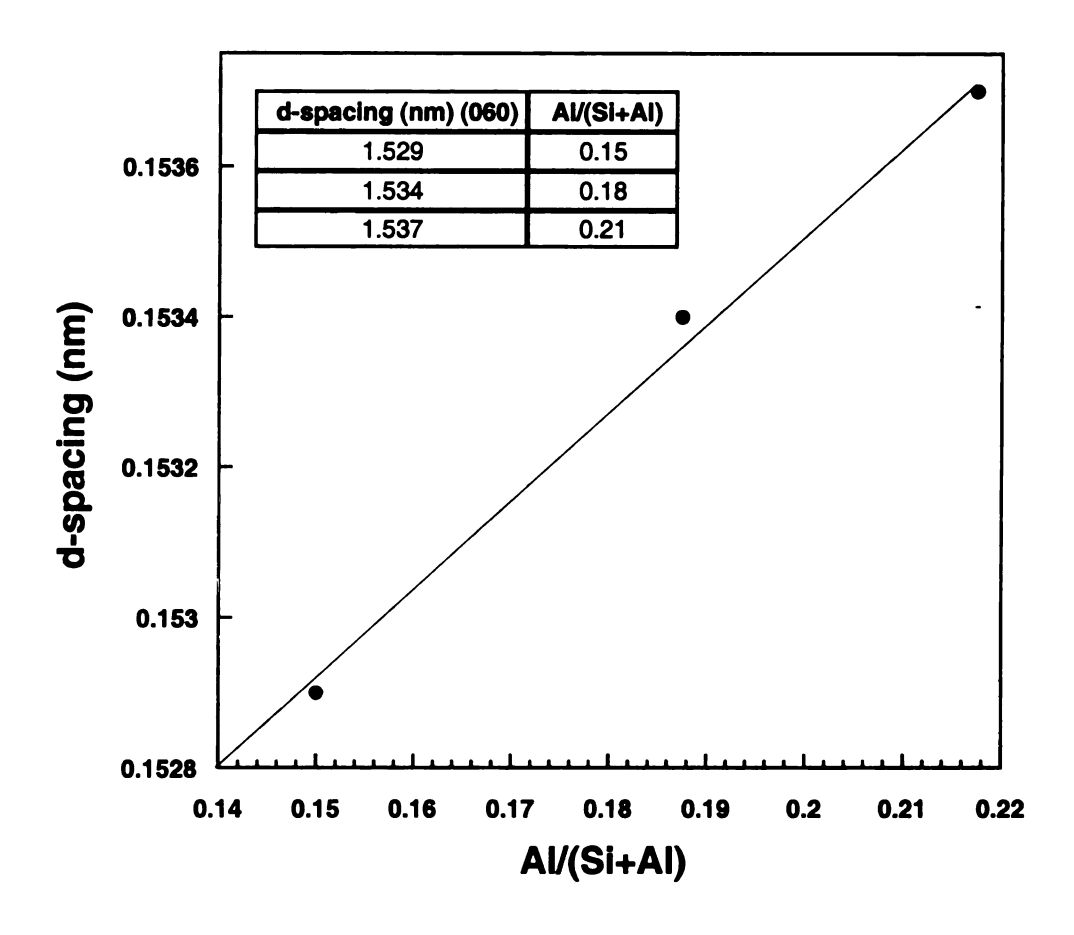


Figure 2.3: Dependence of the (060) spacing on the aluminum content of the tetrahedral layer of synthetic saponites.

On the basis of the analytical results in Table 2.2, the layered structure tends to favor a higher Si/Al ratio than the ratio initially present in the gel prior to crystallization, and the deviations from the initial gel compositions increase with increasing layer charge density.

In order to further investigate the environment of the aluminum centers, ²⁷Al MAS-NMR of the saponite was performed. The spectrum show in Figure 2.5 gives one resonance at 64 ppm. This signal is assigned to tetrahedrally coordinated aluminum where the metal is covalently bonded to three silicon atoms and one magnesium atom via oxygen bridges.³⁹ The absence of a resonance around 0 ppm indicates that all aluminum has been incorporated in the clay structure. The ²⁷Al MAS-NMR results are in good agreement with the XRD and ²⁹Si MAS-NMR data.

Figure 2.6 shows a typical TEM image of synthetic saponite SAP-1.5. The large particles consist of aggregated domains of several layers. However, the lamellar structure can be observed only for the particles with the *ab* plane oriented parallel to the optic axis of the microscope. Our reaction conditions seem to favor a limited layer stacking in the *c* direction, which correlates very well with the XRD data. As a result, the clay layers are more flexible, inducing a certain degree of curvature to the saponite structure.

We note that the CEC values, which were determined by the exchange of sodium ions in the gallery by ammonium ions, increase in proportion to the aluminum content of the layers, as expected. However, the experimentally

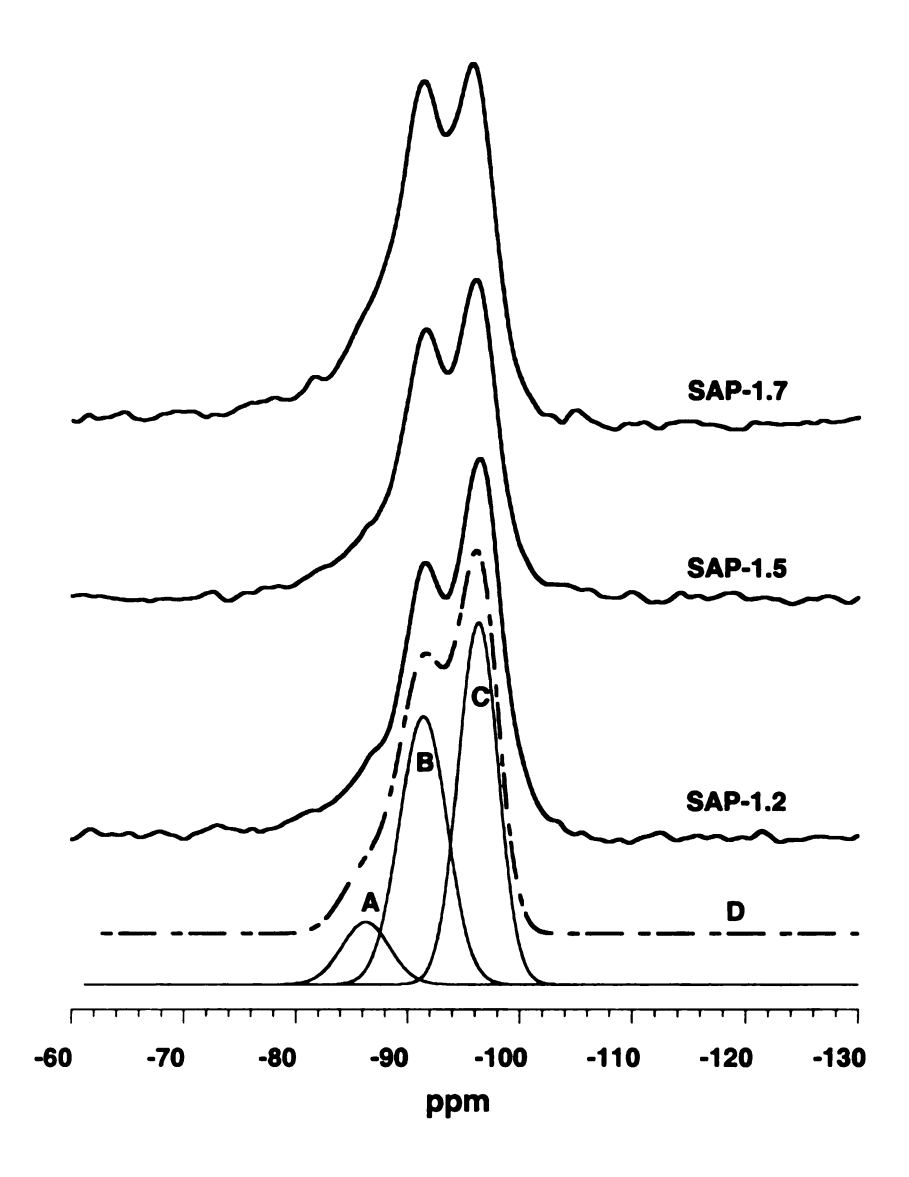


Figure 2.4: ²⁹Si MAS NMR spectra of synthetic saponites. The spectral components of the SAP-1.2 pattern (curves A, B and C) were obtained by deconvolution of the observed spectrum. Curve D represents the sum of the components.

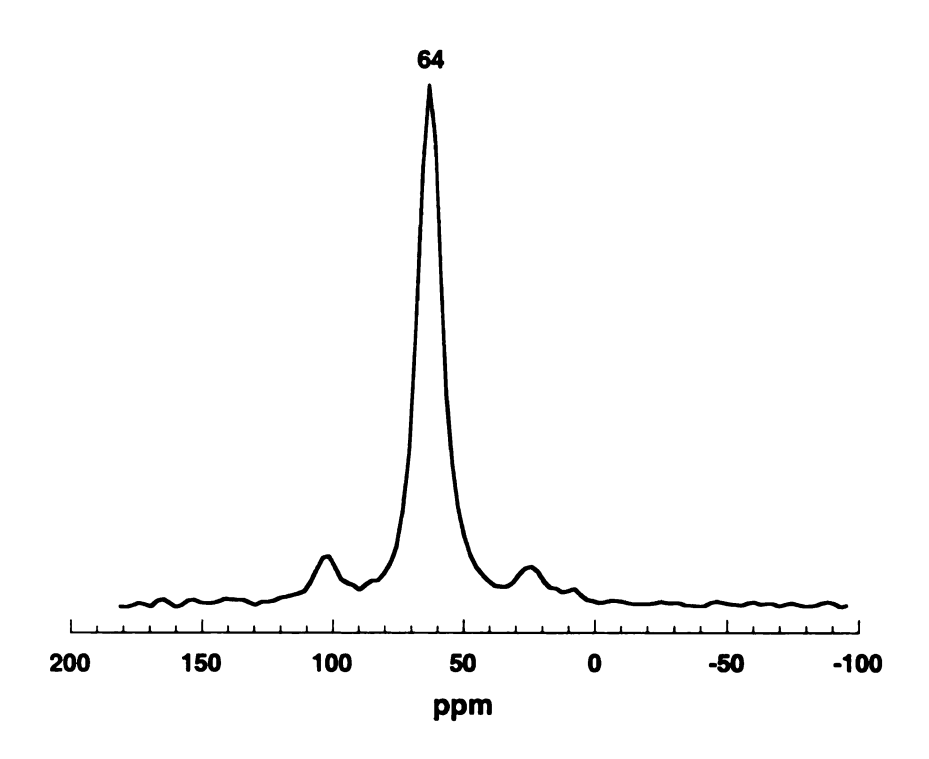


Figure 2.5: ²⁷Al MAS-NMR spectrum of synthetic saponite SAP-1.2.

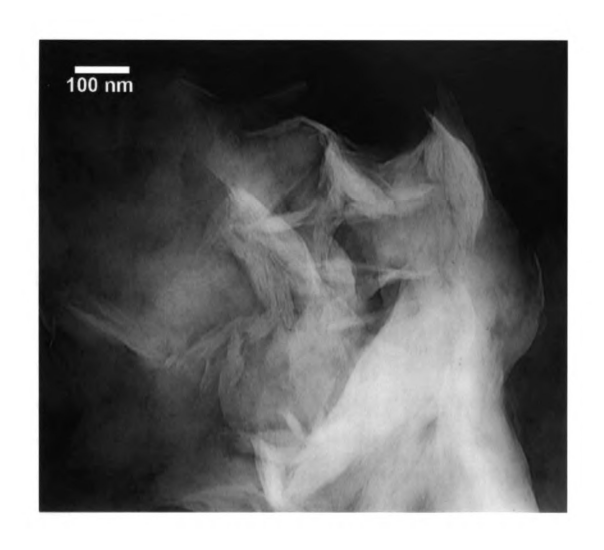


Figure 2.6: Representative TEM image of saponite SAP-1.5.

Served CEC values represent only ~70% of the values expected on the basis of the unit cell formulas in Table 2.2. It appears that sodium ion binding is preferred over ammonium ions under the conditions used in the exchange reaction, and this aspect of the exchange properties will require future investigation. Taken together, the above XRD, NMR and analytical results clearly indicate that the synthetic saponite clays are very well crystallized and have compositions very near those targeted in the initial reaction stoichiometry.

2.5 Conclusion

An effective method for the preparation of high quality saponite clays has been developed. The products were free of impurities and obtainable from readily accessible starting reactants under hydrothermal conditions. They are well-crystallized materials that possess intrinsic acidity. The incorporation of increasing amounts of aluminum in the clay layer was verified by NMR data, which are in good agreement with elemental analysis. In this smectic clay, aluminum substituting for silicon in the tetrahedral sheet of the 2:1 layer regulates the layer charge. A variation in the Si/Al ratios in the reaction stoichiometry from 3.5 to 5.7 increases the corresponding acidity of the clay layer.

As noted in the introduction to this chapter, there have been at least 28 previous procedures reported for the preparation of trioctahedral saponite clays containing various elements in the 2:1 tetrahedral and octahedral layers. Most of the procedures require dilute starting gels, hydrothermal conditions ranging from 23 – 450 °C, pressures from ambient to 1500 bar and reaction times from days to

months. The previously reported procedure that most closely resembles the procedure of the present work is the method of Vogel¹⁹, where the saponite is synthesized in 20 h at 90 °C from a Si/Al gel and magnesium nitrate in the presence of urea. However, the obtained product has low layer charge density since only part of aluminum present in the initial reaction mixture is incorporated in the tetrahedral layer of the clay. Also the poor crystallinity of the saponite along with a high cost of the starting materials make this procedure unattractive for production on a large scale.

The saponites possess a charge density sufficiently high to allow for supramolecular assembly in two-dimensions and therefore they can be employed as layered hosts for the synthesis of porous clay heterostructures.

2.6 References

- (1) Bailey, S. W. Rev. Mineral. 1988, 19, 347-403.
- (2) Nemecz, E. Clay Minerals, 1979.
- (3) Newman, A. C. D.; Brown, G. *Mineral. Soc. Monogr.* **1987**, *6*, 1-128.
- (4) Fripiat, J. J. ACS Symposium Series 1976, 34, 261-264.
- (5) Mortland, M. M. *Physical Chemistry* **1963**, *67*, 248-253.
- (6) Lagaly, G. Solid State Ion. 1986, 22, 43-51.
- (7) Galarneau, A.; Barodawalla, A.; Pinnavaia, T. J. *Nature* **1995**, *374*, 529-531.
- (8) Butruille, J.-R.; Pinnavaia, T. J. Clays Controlling Environ., Proc. Int. Clay Conf., 10th 1995, 92-101.
- (9) Kloprogge, J. T.; Komarneni, S.; Amonette, J. E. *Clays Clay Miner.* **1999**, *47*, 529-554.
- (10) Brat, S.; Rajan, N. S. S. *Indian J. Chem., Sect. A* **1981**, *20A*, 311-312.
- (11) Brat, S. Indian J. Technol. 1985, 23, 345-347.
- (12) Decarreau, A. C. R. Seances Acad. Sci., Ser. 2 1981, 292, 61-64.
- (13) Decarreau, A. Sciences Geologiques. Memoire 1983, 74, 1-191.
- (14) Farmer, V. C.; Krishnamurti, G. S. R.; Huang, P. M. *Clays Clay Miner.* **1991**, *39*, 561-570.
- (15) Farmer, V. C.; McHardy, W. J.; Elsass, F.; Robert, M. Clays Clay Miner.1994, 42, 180-186.
- (16) Kloprogge, J. T.; Breukelaar, J.; Geus, J. W.; Jansen, J. B. H. *Clays Clay Miner.* **1994**, *42*, 18-22.

- (17) Kloprogge, J. T.; Breukelaar, J.; Wilson, A. E.; Geus, J. W.; Jansen, J. B.H. Clays Clay Miner. 1994, 42, 416-420.
- (18) Kloprogge, J. T.; Breukelaar, J.; Jansen, J. B. H.; Geus, J. W. *Clays Clay Miner.* **1993**, *41*, 103-110.
- (19) Vogels, R. J. M. J.; Kerkhoffs, M. J. H. V.; Geus, J. W. Stud. Surf. Sci. Catal. 1995, 91, 1153-1161.
- (20) Grauby, O.; Petit, S.; Decarreau, A.; Baronnet, A. *Eur. J. Mineral.* **1993**, *5*, 623-635.
- (21) Grauby, O.; Petit, S.; Decarreau, A.; Baronnet, A. *Eur. J. Mineral.* **1994**, *6*, 99-112.
- (22) Booij, E. M. Sc. Thesis, Utrecht University 1992, 78pp.
- (23) Breukelaar, J.; Kellendonk, F. J. A.; Van Santen, R. A. In *Eur. Pat. Appl.*; (Shell Internationale Research Maatschappij B. V., Neth.). Ep, 1989, p 8 pp.
- (24) Breukelaar, J.; Van Santen, R. A.; De Winter, A. W. In *Eur. Pat. Appl.*; (Shell Internationale Research Maatschappij B. V., Neth.). Ep, 1990, p 8 pp.
- (25) Harward, M. E.; Brindley, G. W. Clays and Clay Minerals 1965, 6, 209-222.
- (26) Hickson, D. A. In U.S.; (Chevron Research Co.). US, 1974, p 9 pp.
- (27) Hickson, D. A. In *U.S.*; (Chevron Research Co., USA). Us, 1975, pp 9 pp. Division of U.S. 3,844,978.
- (28) Iiyama, J. T.; Roy, R. Clays and Clay Minerals: Proc. 10th national conference on clays and clay minerals. 1963, 4-22.

- (29) Iwasaki, T.; Onodera, Y.; Torii, K. *Clays and Clay Minerals* **1989**, *37*, 248-257.
- (30) Kuchta, L.; Fajnor, V. S. Chem. Pap. 1988, 42, 339-345.
- (31) Li, L.; Liu, X.; Ge, Y.; Xu, R.; Rocha, J.; Klinowski, J. *J. Phys. Chem.* **1993**, *97*, 10389-10393.
- (32) Suquet, H.; Iiyama, J. T.; Kodama, H.; Pezerat, H. *Clays Clay Miner*. **1977**, *25*, 231-242.
- (33) Vogels, R. J. M. J.; Breukelaar, J.; Kloprogge, J. T.; Jansen, J. B. H.; Geus, J. W. *Clays Clay Miner.* **1997**, *45*, 1-7.
- (34) Whitney, G. Clays and Clay Minerals 1983, 31, 1-8.
- (35) Urabe, K.; Koga, M.; Izumi, Y. *Journal of the Chemical Society-Chemical Communications* **1989**, 807-808.
- (36) Jiang, D.; Sun, T.; Liu, Z.; Min, E.; He, M. *Proc. 9th International Zeolite Conference, Montreal* **1993**, 631-638.
- (37) Xie, X.-m.; Yao, Y.-Z.; Cheng, G.; Cao, J.-h.; Zhang, S. *Cuihua Xuebao* **1993**, 166-171.
- (38) Lipsicas, M.; Raythatha, R. H.; Pinnavaia, T. J.; Johnson, I. D.; Giese, R. F., Jr.; Costanzo, P. M.; Robert, J. L. *Nature (London)* **1984**, *309*, 604-607.
- (39) Woessner, D. E. Am. Mineral. 1989, 74, 203-215.

Chapter 3

Mesostructured Clay Catalysts: Synthesis,
Characterization and Catalytic Activity of a New Porous
Clay Heterostructure (SAP-PCH) Derived from Synthetic
Saponite

3.1 Abstract

Mesostructured intercalates belonging to the class of solid acids known as porous clay heterostructures (PCH) have been prepared through the surfactant - directed assembly of mesoporous silica within the galleries of synthetic saponite clays. The removal of the intragallery mixture of neutral alkyl amine and quaternary ammonium ion surfactant (Q⁺) by calcination afforded PCH intercalates with basal spacings of 33 - 35 Å, BET specific surface areas of 800 - 920 m² g⁻¹, and pore volumes of 0.38 - 0.44 cm³ g⁻¹. The framework pore sizes were in the super - micropore to small mesopore region ~15 - 23 Å. Temperature - programmed desorption of chemisorbed cyclohexylamine (CHA) indicated the

presence of both weak and strong acid sites, corresponding to desorption temperatures near 220 and 410 °C, respectively. The total acidity (0.64 - 0.77 mmole CHA g⁻¹) increased with the saponite layer charge density (x), indicating that the acidity is correlated with the number of protons balancing the clay layer charge after calcination. The high acidity, structural stability to 750 °C, and supermicroporous to small mesoporous pore structure were verified by employing these PCH materials as catalysts for Friedel-Crafts alkylation and cumene cracking reactions.

3.2 Introduction

Owing to growing environmental concerns, there is a large interest in replacing traditional catalysts, such as aluminum trichloride, sulfuric acid and hydrofluoric acid with recyclable solid acids. The engineering of porosity in common materials like silica, zeolites and clays is emerging as an area of great scientific and technological interest. Materials with tunable pores become particularly important towards applications in the field of adsorption and catalysis.^{1,2}

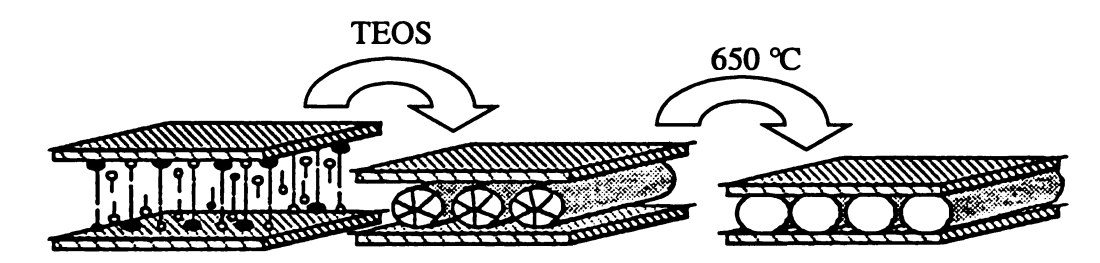
Pillared interlayered clays have been extensively studied and are very attractive as solid acid catalysts.^{3,4} These solids exhibit a tunable acidity, regular microporosity and relatively high thermal stability. Montmorillonite, beidelite, hectorite and saponite pillared by Al₁₃ hydroxyl cations have been studied the most. These microporous materials revealed a substantial activity for petroleum cracking and for fine chemical synthesis via alkylation and isomerization. Butruille and co-workers^{5,6} reported an improvement in the acidic catalytic properties of alumina-pillared fluorohectorite relative to other pillared clays. The presence of fluorine in the layer structure enhanced the Bronsted acidity of the pillared clay at outgassing temperatures below 350 °C. This catalyst exhibited significant Bronsted acidity, which is unusual for smectites clays.

Also the mesoporous molecular sieves developed recently^{7,8} have stimulated a great deal of interest in large-pore materials for selective catalysis⁹⁻¹¹ and other applications.¹² The synthesis of these materials involves the use of ionic surfactants, which interact with the inorganic ions in a cooperative process

to form a range of ordered mesostructures.^{13,14} Many of the same ionic surfactants used for the assembly of mesostructured molecular sieve catalysts^{7,9,11} and related bulk phases¹² can be intercalated in a variety of layered host structures.¹³ Recently has been demonstrated that some of these mesostructure - forming surfactants retain their structure directing properties when intercalated in the galleries of smectite clays. In a manner quite analogous to bulk mesostructure formation, the intercalated surfactants direct the assembly of an open framework metal oxide (silica) structure within the constrained gallery regions of the layered host.¹⁵ The resulting porous intercalates referred to as porous clay heterostructures (PCH), showed promising acidic properties for catalytic organic conversions.^{16,17} They were prepared by the surfactant - directed assembly of mesostructured silica in the two - dimensional galleries of 2:1 mica - type layered silicate with high charge density, such as in fluorohectorite, rectorite, and vermiculite.

PCH synthesis makes use of the intragallery ordering of silicate species and surfactants into organic/inorganic micelles (Figure 3.1), similar to the ordering processes observed for MCM-41 molecular sieves. However, the difference between PCH and MCM-41 synthesis is that this micellar organization occurs inside the restricted gallery region of the clay, not in bulk solution.

In general, PCH materials offer special opportunities for the rational design of a heterogeneous catalyst system, in part, because the pore size



A. Q*-Amine Solvated Clay B. Templated Heterostructure C. Porous Clay Heterostructure

Figure 3.1: Proposed mechanism for the formation of a porous clay heterostructures (PCH) by gallery assembly: (A) the initial amine-solvated bilayer structure with a thickness equivalent to the length of the quaternary cation (filled head groups) and the neutral amine (open head groups) surfactants; (B) the templated heterostructure in which a 2D hydrated silica is organized around micellar assemblies of Q+ and neutral amine; (C) the calcined PCH with a 2D framework of porous silica intercalated between the clay layers.

distribution can be tailored in the rarely encountered supermicropore to small mesopore range (14-25 Å) through the choice of the structure-directing surfactant in the galleries. However, the choice of a host clay with a charge density suitable for the intragallery assembly is somewhat problematic. Although vermiculite occurs abundantly in nature, this mineral is almost always contaminated with iron impurities that can compromise catalytic properties. Rectorite, although found abundantly in China, is not commercially available. Neither mineral is easily synthesized. Fluorohectorite, on the other hand, can be easily synthesized from molten fluxes, but PCH derivatives based on fluorohectorite are thermally unstable and undergo defluorination above 350 °C. 18 Therefore, more readily accessible synthetic smectite clays with high layer charge density are needed to fully develop the chemistry of PCH materials.

Here we report the synthesis and properties of a new family of porous clay heterostructures derived from synthetic saponite clay. In this smectic clay the layer charge density can be regulated by controlling the extent of silicon substitution by aluminum in the tetrahedral sheet of the 2:1 layer. Also, saponite can be synthesized free of impurities from readily accessible starting materials under hydrothermal conditions. Moreover, intercalated derivatives of saponite are intrinsically acidic, as has been demonstrated previously for alumina-pillared forms of the mineral. However, their catalytic utility is limited in part by a pore structure in the micropore domain.

Based on PCHs unique porosity and acidic nature, their interesting properties to potentially function as a heterogeneous catalyst will be explored. In

order to test the porosity of our materials Friedel-Crafts alkylation of bulky 2, 4-ditert-butylphenol (DBP) (molecular size (Å): 9.5×6.1×4.4) with cinnamyl alcohol to produce 6,8-di-tert-butyl-2, 3-dihydro[4H] benzopyran (molecular size (Å): 13.5×7.9×4.9) was used as a probe reaction for SAP-PCH. This large substrate reaction also was selected in part because only mesoporous molecular sieves are known to provide the accessible acid sites for catalysis.²² Conventional zeolites and pillared clays are poor catalysts for this reaction because the reagents cannot readily access the small micropores.

Also, by utilization as solid acid catalysts in the cumene cracking reaction, the acidity of our saponite derivatives was tested.

3.3 Experimental

3.3.1 PCH Synthesis

Cetyltrimethylammonium (CTMA) as the clay exchange cation and decylamine as the co-surfactant were used to form the PCH forms of the synthetic saponites. A 1.0 wt % suspension of previously prepared saponite was allowed to react at 50 °C with a 0.5 M aqueous cetyltrimethylammonium bromide solution in two-fold excess of the clay cation exchange capacity. After a reaction time of 24 hours, the product was washed with ethanol and water to remove excess surfactant and air-dried. The organoclay, denoted Q⁺-clay, was then added to decylamine at a Q⁺-clay: decylamine molar ratio of 1:20 and the resulting suspension was stirred for 20 minutes at room temperature. The amine

co-surfactant swells the galleries and participates in the gallery assembly process. Tetraethylorthosilicate (TEOS) was added to achieve the molar ratio decylamine: TEOS = 1:6. After a reaction time of 3 hours at room temperature the gel was recovered by centrifugation and exposed to a controlled relative humidity of 50 % for a period of 72 hours to form the as-synthesized product. The resulting white powder was subsequently calcined in air at 650 °C using a temperature ramp rate of 1 °C / min to remove the surfactant.

All reactants were obtained from Aldrich Chemical Co. and used without further purification.

3.3.2 Catalytic Alkylation of 2,4-Di-tert-butylphenol (DBP) with Cinnamyl Alcohol (CA)

The alkylation of 2,4-di-tert-butylphenol with cinnamyl alcohol was carried out in a 25 ml flask with 0.25 mmol 2,4-di-tert-butylphenol (Aldrich) and 0.25 mmol cinnamyl alcohol (Aldrich) using 12.5 ml isooctane as solvent. When the solution was heated and maintained at 60°C, 125 mg catalyst was added. After 6 hours reaction, the catalyst was filtered and extracted with dichloromethane to recover adsorbed reaction products. 1,3 - Di-tert-butylbenzene was used as internal standard and the products were analyzed by GC (HP5890) and GC-MS (HP5890). The reaction is illustrated in Figure 3.2.

Figure 3.2: Catalytic Alkylation of 2,4-Di-tert-butylphenol (DBP) with Cinnamyl Alcohol (CA).

3.3.3 Cumene Cracking Reaction

Cumene cracking reactions were performed in a 6 mm i.d. fixed bed quartz reactor with 200 mg catalysts. The cumene flow rate was 4.1 μ mol min⁻¹ in a 20 mL min⁻¹ carrier gas of N₂. Cumene conversions were reported under steady-state conditions after 30 min. on steam at 300 $^{\circ}$ C.

3.3.4 Physical Measurements

Powder X-ray diffraction patterns were obtained on a Rigaku Rotaflex diffractometer equipped with a rotating anode (CuK_{α} radiation) operated at 45 kV and 100 mA. The scattering and receiving slits were 1/6 and 0.3 degrees, respectively.

 N_2 adsorption-desorption isotherms were obtained at -196 °C on a Micromeritics ASAP 2010 Sorptometer using static adsorption procedures. Samples were outgassed at 175 °C and 10^{-6} Torr for a minimum of 12 hours prior to analysis. BET specific surface areas were calculated from the linear part of the BET plot according to IUPAC²³ recommendations.

Elemental analyses were carried out by inductively coupled plasma emission spectroscopy at the University of Illinois Elemental Analysis Laboratory.

TEM images were obtained on a JEOL JEM-100CX II microscope with a CeB₆ filament and an accelerating voltage of 120 kV, a beam diameter of approximately 5 µm and an objective lens aperture of 20 µm. TEM samples were prepared either by sonication of the powder in ethanol for 20 minutes and

evaporating one drop onto a holey carbon film or by thin sectioning. Thin sections were prepared by embedding the powder in L.R. White acrylic resin (hard) and sectioning on an ultramicrotome. The holey carbon film and the thin sections (~80 nm) were supported on 300 mesh copper grids.

Temperature programmed cyclohexylamine desorption (CHA-TPD) spectra were recorded on a Cahn TG system 121 analyzer. Samples (~ 30 mg) were transferred directly out of the cyclohexylamine vapor to the thermobalance and they were kept at 150 °C for 2 hours. Desorption thermograms were recorded at a heating rate of 10 °C /min under nitrogen flow. The mass loss between 200 °C and 420 °C was used to determine the acid content of the samples (in mmoles CHA g⁻¹ adsorbent).

3.4 Results and Discussion

All three saponite compositions were used to assemble porous clay heterostructures that were denoted SAP1.2-, SAP1.5-, and SAP1.7-PCH, respectively. The process used to assemble the intragallery mesostructure, which is illustrated schematically in Figure 3.3, was analogous to the one previously reported for the preparation of PCH derivatives of fluorohectorite (FH-PCH).¹⁵ This scheme illustrates the conversion of these lamellar hosts into the mesoporous heterostructures analogs. The saponites were first converted to an onium form by ion exchange with aqueous solution of an cetyltrimethylammonium bromide (CTAB), and then solvated with decylamine as a co-surfactant and tetraethylorthosilicate (TEOS) as a silica precursor to achieve

a Q⁺-clay: decylamine: TEOS molar ratio of 1:20:120. The TEOS preferentially intercalates into the gallery and the presence of the intragallery water converts that TEOS into mesostructured silica. Upon calcination the corresponding porous derivative is obtained.

The XRD patterns (the 001 reflections) of the 3 derivatives before and after calcinations (Figure 3.4) show the dependence of the gallery height with the charge density. If 10 Å, the approximate height of the clay layer are subtracted from these values, the gallery height of the saponite derivatives will be in the range of 22 to 25 Å.

The basal spacings for the as-synthesized and calcined forms of the SAP-PCH derivatives (Table 3.1), as well as for the initial quaternary ammonium saponite precursors, increase with increasing aluminum content of the layers. The quaternary ammonium ions adopt paraffin-type arrangements in the interlayer space with chains radiating away from the clay surface.²⁴ As the layer charge density increases with increasing aluminum content, the onium ion orientation in the gallery becomes more vertical, resulting in an expansion of the gallery height (Figure 3.5). The increase in gallery height is accompanied by an increase in TEOS loading and, consequently in the amount of mesostructured silica in the gallery region of the final PCH. For instance, the gallery silica content per O₂₀(OH)₄ unit cell of the calcined product increases from 13.7 for SAP1.2-PCH to 15.7 mole for SAP1.7-PCH.

SAP-PCH derivatives exhibit specific surface areas and pore volumes that are even larger than those obtained for FH-PCH assembled from the same

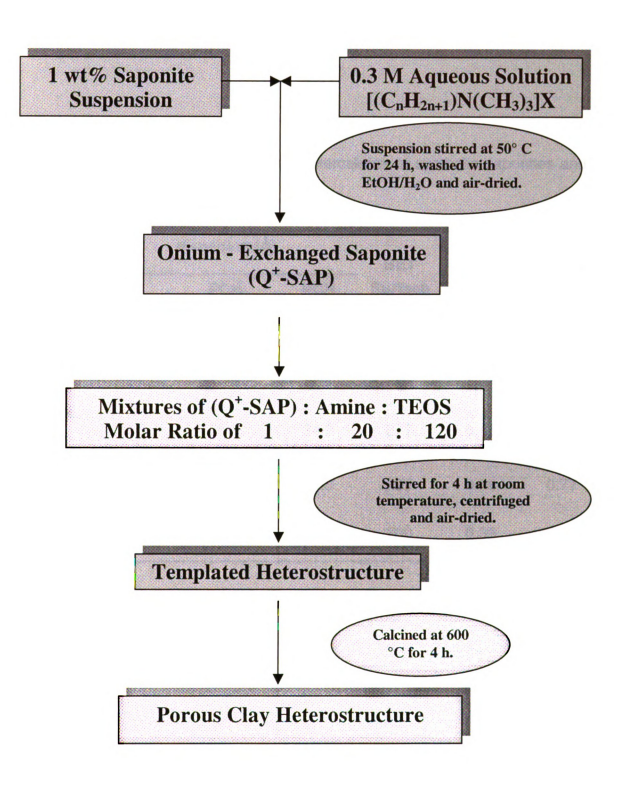
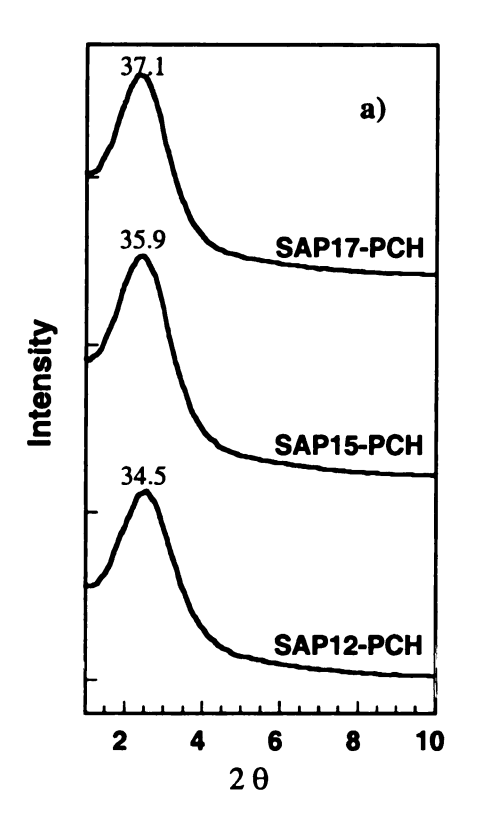


Figure 3.3: Schematic illustration of the main steps involved in the porous clay heterostructures synthesis.

Table 3.1. Properties of Q⁺ and PCH intercalates of synthetic saponites and fluorohectotrite.

		d spacing (Å)		BET	Pore	Acidity
Sample	Q ⁺ - saponite	PCH As- synthesized	PCH calcined	Surface Area ^a (m ² g ⁻¹)	Volume ^a (cm ³ g ⁻¹)	(mmol CHAg ⁻¹)
SAP1.2- PCH	20.5	34.5	32.9	921	0.44	0.64
SAP1.5- PCH	24.2	35.9	34.2	877	0.42	0.73
SAP1.7- PCH	25.8	37.1	35.3	797	0.38	0.77
FH-PCH	27.0	38.0	32.0	700	0.35	0.10

^aThe surfaces areas and pore volumes are for the calcined forms of the PCH derivatives.



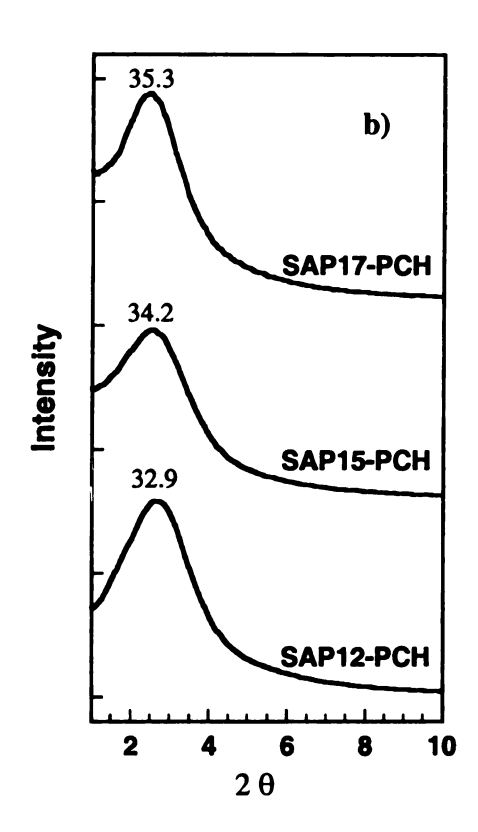


Figure 3.4: XRD profiles for a) as-synthesized and b) calcined SAP-PCH materials.

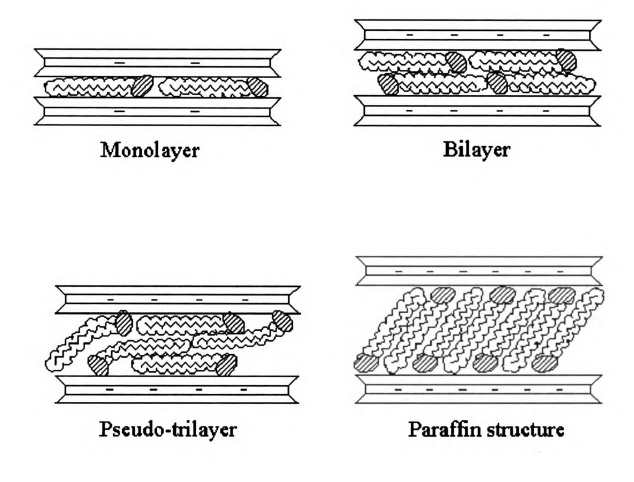


Figure 3.5: Various orientations of alkylammonium ions in the galleries of layered silicates with different charge densities.

surfactant/co-surfactant system¹⁵ (Table 3.1). Also, whereas FH-PCH begins to undergo defluorination above 350 °C and structural decomposition above ~550 °C, the SAP-PCH derivatives retain structural integrity even when calcined at 750 °C.

As shown in Figure 3.6, the SAP-PCH products exhibit type IV adsorption isotherms. The near-linear uptake of nitrogen in the knee region corresponding to the partial pressure range 0.05-0.25 is indicative of a super-micropore to small mesopore structure in the super - micropore to small mesopore region, ~15 - 25 Å. The inset to Figure 3.6 provides a typical pore size distribution. The BET specific surface areas progressively decrease with increasing aluminum loading from 921 to 797 m² g⁻¹ and the framework pore volumes decrease form 0.44 to 0.37cm³ g⁻¹. This behavior is explained by the increased layer charge density, which results in an increase in the amount of mesostructured gallery silica.

Previous efforts to obtain TEM images of PCH materials have met with limited success. ¹⁵ Though the clay layers have been easily observed, resolving the intragallery pore structure has been more difficult due to the turbostratic nature of these materials. In the present work, direct imaging of the framework pores of SAP-PCH derivatives was achieved by thinning the samples along the *ab* plane through microtoming. Figure 3.7 is a typical TEM image of a SAP-PCH that has been suspended in ethanol and evaporated onto a holey carbon film. The low magnification image (see Figure 3.7A) shows that the larger particles consists of aggregated domains of several layers oriented in all directions, similar

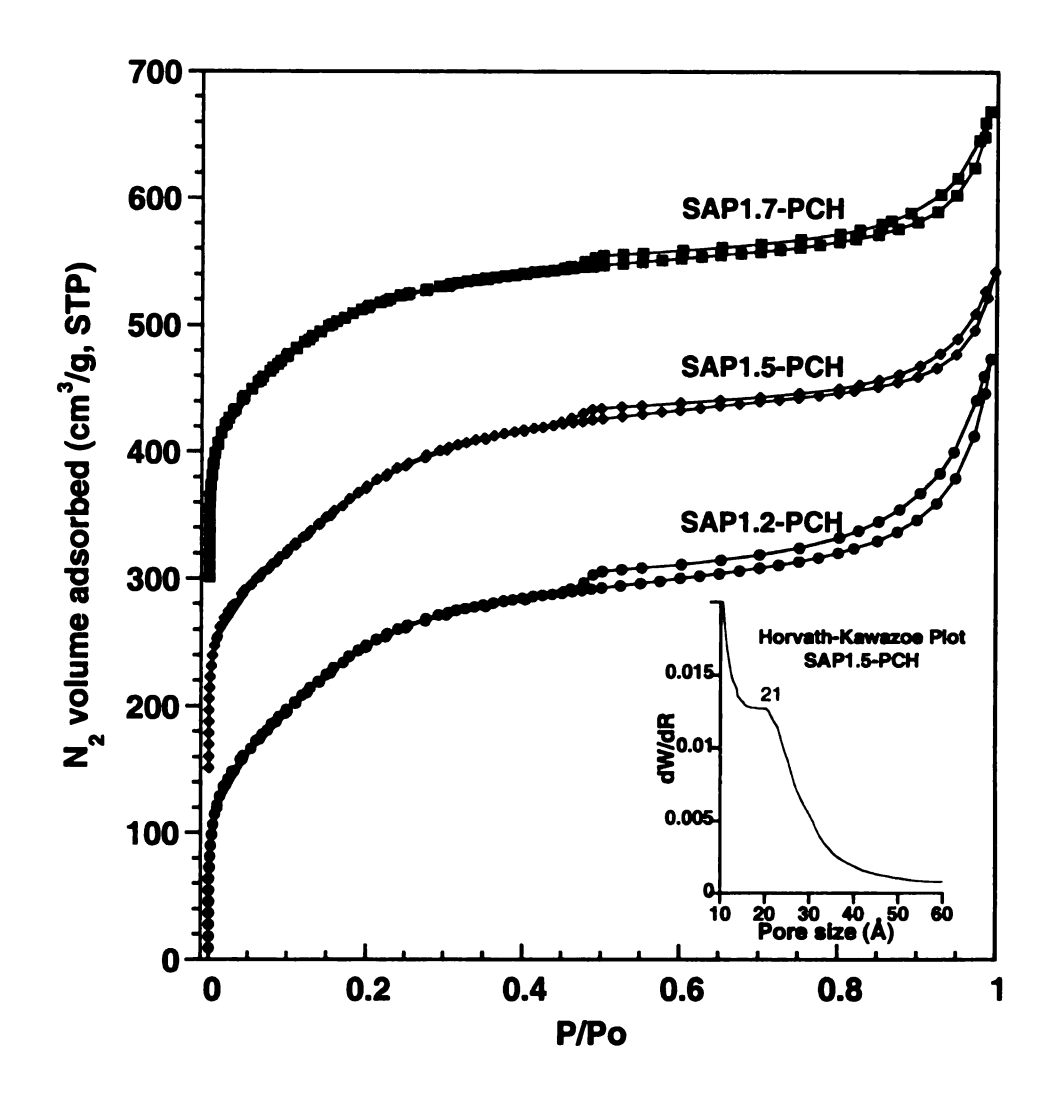


Figure 3.6: N_2 adsorption/desorption isotherms for porous clay heterostructures derived from synthetic saponites. The isotherms for SAP1.5 and SAP1.7-PCH are vertically displaced by 150 and 300 cm³ g⁻¹, respectively. **Insert:** Horvath-Kawazoe pore size distribution curve. dW/dR is the derivative of the normalized adsorbate (N_2) volume adsorbed with respect to the pore diameter of the adsorbent in units of cm³ g⁻¹ Å⁻¹.

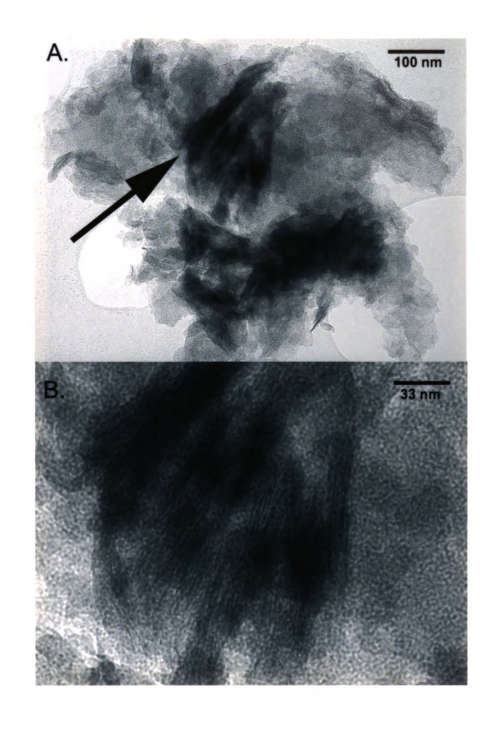


Figure 3.7: Representative TEM image of a calcined SAP1.5-PCH.

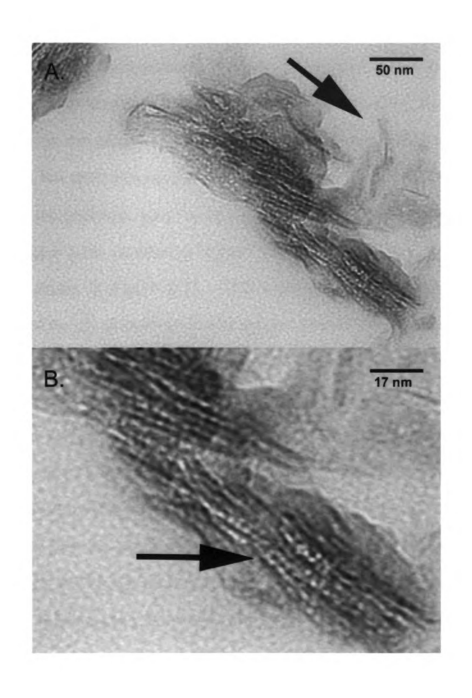


Figure 3.8: TEM of a thin-sectioned SAP1.5-PCH.

to the layer aggregation in the synthesized clay. The arrow in Figure 3.7A highlights the domains within the particle that are oriented with their *ab* planes parallel to the optic axis of the microscope. The lamellar phase is visible for this orientation of the domains. Other orientations of the *ab* planes reveal wormhole-like pores at the external surfaces of the clay plates. Tilting of the particle relative to the optic axis results in the reorientation of some of these domains parallel to the optic axis, again revealing the layered structure of these regions.

Figure 3.7B provides a higher magnification image of the oriented domains shown in Figure 3.7A. The lamellar phase and intragallery pore structure is clearly evident within this image. Due to the disorder of the pores within the gallery and the thickness of the particles, enhanced imaging of the intragallery pore structure is precluded.

Improved imaging of the intragallery pore structure is possible, however, by sectioning the materials prior to imaging. Figure 3.8 shows typical TEM images of thin-sectioned a SAP-PCH in which the *ab* planes of the particle domain are oriented parallel to the optic axis. In the image provided in Figure 3.8A, the clay layers are discernable as solid dark lines and the pores appear in lighter contrast between the layers. The arrow in Figure 3.8A points to a small domain of three layers of SAP-PCH in which only the middle clay layer and the two adjacent gallery pore structures are clearly evident. The two outer clay layers are barely visible in this image.

Figure 3.8B is a higher magnification image of the intragallery pore structure. The pores within a gallery have a uniform size (arrow), as do the clay layers. The framework pore orientation is not persistent, however, indicating a significant degree of disorder within the gallery. A disorder wormhole - like pore structure in the *ab* plane is suggested by the changes in contrast levels between the layers.

The SAP-PCH materials reported here represent heterostructures comprising the smectite clay host and a mesostructured silica phase within the galleries of the host. The lattice substitution of silicon by aluminum in the clay layer and the replacement of the initial gallery ions (Na⁺) by surfactant cations and subsequently by protons upon calcination, generate significant Bronsted acidity within the mesostructured galleries. The acid content of the SAP-PCH derivatives was determined using thermally programmed desorption of cyclohexylamine (CHA-TPD).^{27,28} After being exposed to CHA vapor, the samples were heated at 150 °C for 2 hours in order to remove the physically adsorbed amine.

As shown in Figure 3.9, the SAP-PCH materials exhibit two types of acidic sites. The intensity of the first desorption peak at 210 °C is directly correlated with the Si/Al ratio or the clay layers. This weaker acid site most likely is associated with the internal gallery surfaces of the PCH. The stronger acid site represented by the desorption peak near 400 °C is independent of the layer chemical composition and may related to sites at the external surfaces of the heterostructure. The weight loss of CHA between 150 and 450 °C was used to

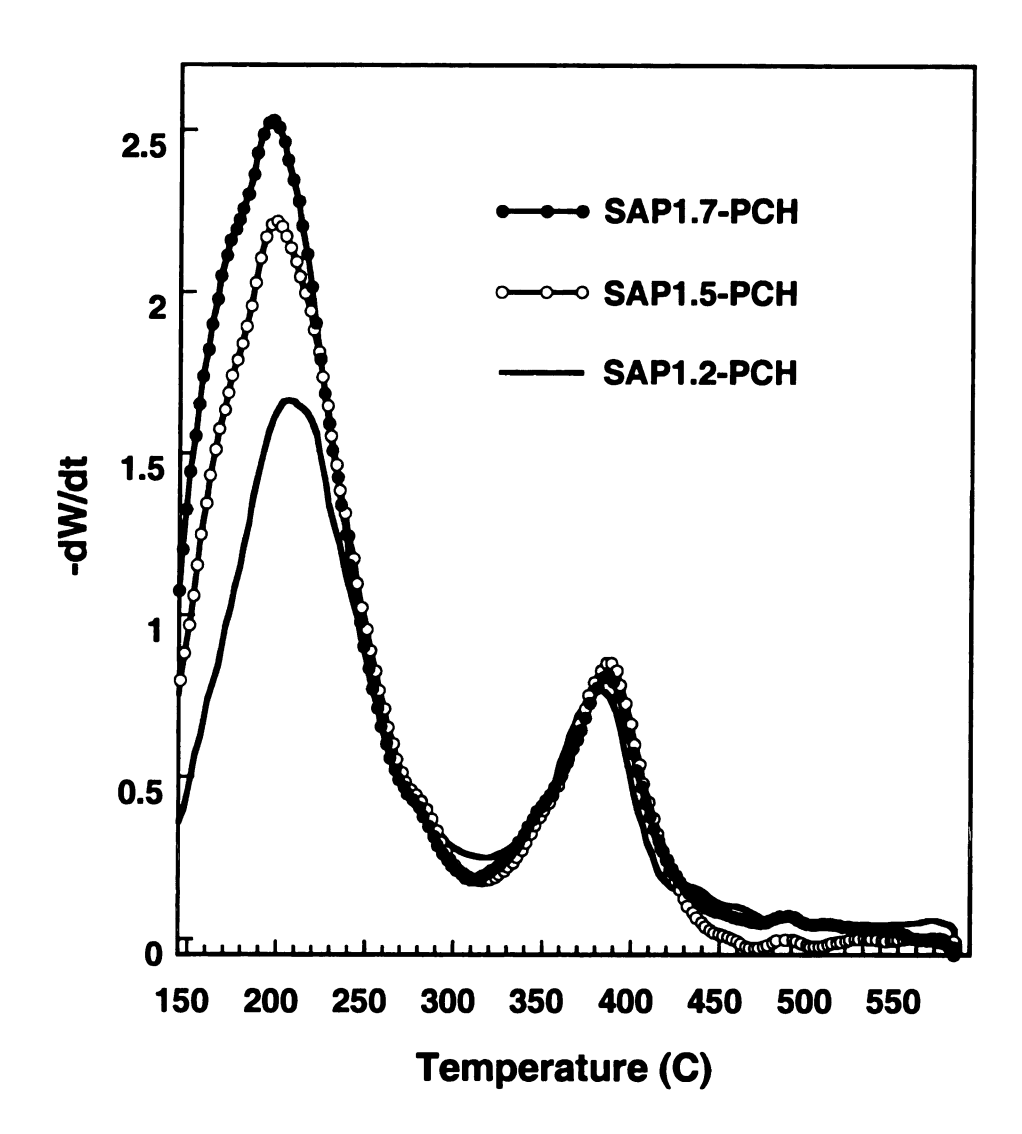


Figure 3.9: Profiles for the thermal desorption of cyclohexylamine from SAP-PCH samples. dW/dT is the differential weight with respect to temperature in units of g/°C.

quantify the acidity, assuming that each base molecule interacts with one acid site. As expected, the number of acid sites increases due to an increase in the number of intragallery acid sites with increasing aluminum loading (Table 3.1).

Therefore we can conclude that our new materials have acidity and the issue is what can be done with it. One of the reactions used to test the reactivity of mesoporous materials is the one that Corma reported few years ago²² where the 2,4-di-tert-butylphenol phenol reacts with cynamil alcohol to form the flavan molecule (Figure 3.2). This is mainly used as a probe reaction because in order to obtain a significant yield of falvan we need to have a very rapid access to the active sites of the catalyst. These two reagents must be brought close together at a reactive site to form the activated complex; otherwise each reactant may undergo undesirable transformations such as dealkylation or intermolecular dehydration to ether.

Mesostructures are very suitable catalysts for this reaction as compared with the traditional catalysts such as HY zeolites or K-10 layered silicate. As shown in Table 3.2, in agreement with an earlier result reported by Corma and his co-workers, the yields of flavan for HY, K-10 and protonated saponite are almost not existent whereas for Al-MCM41 or Al-HMS mesostructures a significant amount of the product is obtained. This means that the diffusion of DBP through the windows of faujastites of HY is strongly restricted. Similarly, in the cases of K-10 Montmorillonite and H⁺-saponite, the main product is dealkylated 4-tert butylphenol. Consequently besides the difficulty of the diffusion of DBP through the interclays, the accessibility of reactants and the

shape selectivity are big problems. This proves that HY, K-10 and protonated saponite lack the needed framework porosity and are incapable of shape selectivity catalysts. By contrast, in the case of PCH, based on their pore size and structure, a higher yield of flavan, 15.3%, was obtained. The limitation of the diffusions of the bulk reactant and product (flavan) were in some way overcome by the PCH structure. Obviously, the formation of mesoporosity in PCH does appreciably alter the accessibility of reactants and this increases its ability of shape selectivity to catalyze the alkylation reaction. For that reason the yields of flavan are correlated with the concept of access. We did not expect PCH's to be competitive with the HMS or MCM-41 materials but they are significantly better than the traditional acid catalysts.

We believe that these types of materials will really make a difference in cracking of hydrocarbons. Catalytic hydrocarbon cracking is an important step in the conversion of crude oil to transportation fuels. Industrial cracking catalysts contain a significant component of zeolite (such as H-USY), which provides Bronsted acid sites for the cracking of hydrocarbons. It is well know that the strength and the amount of Bronsted acid sites in the cracking catalysts are crucial to enhance the cracking activity.

Cumene cracking is generally considered as a probe reaction to investigate the Bronsted acidity of the zeolite and related aluminosilicate materials. Our materials proved to own a significant number of acidic sites. As a result, they were employed as solid acid catalysts for the cumene cracking reaction. The initial results of the cumene cracking are summarized in Table 3.3.

Table 3.2. Alkylation of 2,4-di-tert-butylphenol with cinnamyl alcohol in the presence of various solid acid catalysts.*

Catalysts	Conversion	Selec	Yield of	
	(%)	4-tert- butylphenol	Flavan	Flavan (%)
HY	13.3	57.8	11.1	1.5
K-10	47.6	59.7	-	<1
H⁺-Saponite	36.1	87.7	3.3	1.2
SAP1.2-PCH	28.9	51.0	29.0	8.38
SAP1.5-PCH	26.5	43.7	35.8	9.48
SAP1.7-PCH	36.6	32.1	41.9	15.3
2% Al-MCM-41	47.2	-	71.8	33.9
2% AI-HMS	56.5	-	74.2	41.4

^{*}Reaction conditions: 125 mg catalyst, 0.25 mmol 2,4-di-tert-butylphenol, 0.25 mmol cinnamyl alcohol, 12.5 mL isooctane, 60°C, 6 hours.

^{*}The total selectivity is less than 100% because part of the products is adsorbed on the catalysts. TGA profiles of the catalysts after reaction established ~15% weight loss of non-recoverable organic material.

Table 3.3. Cumene cracking activity of different mesoporous materials.*

Catalysts	Conversion (%)
H ⁺ -Saponite	20.2
SAP1.7-PCH	36.2
5% AI-HMS	48.9
5% AI-MCM-41	34.5

^{*}Reaction temperature 300°C, 200 mg catalyst. The cumene flow rate is 4.1 µmol/min.

We see that even standard acid saponite with no mesoporosity is active by virtue of the external surface area. The porous clay heterostructure textural properties significantly enhance the activity approaching the activity of the acidic mesostructures. These results suggest that our mesostructured saponite derivatives are suitable catalysts for the processing of petroleum fractions.

3.5 Conclusion

A novel porous intercalate belonging to the class of mesostructured solid acids known as porous clay heterostuctures (PCH) has been synthesized through the surfactant-directed assembly of silica in the two-dimensional galleries of saponite. The SAP-PCH materials possess basal spacings from 32.9 to 35.3 Å, surface areas in the range of 800 – 920 m² g⁻¹, and pore volumes from 0.38 to 0.46 cm³ g⁻¹. They also exhibit substantially higher acidity (0.64 - 0.77 mmol g⁻¹) than pillared clays (~0.24 mmol g⁻¹).³⁻⁵ This feature of their chemistry, together with their unique pore structure in the supermicropore to small mesopore range and thermal stability to at least 750 °C should make them promising acid catalysts for organic chemical conversions, including gas oil cracking.

The new saponite derivatives were successfully employed as solid acid catalysts in the Friedel-Crafts alkylation of bulky 2, 4-di-tert-butylphenol (DBP) (molecular size (Å): 9.5×6.1×4.4) with cinnamyl alcohol to produce 6,8-di-tert-butyl-2, 3-dihydro[4H] benzopyran (flavan) (molecular size (Å): 13.5×7.9× 4.9). A higher yield of flavan (15.3%) was obtained over PCH as compared with H⁺-Saponite (1.2%). This reaction also confirmed the formation of mesoporosity in

the saponite galleries. Additionally, in order to test the acidity, our compounds were effectively utilized as catalysts for cumene cracking reaction. Their catalytic activity is considerably superior to that of the protonated saponite, and comparable to that of the acidic mesostructures.

3.6 References

- (1) Behrens, P. Advanced Materials 1993, 5, 127-132.
- (2) Davis, M. E. *Nature* **1993**, *364*, 391.
- (3) Figueras, F. Catalysis Reviews-Science and Engineering 1988, 30, 457-499.
- (4) Izumi, Y.; Urabe, K.; Onaka, M. Zeolite, Clay, and Heteropoly Acid in Organic Reactions; VCH, 1992.
- (5) Butruille, J. R.; Pinnavaia, T. J. Catalysis Today 1992, 14, 141-154.
- (6) Butruille, J. R.; Michot, L. J.; Barres, O.; Pinnavaia, T. J. *J. Catal.* **1993**, *139*, 664-678.
- (7) Beck, J. S.; Vartuli, J. C.; Roth, W. J.; Leonowicz, M. E.; Kresge, C. T.; Schmitt, K. D.; Chu, C. T. W.; Olson, D. H.; Sheppard, E. W.; McCullen, S. B.; Higgins, J. B.; Schlenker, J. L. *J. Am. Chem. Soc.* **1992**, *114*, 10834-10843.
- (8) Kresge, C. T.; Leonowicz, M. E.; Roth, W. J.; Vartuli, J. C.; Beck, J. S. *Nature* **1992**, *359*, 710-712.
- (9) Tanev, P. T.; Chibwe, M.; Pinnavaia, T. J. *Nature (London)* **1994**, *368*, 321-323.
- (10) Reddy, K. M.; Moudrakovski, I.; Sayari, A. *Journal of the Chemical Society-Chemical Communications* **1994**, 1059-1060.
- (11) Corma, A.; Navarro, M. T.; Pariente, J. P. *Journal of the Chemical Society-Chemical Communications* **1994**. 147-148.
- (12) Bein, T. ACS Symposium Series 1992, 499, 1-7.

- (13) Huo, Q. S.; Margolese, D. I.; Ciesla, U.; Demuth, D. G.; Feng, P. Y.; Gier,
 T. E.; Sieger, P.; Firouzi, A.; Chmelka, B. F.; Schuth, F.; Stucky, G. D. Chem.
 Mat. 1994, 6, 1176-1191.
- (14) Huo, Q. S.; Margolese, D. I.; Ciesla, U.; Feng, P. Y.; Gier, T. E.; Sieger,P.; Leon, R.; Petroff, P. M.; Schuth, F.; Stucky, G. D. *Nature* 1994, 368, 317-321.
- (15) Galarneau, A.; Barodawalla, A.; Pinnavaia, T. J. *Nature* **1995**, *374*, 529-531.
- (16) Galarneau, A.; Barodawalla, A.; Pinnavaia, T. J. Clays Our Future, Proc. Int. Clay Conf., 11th 1997, 21-29.
- (17) Galarneau, A.; Barodawalla, A.; Pinnavaia, T. J. *Chem. Commun.* (Cambridge) 1997, 1661-1662.
- (18) Butruille, J.-R.; Pinnavaia, T. J. Clays Controlling Environ., Proc. Int. Clay Conf., 10th 1995, 92-101.
- (19) Booij, E.; Kloprogge, T.; Van Veen, J. A. R. *Clays Clay Miner.* **1996**, *44*, 774-782.
- (20) Casal, B.; Merino, J.; Ruiz-Hitzky, E.; Gutierrez, E.; Alvarez, A. *Clay Miner.* **1997**, *32*, 41-54.
- (21) Raimondo, M.; De Stefanis, A.; Perez, G.; Tomlinson, A. A. G. *Appl. Catal. A-Gen.* **1998**, *171*, 85-97.
- (22) Armengol, E.; Cano, M. L.; Corma, A.; Garcia, H.; Navarro, M. T. *J. Chem. Soc., Chem. Commun.* **1995**, 519-520.
- (23) Sing, K. S. W.; Everet, D. H.; Haul, R. A. W.; Moscou, L.; Pierotti, R. A.; Rouquerol, J.; Siemieniewska, T. *Pure Applied Chemistry* **1985**, *57*, 603.

- (24) Lagaly, G. Solid State Ion. 1986, 22, 43-51.
- (25) Horwath, G.; Kawazoe, K. J. *Journal of Chemical Engineering of Japan* **1983**, *16*, 470.
- (26) Gregg, S. J.; Sing, K. S. W. Adsorption, Surface Area and Porosity. 2nd Ed London, 1982.
- (27) Breen, C. Clay Minerals 1991, 26, 473-486.
- (28) Breen, C. Clay Minerals 1991, 26, 487-496.

Chapter 4

Post-Synthesis Grafting of Aluminum into Porous Clay Heterostructures (PCH) Derived from a Synthetic Saponite

4.1 Abstract

Mesostructured intercalates belonging to the new class of solid acids known as porous clay heterostructures (PCH) have been prepared by post-synthesis grafting of aluminum into a silica-intercalated PCH precursor derived from a synthetic saponite. The products designated AI-PCH, were characterized by powder XRD, N₂ adsorption, ²⁷AI MAS NMR, TPD of cyclohexylamine and elemental analysis. Depending on the choice of aluminating agent (AICI₃ or NaAIO₂), intercalates with basal spacings of 32 - 34.8 Å, BET surface areas of 623 - 906 m²/g, pore volumes of 0.32 - 0.45 cm³/g and pore size in the large

micropore to small mesopores range were obtained. The aluminum content was strongly correlated with the reactant composition in the post-synthesis mixture. Nearly all of the grafted aluminum was incorporated into the mesostructured silica in a tetrahedral form. In comparison to the initial silica-intercalated PCH precursor, little or no change in textural porosity was observed when the alumination reaction was carried out under acidic conditions using aqueous AlCl₃ (route 1), whereas small decrease in surface area and pore volume were noted under basic conditions with NaAlO₂ as the aluminating agent (route 2). Both reagents however, afforded acid sites that increased with increasing Al content. The enhanced acidity, structural stability up to 750 °C and the porosity of the Al-PCH materials were verified by using these aluminated derivatives as solid acid catalysts for the cumene cracking reaction.

4.2 Introduction

During the last decade various kinds of mesoporous silica materials¹⁻⁵ have been synthesized using surfactant micelles as the structure directing agents. Heteroatom substituted mesoporous molecular sieves such as MCM-41 have attracted much interest due to their potential use as adsorbents or catalysts.^{6,7} Of particular interest are the aluminum containing compounds that may be employed as solid acid catalysts. Purely siliceous molecular sieve materials have an electrically neutral framework and consequently little or no acidity. Bronsted acid sites can be generated by isomorphous substitution of aluminum for silicon in the silica matrix. Previous studies⁸⁻¹¹ have shown that aluminum can be effectively incorporated into siliceous MCM-41 materials via various post-synthesis procedures by grafting Al onto MCM-41 walls using different aluminum sources, followed by calcination. Post-synthesis alumination increases both acidity and chemical stability of the alumina modified MCM-41 materials.^{12,13}

Recently, the discovery of porous clay heterostructures (PCH) formed by gallery assembly of mesoporous silica in various clays has been reported.¹⁴ PCH synthesis makes use of the micellar ordering of silicate species and surfactants in the restricted two-dimensional gallery region of the clay. PCH also combines the mesoporous structure of the gallery with the chemistry of the clay layer. Modifying the chemical composition of the layered host can control intrinsic acidity of these materials.¹⁵ Moreover the PCH's acidic character¹⁶⁻¹⁸ can

be enhanced by a post-synthesis treatment in a manner quite analogous to the alumination of MCM-41.

Here we report the incorporation of aluminum into the mesoporous structure of the clay gallery of a PCH material derived from synthetic saponite via two different post-synthesis procedures. We show that during the alumination process, the structural integrity of the original PCH is preserved and the acidity of the resultant mesoporous clay denoted Al-PCH is significantly enhanced.

The aluminum grafted porous clay heterostructures, denoted AI-PCH exhibit considerable catalytic activity for cumene cracking reaction and are notably superior to that of parent PCH and aluminated mesostructures (AI-HMS, AI-MCM-41).

4.3 Experimental

4.3.1 Al-PCH Synthesis

A saponite PCH was prepared according to the previously described procedure (Chapter 3). Synthetic saponite with the anhydrous unit cell formula Na_{1.2}[Mg₆](Si_{6.8}Al_{1.2})O₂₀(OH)₄ was hydrothermally synthesized at 175 °C and converted to quaternary ammonium form by ion exchange reacting with cetyltrimethylammonium chloride. Mixtures of organoclay, neutral amine cosurfactant and TEOS at molar ratios 1:20:150 were allowed to react for 4 hours at room temperature. The product was recovered by centrifugation, dried under controlled humidity and subsequently calcined at 650 °C using a temperature

ramp rate of 1 degree/min. The obtained silica-intercalated SAP-PCH with anhydrous unit cell formula (SiO₂)_{13.7}· H_{1.2}[Mg₆](Si_{6.8}Al_{1.2})O₂₀(OH)₄ was used to produce aluminated PCH derivatives via two synthetic routes.

In the first route PCH (0.5 g) was combined with 50 mL aqueous AlCl₃ solution to give gallery Si/Al ratios 10 and 20. After a reaction time of 12 hours at 55 °C, the solid products were filtered, washed with water, dried at room temperature and calcined at 600 °C for 4 hours.

In the second route 0.5 g of PCH in 50 mL water was allowed to react with NaAlO₂ at room temperature for 3 hours at gallery Si/Al ratio 5 and 10. The solid powder was recovered by filtration and washed thoroughly with water. Prior to calcination at 600 °C for 4 hours the sodium ions in the aluminated product were exchanged for ammonium ions by stirring the aluminated solids in a 1 M NH₄NO₃ solution.

The products are designated as Al-PCH1 or 2-X, where 1 or 2 are the corresponding routes and X is the gallery Si/Al ratio used in the reaction mixtures.

4.3.2 Cumene Cracking Reaction

Cumene cracking reactions were performed in a 6 mm i.d. fixed bed quartz reactor containing 200 mg catalysts. The cumene flow rate was 4.1 μmol min⁻¹ in a 20 mL min⁻¹ carrier gas of N₂. Cumene conversions were reported under steady-state conditions after 30 min. on steam at 300 °C.

4.3.3 Physical Measurements

Powder X-ray diffraction patterns were obtained on a Rigaku Rotaflex diffractometer equipped with a rotating anode (CuK_{α} radiation) operated at 45 kV and 100 mA. The scattering and receiving slits were 1/6 and 0.3 degrees, respectively.

N₂ adsorption-desorption isotherms were obtained at -196 °C on a Micromeritics ASAP 2010 Sorptometer using static adsorption procedures. Samples were outgassed at 175 °C and 10⁻⁶ Torr for a minimum of 12 h prior to analysis. BET surface areas were calculated from the linear part of the BET plot according to IUPAC recommendations.¹⁹ The pore size distributions were calculated by BJH method using the adsorption branch of the N₂ isotherm.

²⁷Al MAS (magic angle spinning) NMR spectra were obtained on a Varian VXR 400 MHz spectrometer at 104.26 MHz using a 7 mm zirconia rotor and a sample spinning frequency of 4 kHz. A pulse duration of 9 μs and a delay time of 1 sec. allowed for a full relaxation of the Al nucleus. External Al(H₂O)₆³⁺ was used as a reference to determine the chemical shift values.

Temperature programmed cyclohexylamine desorption (CHA-TPD) profiles were recorded on a Cahn TG system 121 analyzer. Calcined samples (~30 mg) were transferred directly out of the cyclohexylamine vapor to the thermobalance and were kept at 150 °C for 2 hours to remove physisorbed CHA. Desorption thermograms were recorded at a heating rate of 10 °C /min under a nitrogen flow. The mass loss between 300 °C and 450 °C was used to determine the acid content of the samples (in mmoles CHA/q adsorbent).

Elemental analyses were provided by inductively coupled plasma emission spectroscopy at the University of Illinois Elemental Analysis Laboratory.

4.4 Results and Discussion

All of the Al-PCH derivatives obtained by AlCl₃ and NaAlO₂ grafting gave the same XRD patterns equivalent to parent PCH, as shown in Figure 4.1. There were no significant changes in the XRD peak intensities and line widths, and no additional peaks appeared beyond the 2Θ region shown in Figure 4.1, indicating that the grafted aluminum centers are well dispersed. The basal spacings of the Al-PCH materials (Table 4.1) were larger that the spacing observed for the starting PCH and generally increased with the amount of incorporated aluminum. This is consistent with the incorporation of increasing amounts of tetrahedral aluminum into the gallery mesostructure.

The textural parameters for the parent PCH and its Al derivatives are given in Table 4.1. Figure 4.2 provides representative N_2 isotherm and BJH pore size distribution for Al-PCH1-10 and Al-PCH2-10. All the Al-PCH derivatives exhibited a type IV isotherm typical for mesoporous materials. They display a linear region in the partial pressure range 0.05 - 0.25 indicating the presence of small mesopores or supermicropores (14 - 25 Å).

The textural information derived from the nitrogen isotherms is in good agreement with the XRD patterns and confirms the retention of the structural integrity of the PCH after aluminum grafting. Alumination by grafting with AlCl₃ (route 1) does not affect the original pore structure of the parent PCH (Al-PCH1-

20 and Al-PCH1-10). When sodium aluminate is used as aluminum source (route 2) a slight decrease in the surface area and pore volume is observed as the aluminum loading increases from a gallery Si/Al ratio of 10 to 5. The basic NaAlO₂ solution may promote the cleavage of Si – O bond, resulting in a partial collapse of the interlayer mesostructure. Part of the observed decrease in surface area and pore volume is related to the added weight of the materials due to aluminum incorporation.¹¹ However, the BET surface area (623 m²/g) and pore volume (0.32 cm³/g) obtained for the sample with the highest aluminum loading (Al-PCH2-5) are still within the range usually obtained for PCH materials.¹⁴

In order to elucidate the nature of the incorporated aluminum, ²⁷Al MAS NMR spectra were obtained for the calcined aluminum PCH derivatives. As shown in Figure 4.3 and 4.4, each aluminum derivative exhibits two resolved lines at 65 and 53 ppm. The 65 ppm resonance is assigned to tetrahedral aluminum in the 2:1 layer of the synthetic saponite, where the metal is covalently bonded to three Si atoms and one Mg atom via oxygen bridges. ²¹ The line at 53 ppm can be assigned to tetrahedral aluminum grafted onto the gallery silica. ²² The absence of a signal around 0 ppm for octahedral aluminum indicates that nearly all the aluminum has been incorporated into the siliceous framework. The ²⁷Al MAS NMR spectra in Figure 4.3 for Al-PCH1-10 and Al-PCH1-20 synthesized by reacting PCH with AlCl₃ in water (route 1) show that the aluminum content in the PCH increases with the aluminum content of the

Table 4.1. Properties of the PCH intercalate and Al-PCH derivatives.

Sample	Si/Alª	Basal spacing ^b (Å)	BET Surface Area ^b (m²/g)	Pore Volume ^b (cm³/g)	Acidity (mmoles CHA/g)
AI-PCH1-20	24.1	32.0	906	0.45	1.230
AI-PCH1-10	15.4	33.7	834	0.43	1.450
Al-PCH2-10	12.7	34.5	786	0.40	1.510
AI-PCH2-5	8.5	34.8	623	0.32	1.820
PCH	-	31.3	860	0.45	0.630

^aThe galley Si/Al ratios found by elemental analysis.

^bThe basal spacings, surface areas and pore volumes are for the calcined forms of the Al-PCH derivatives.

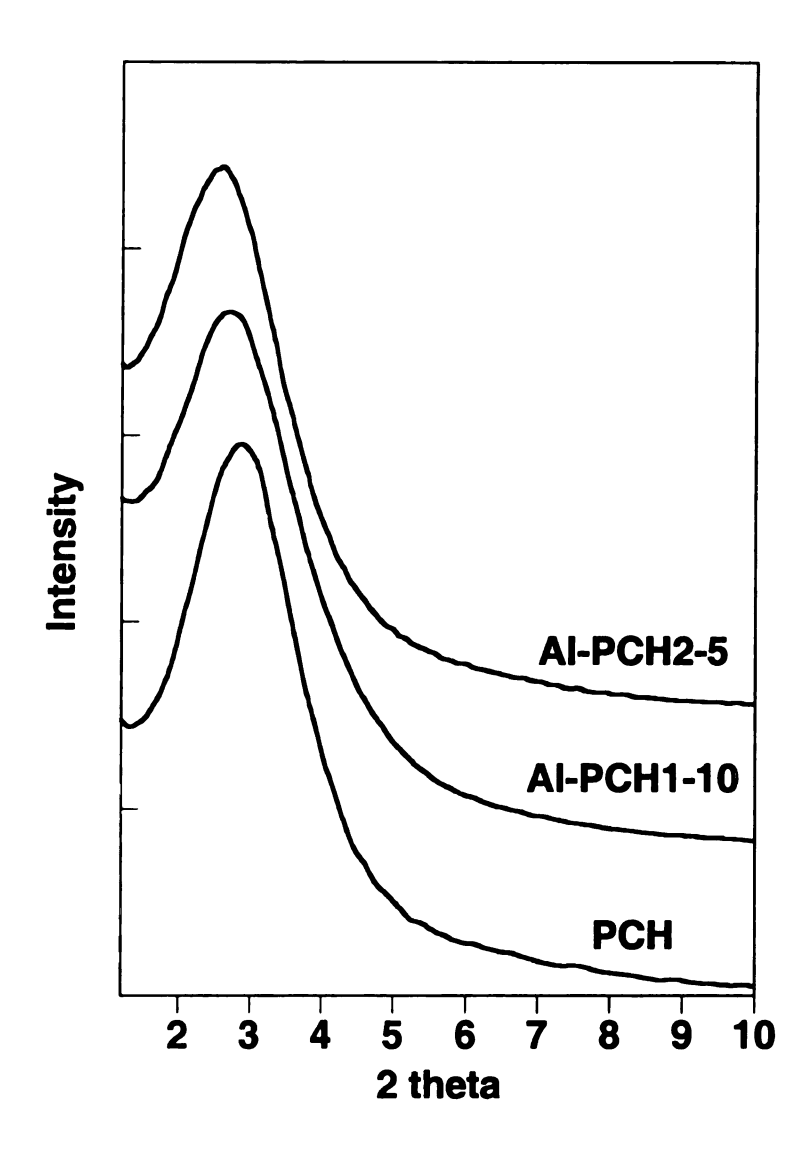


Figure 4.1: XRD patterns for calcined PCH and the calcined Al-SAP-PCH derivatives.

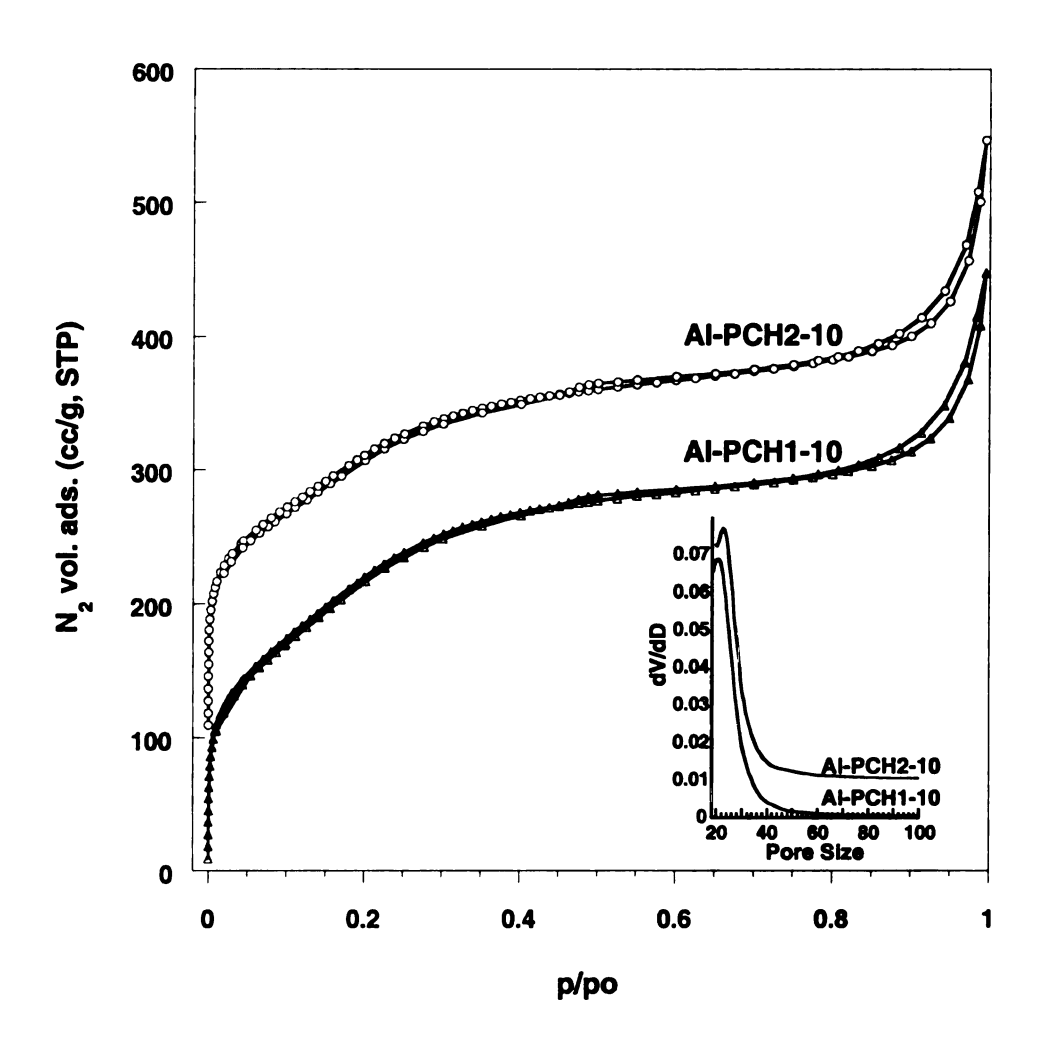


Figure 4.2: Nitrogen adsorption/desorption isotherms for Al-PCH intercalates formed by using NaAlO₂ and AlCl₃ as aluminating agents. The isotherms are offset by 100 cc/g for clarity. Inset shows the BJH pore size distribution.

reactant mixture, which suggests that the aluminum incorporation can be controlled by the reaction stoichiometry. However, a further increase in AlCl₃ concentration at Si/Al ratios below 10 resulted in the appearance of the undesired octahedral resonance at 0 ppm.

On the other hand, as shown by the ²⁷Al NMR spectrum for Al-PCH2-5 in Figure 4.4 the loading of tetrahedral aluminum could be increased by using NaAlO₂ in the grafting reaction without forming octahedral aluminum. Essentially all the aluminum incorporated into the Al-PCH2-5 sample is in a tetrahedral coordination. The strongly basic NaAlO₂ solution facilitates the insertion of the aluminum in the gallery silica matrix. In comparison with the spectrum for the Al-PCH1 samples the line at 53 ppm is much more intense. This indicates that a higher percentage of aluminum is incorporated into Al-PCH via route 2. However, grafting reactions carried out at higher concentrations of NaAlO2 result in a loss of greater than 50 % of the surface area. For both alumination procedures we observe an excellent correlation between the NMR peak intensities and the amount of the incorporated aluminum found by elemental analysis (Table 4.1). Taken together these observations indicate that both procedures are effective methods for aluminum grafting (no extra framework aluminum present) onto sites on the clay gallery mesostructure. Such aluminum sites generate acid centers that are accessible and therefore very useful for catalysis.

The acidities of the Al-PCH derivatives and the initial PCH materials, as determined using temperature programmed desorption of chemisorbed

cyclohexylamine, 23 are given in Table 4.1. The samples were exposed to CHA vapors and then heated at 150 °C for 2 hours to remove the physically adsorbed The weight loss between 200 °C and 450 °C was used to quantify the amine. acidity, assuming that each base molecule interacts with one acid site. As shown in Figure 4.5, the TPD profiles for Al-PCH1-10, Al-PCH2-5 and the starting PCH materials exhibit two types of acidic sites. The intensity of the first desorption peak at 230 °C is correlated with the clay layer acidity. 15 The stronger acid site represented by the desorption peak at 380 °C is directly related to the grafted aluminum centers onto the mesostructured silica. It is evident that the incorporation of aluminum in the mesostructured gallery silica generates significant Bronsted acidity. The relative peak intensities are in close agreement with the amount of incorporated aluminum, revealing the superiority of NaAlO2 as alumination agent. It is clear from the acidity values provided in Table 4.1 that the aluminum grafting process creates acid sites and the number of acid sites increases as the amount of incorporated aluminum increases. The enhanced acidity is correlated with the increase in the aluminum content and is compatible with our interpretation of the NMR data.

Previous studies²⁴ indicated that samples with high AI content prepared using NaAIO₂ present practically no Bronsted acidity due to the presence of Na⁺ ions. This problem can be addressed by exchanging the sodium ions after alumination, first with ammonium ions and then ultimately with protons upon calcination.

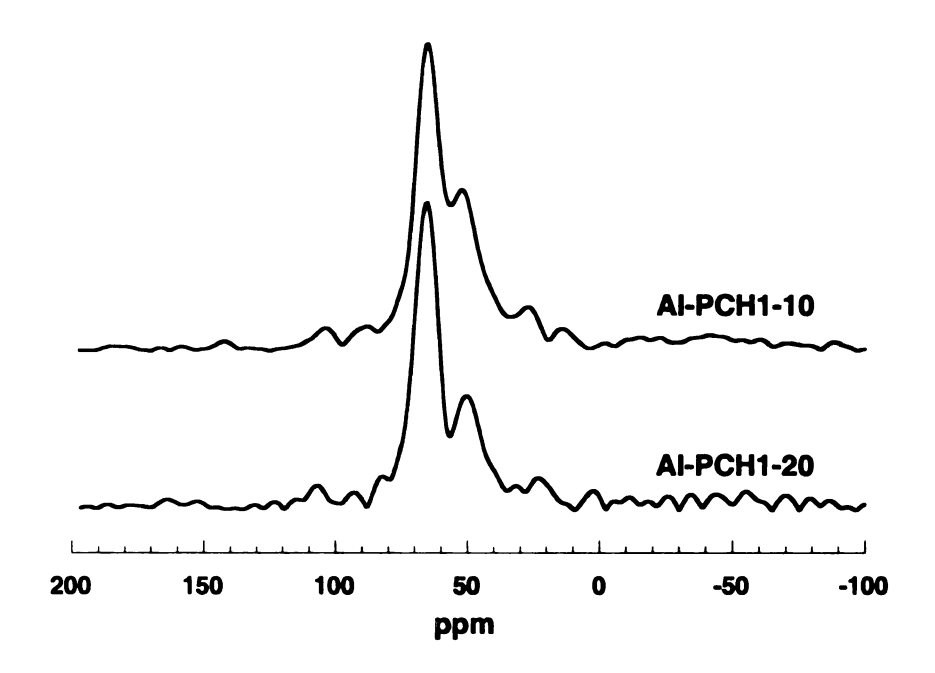


Figure 4.3: ²⁷Al MAS NMR spectra for the calcined Al-PCH1-20 and Al-PCH1-10 samples, prepared by post-synthesis grafting with AlCl₃.

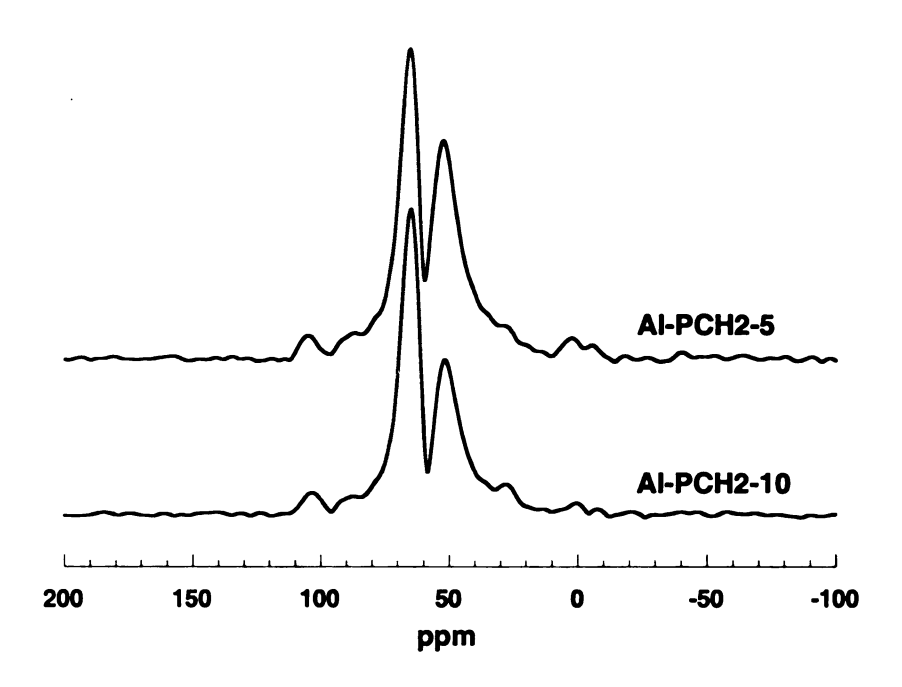


Figure 4.4: ²⁷Al MAS NMR spectra for the calcined Al-PCH2-10 and Al-PCH2-5 samples, prepared by post-synthesis grafting with NaAlO₂.

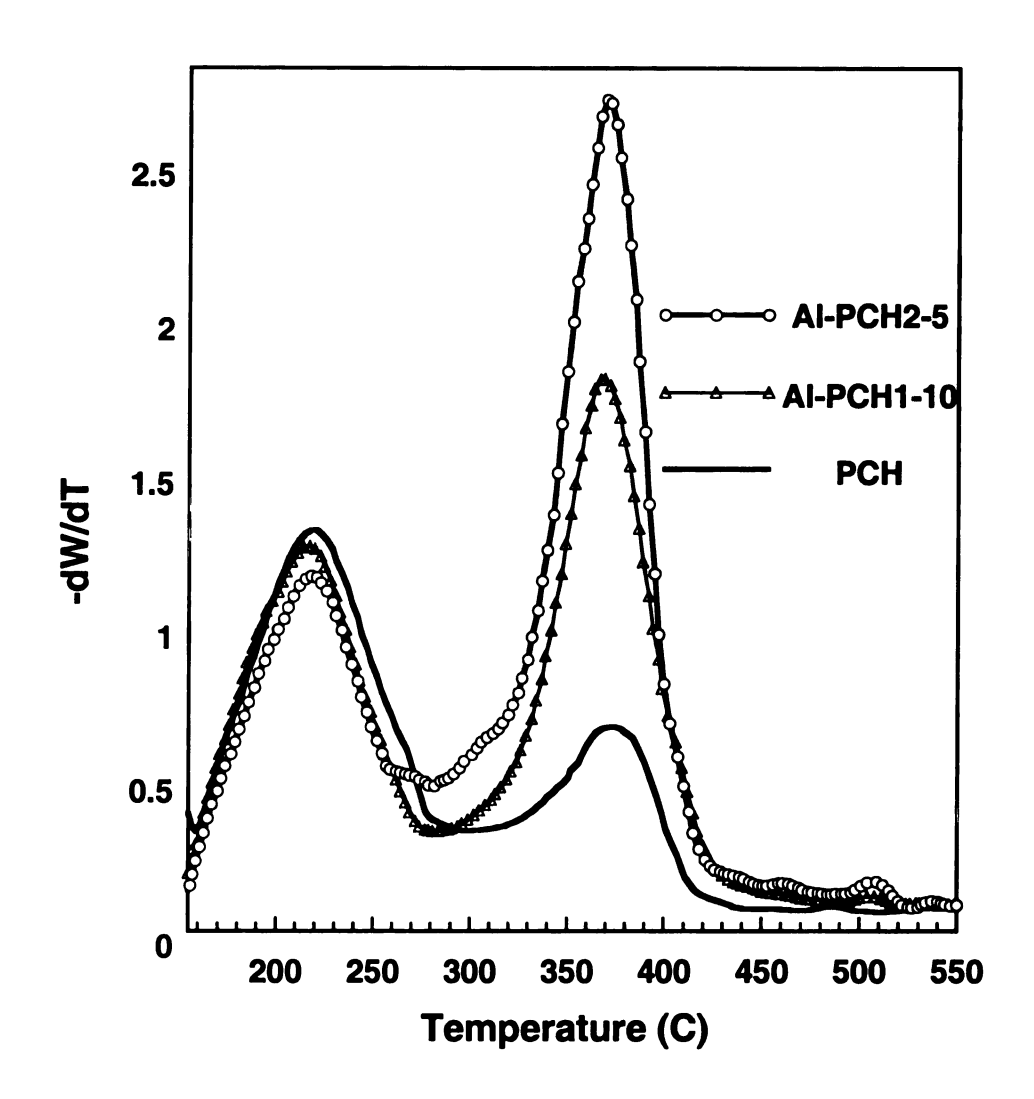


Figure 4.5: TPD Profiles for the desorption of cyclohexylamine from the parent PCH and Al-PCH derivatives.

In the present work we compared the cumene cracking activity of our AI-PCH compounds with those for acidic derivatives of hexagonal AI-MCM-41 and wormhole AI-HMS molecular sieves containing 5% aluminum (Si/AI = 19). At this aluminum loading all the aluminum centers in the mesoporous molecular sieves are in tetrahedral sites. The conversion of cumene requires medium to strong acid sites. Catalytic cracking to benzene and propene was the main reaction with only trace amounts of other products being formed, indicating that the active sites are Bronsted acid sites. The catalytic data provided in Table 4.2 show that the AI-PCH materials substantially outperform the aluminated MCM-41 and HMS mesostructures as well as the protonated form of saponite and non-aluminated saponite PCH. It should be also noted that as expected, the increase in activity is in line with the change in acid content and aluminum loading of the AI-PCH.

Table 4.2. Cumene cracking activity of Al-PCH's, parent SAP-PCH and aluminated mesostructures*.

Catalyst	Aluminating Agent	Conversion (%)	
H ⁺ -Saponite	-	20.2	
PCH	-	36.2	
Al-PCH1-10	AICI ₃	55.2	
Al-PCH2-10	NaAlO ₂	58.8	
AI-PCH2-5	NaAlO ₂	66.7	
5% AI-HMS	NaAlO ₂	48.9	
5% AI-MCM-41	NaAlO ₂	34.5	

^{*}Reaction temperature 300 °C, 200 mg catalyst. The cumene flow rate is 4.1 μ mol/min.

4.5 Conclusion

A porous clay heterostructure derived from synthetic saponite has been synthesized and subsequently functionalized with aluminum to produce aluminated PCH via two post-synthesis procedures using AlCl₃ and NaAlO₂ as aluminating agents. The resulting materials (herein designated Al-PCH) retain almost all the supermicroporous to small mesoporous integrity of the parent PCH and possess significantly enhanced acidity. The amount of aluminum incorporated into the saponite gallery structure depends on the concentration of aluminum in the grafting solution. ²⁷Al MAS NMR confirms that all aluminum is inserted into tetrahedral position within the gallery silica framework. The incorporation of aluminum has either no effect on the texture properties of the original PCH or results in a small decrease in surface area and pore volume. The aluminum grafting generates Bronsted acid sites that increase in number as the Si/Al ratio decreases. The acidity of the new Al-PCH materials is significantly greater than that of the parent material and can be tuned by controlling the stoichiometry in the initial reaction mixture.

The Al-PCH materials demonstrate high catalytic activity for cumene cracking reaction, being superior to that of the parent PCH, protonated saponite and representative mesoporous molecular sieves with hexagonal and wormhole framework structures. Their enhanced acidity combined with a stable, well-ordered supermicropore to small mesopores structure opens up new opportunities for application in acid catalysis.

4.6 References

- (1) Sayari, A. Chem. Mat. 1996, 8, 1840-1852.
- (2) Ryoo, R.; Kim, J. M.; Ko, C. H.; Shin, C. H. *Journal of Physical Chemistry* **1996**, *100*, 17718-17721.
- (3) Kresge, C. T.; Leonowicz, M. E.; Roth, W. J.; Vartuli, J. C.; Beck, J. S. *Nature* **1992**, *359*, 710-712.
- (4) Hue, Q.; Leon, R.; Petroff, P. M.; Stucky, G. D. *Science* **1995**, *268*, 1324-1327.
- (5) Corma, A. Chemical Reviews 1997, 97, 2373-2419.
- (6) Mokaya, R.; Jones, W. J. Catal. 1997, 172, 211-221.
- (7) Corma, A.; Grande, M. S.; GonzalezAlfaro, V.; Orchilles, A. V. *J. Catal.*1996, 159, 375-382.
- (8) Hamdan, H.; Endud, S.; He, H. Y.; Muhid, M. N. M.; Klinowski, J. *Journal of the Chemical Society-Faraday Transactions* **1996**, *92*, 2311-2315.
- (9) Luan, Z. H.; Hartmann, M.; Zhao, D. Y.; Zhou, W. Z.; Kevan, L. *Chem. Mat.* **1999**, *11*, 1621-1627.
- (10) Mokaya, R.; Jones, W. *Chemical Communications* **1997**, 2185-2186.
- (11) Ryoo, R.; Jun, S.; Kim, J. M.; Kim, M. J. *Chemical Communications* **1997**, 2225-2226.
- (12) Mokaya, R. Angewandte Chemie-International Edition 1999, 38, 2930-2934.
- (13) Shen, S. C.; Kawi, S. *Chemistry Letters* **1999**, 1293-1294.

- (14) Galarneau, A.; Barodawalla, A.; Pinnavaia, T. J. *Nature* **1995**, *374*, 529-531.
- (15) Polverejan, M.; Pauly, T. R.; Pinnavaia, T. J. *Chem. Mat.* **2000**, *12*, 2698-2704.
- (16) Polverejan, M.; Liu, Y.; Pinnavaia, T. J. *Stud. Surf. Sci. Catal.* **2000**, *129*, 401-408.
- (17) Galarneau, A.; Barodawalla, A.; Pinnavaia, T. J. Clays Our Future, Proc. Int. Clay Conf., 11th 1997, 21-29.
- (18) Galarneau, A.; Barodawalla, A.; Pinnavaia, T. J. Chem. Commun. (Cambridge) 1997, 1661-1662.
- (19) Sing, K. S. W.; Everet, D. H.; Haul, R. A. W.; Moscou, L.; Pierotti, R. A.; Rouquerol, J.; Siemieniewska, T. *Pure Applied Chemistry* **1985**, *57*, 603.
- (20) Gregg, S. J.; Sing, K. S. W. Adsorption, Surface Area and Porosity. 2nd Ed London, 1982.
- (21) Woessner, D. E. Am. Mineral. 1989, 74, 203-215.
- (22) Stocker, M. Microporous and Mesoporous Materials 1998, 22, 533-535.
- (23) Breen, C. Clay Minerals 1991, 26, 487-496.
- (24) Mokaya, R.; Jones, W. J. Mater. Chem. 1999, 9, 555-561.
- (25) Mokaya, R.; Jones, W. Chem. Commun. (Cambridge) 1998, 1839-1840.
- (26) Ward, J. W. J. Catal. 1967, 9, 225-236.

Chapter 5

Covalent Grafting of Titanium on the Hydroxyl Groups Lining the Pore Walls of SAP-PCH

5.1 Abstract

This chapter describes the introduction of titanium centers onto the silica framework of the porous clay heterostructure materials (SAP-PCH) derived from synthetic saponite, by a post-synthesis grafting technique. Porous clay heterostructures were prepared through the use of intercalated quaternary ammonium cations and neutral amine surfactants to direct the condensation polymerization of tetraethylorthosilicate (TEOS) in the galleries of the saponite clay. These mesostructured intercalates have been used as parent materials for titanium incorporation via a post-synthesis grafting procedure that uses titanium (IV) butoxide as the titanium source. Samples were characterized by XRD, nitrogen adsorption, UV-Vis reflectance spectroscopy and elemental analysis. X-ray powder diffraction and nitrogen adsorption show that the pore structure is preserved upon grafting despite the moderate decrease in the surface area at higher titanium loadings. UV-Vis spectroscopy indicates that the grafting method

produces minimal amounts of Ti-O-Ti bonds favoring the isolated tetrahedral titanium centers. Taken together these features make the new grafted porous clay heterostructures (denoted Ti-PCH) promising candidates for catalyzed conversions of organic molecules. They were effectively utilized as catalysts for cyclohexene oxidation, their catalytic activity being comparable to that of the titanium grafted MCM-41.

5.2 Introduction

Today's environmental concerns demand the streamlining of the catalytic processes for the production of fine chemicals. The utility of hydrogen peroxide as an oxidant is a significant step in this direction due to the fact that its only byproduct is water. Titanium incorporation in several silicates such as silicalite-1, ZSM-12, ZSM-48 and zeolite-β are well documented and focused to be effective for the selective oxidation of alkanes, the hydroxylation of phenols and the epoxidation of alkenes using hydrogen peroxide.¹⁻⁶ These materials have been successfully employed as catalysts for the above-mentioned reactions, but their use is limited to molecules small enough to fit their pores.

The mesoporous silicas with larger channel diameters could be used to extend the catalyst capabilities to molecules with larger sizes. The discovery of titanium containing siliceous mesoporous materials MCM-41 and MCM-48, where titanium is incorporated in the framework of mesoporous silica, leads to remarkable catalytic performance utilizing both diluted hydrogen and organic peroxides. Titanium incorporation into a molecular sieve can be achieved either by direct synthesis sortium incorporation into a molecular sieve can be achieved either by direct synthesis sortium in by post-synthesis modification. The grafting method showed promising results for developing active oxidation catalysts in a simple and convenient way. It has been observed for example that the reaction of titanium isopropoxide with silica surface followed by calcination, gives highly dispersed titanium centers 15,18,19 with strong Ti-O-Si bonds. In

We recently reported the discovery of a new class of solid porous materials derived from synthetic saponite denoted porous clay heterostructures

(SAP-PCH) that showed promising acidic properties for catalytic organic conversions.^{21,22} They were prepared by surfactant directed assembly of mesostructured silica in the two-dimensional galleries of a layered aluminosilicate such as saponite.

Here we report the covalent grafting of titanium on the inner lining of the intragallery nanostructure of SAP-PCH used as parent material and titanium butoxide as a Ti source. We synthesized three Ti-PCH compositions with the initial gallery Si/Ti ratio 10, 15 and 20. The products were designated Ti-PCH10, 15 and 20 respectively. We show that the final Si/Ti ratio can be controlled from the initial reaction composition. Using this synthetic approach the structural integrity of the original SAP-PCH is preserved, generating a promising bifunctional catalyst.

5.3 Experimental

5.3.1 Ti-PCH Synthesis

A PCH with the anhydrous unit cell formula $(SiO_2)_{13.7}$ $H_{1.2}[Mg_6](Si_{6.8}Al_{1.2})O_{20}(OH)_4$ where $(SiO_2)_{13.7}$ is the mesostructured galley silica, was prepared according to the previously explained procedure (Chapter 3). Synthetic saponite was hydrothermally synthesized at 175 °C and converted to quaternaryammonium form by ion exchange. Mixtures of organoclay, neutral amine and TEOS at molar ratios 1:20:150 were allowed to react for 4 hours at room temperature. The product was recovered by

centrifugation and dried under controlled humidity. In order to prevent the loss of Si-OH groups from the gallery framework, the as-synthesized SAP-PCH was not calcined to remove the surfactants. Instead, the surfactants were removed from the structure first by treatment 0.1 M HCl to protonate the decylamine and exchange the cetyltrimethylammonium cation. Refluxing the PCH in ethanol followed the exchange reaction. The obtained powder is used as the parent material to produce Ti-PCH via grafting method.

A 1.0 g sample of surfactant-extracted SAP-PCH was refluxed in 50 mL dry toluene containing titanium (IV) butoxide for 20 hours. The ratio of gallery Si/Ti was varied in the range of 10 to 20. The product designated Ti-PCH was then filtered, thoroughly washed with toluene and ethanol, dried at room temperature and calcined in air at 600 °C for 4 hours.

5.3.2 Catalytic Oxidation of Cyclohexene with *tert*-butylhydroperoxide (TBHP)

The catalytic oxidation of cyclohexene (Figure 5.1) was carried out as bath reaction in sealed glass vials at 40 °C in a shaking bath for 6 h. The reactor was loaded with 100 mg of catalyst, 10 mmmol of cyclohexene, 11 mmol of TBHP and 10 mL of CH₂Cl₂. All reaction products were sampled by a syringe through a rubber septum. Products were analyzed by GC HP5890 with FID detector.

Figure 5.1: Reaction scheme for the condensed phase oxidation of cyclohexene with tetrabutylhydroperoxide, catalyzed by Ti-PCH.

5.3.3 Physical Measurements

Powder X-ray diffraction patterns were obtained on a Rigaku Rotaflex diffractometer equipped with a rotating anode (CuK $_{\alpha}$ radiation) operated at 45 kV and 100 mA. The scattering and receiving slits were 1/6 and 0.3 degrees, respectively.

N₂ adsorption-desorption isotherms were obtained at -196 °C on a Micromeritics ASAP 2010 Sorptometer using static adsorption procedures. Samples were outgassed at 175 °C and 10⁻⁶ Torr for a minimum of 12 h prior to analysis. BET surface areas were calculated from the linear part of the BET plot according to IUPAC recommendations.²³

Elemental analyses were carried out by inductively coupled plasma emission spectroscopy at the University of Illinois Elemental Analysis Laboratory.

UV-Vis spectroscopic measurements were carried out on a shimadzu UV-310PC UV-Vis-nearIR scanning spectrophotometer equipped with an integrating sphere. A reflection mode with a resolution of 10 Å and BaSO₄ reference was used for the measurements. The collected relative reflection intensity ($R_{-} = R_{\text{sample}}/R_{\text{reference}}$) was transformed into F(R_{-}) by using the Kubelka-Munk function F(R_{-}) = $(1-R_{-})^2/(2R_{-})$. All spectra were plotted in terms of F(R_{-}) versus wavelengths.

5.4 Results and Discussion

Generally, the incorporation of large transition metal cations into the silica lattice often results in lowered crystallinity and surface area. However, Figure 5.2 shows that all Ti-PCH derivatives obtained by the present metal-implantation routes gave the same XRD patterns as that for the parent PCH. There were no significant changes in the XRD peak intensities and line widths resulting from the titanium incorporation. No additional peaks appeared beyond the 2Θ region shown in Figure 5.2, indicating that the implanted metal is well dispersed. The dspacing of the Ti-PCH materials (Table 5.1) is higher than that of the starting PCH and generally increases with the amount of incorporated titanium. This is consistent with the incorporation of increasing amounts of tetrahedral titanium into the gallery mesostructure and is partly due to the longer Ti-O bond length compared to the Si-O bond. It should be also noted that the gallery Si/Ti ratios in the starting reaction mixture and found by elemental analysis are in a close agreement (Table 5.1).

The textural parameters of the parent PCH and its Ti derivatives are given in Table 5.1. The nature of the mesoporous structure and pore uniformity for parent PCH and the Ti derivative with the highest Ti loading are illustrated by the nitrogen sorption isotherms in Figure 5.3. All the materials show a type IV isotherm typical for mesoporous materials. They display a linear region in the partial pressure range 0.05 - 0.25 indicating the presence of small mesopores or supermicropores $(14 - 25 \text{ Å}).^{24}$ The information derived from the nitrogen isotherms is in good agreement with the XRD patterns and confirms the retention

of the structural integrity after titanium grafting. At lower Ti loadings the original pore structure is not affected. However when more titanium is incorporated a slight decrease in the surface area and pore volume is observed, indicating a limited collapse of the interlayer mesostructure. Part of the observed decrease in surface area and pore volume is related to the increased weight of the materials due to metal incorporation. However, despite this decrease the lowest BET surface area (610 m²/g) and pore volume (0.32 cm³/g) obtained for a sample with the lowest Si/Ti ratio (Ti-PCH10) are still with in the range usually obtained for PCH materials. Attempts to obtain titanium PCH derivatives with a Si/Ti ratio lower that 10 resulted in a more than 50% loss in surface area.

Table 5.1. Properties of the PCH intercalate and Ti-PCH derivatives.

Sample	Si/Ti ^a	Si/Ti ^b	dspacing (Å)	BET Surface Area (m²/g)	Pore Volume (cm³/g)
Ti-PCH-10	10	13.3	36.8	610	0.32
Ti-PCH-15	15	17.8	36.1	680	0.37
Ti-PCH-20	20	22.7	35.2	790	0.40
PCH	-	-	34.0	850	0.43

^aGallery Si/Ti ratios in the initial reaction mixture.

^bGallery Si/Ti ratios found by elemental analysis.

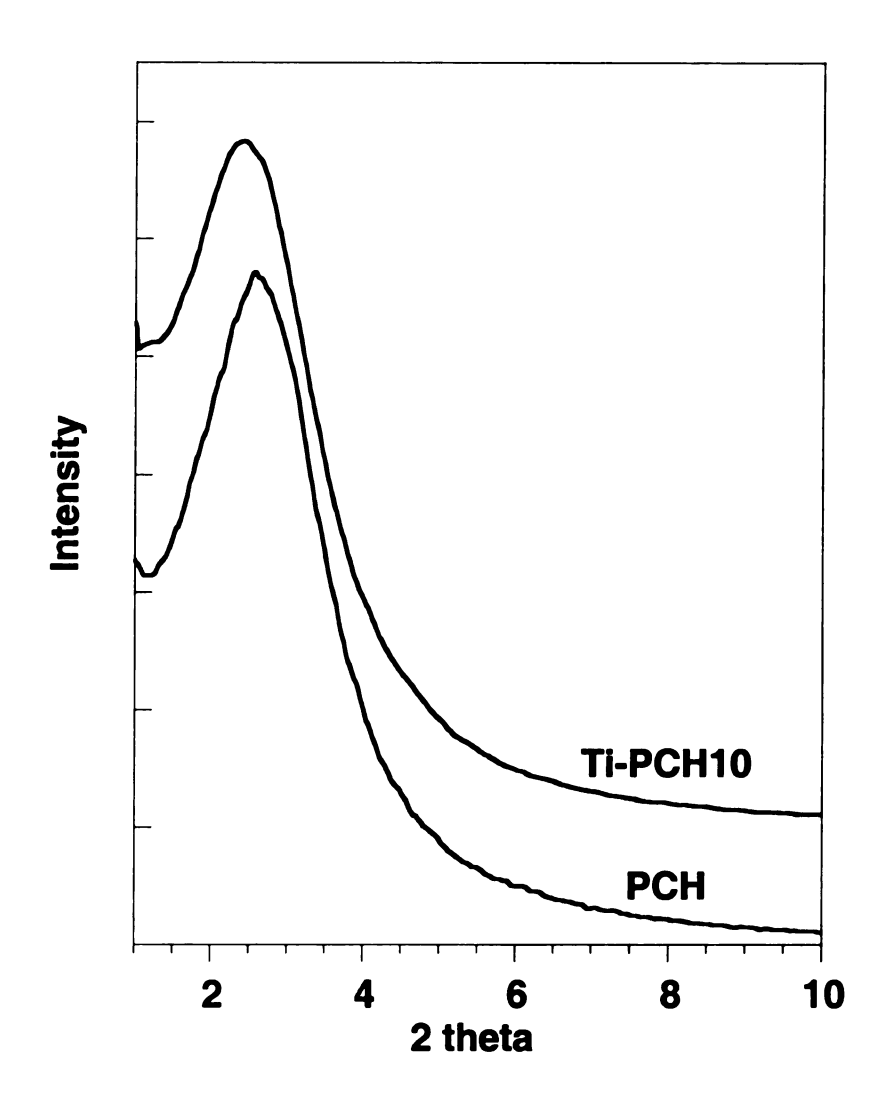


Figure 5.2: XRD patterns for the calcined PCH and Ti grafted samples.

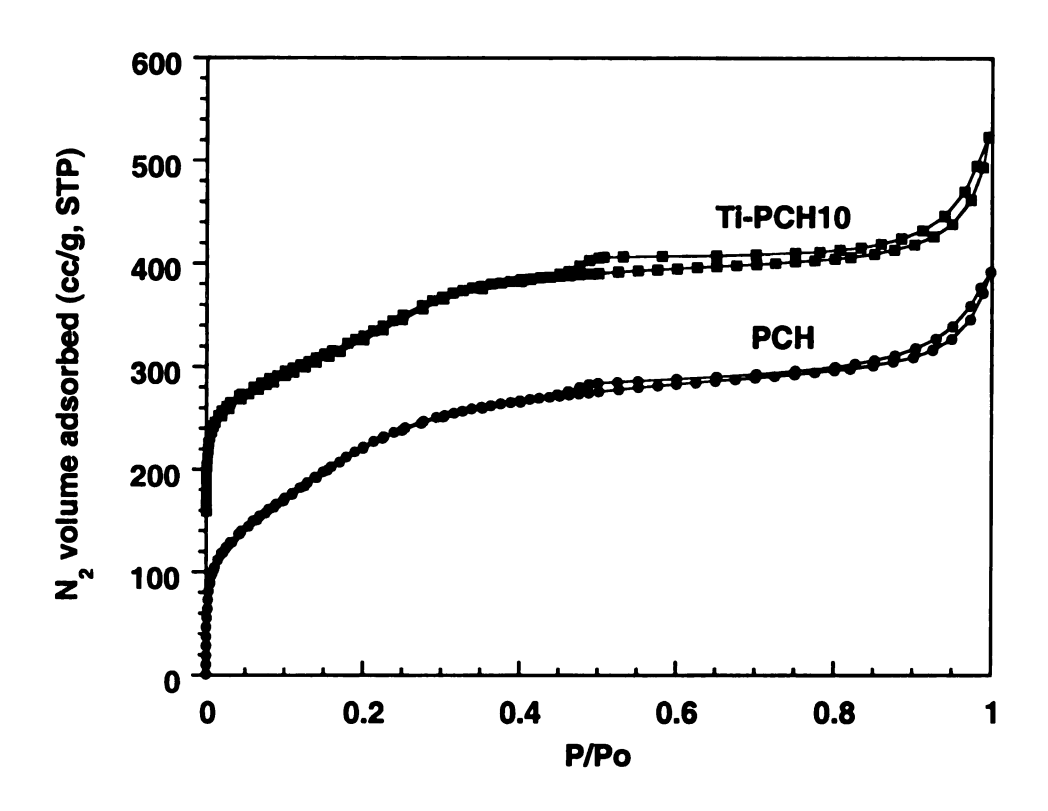


Figure 5.3: Nitrogen adsorption/desorption isotherms for the calcined parent PCH and Ti-grafted compounds.

After confirming by both XRD and nitrogen adsorption that the bulk structure is maintained upon introduction of titanium, UV-Vis spectroscopy was applied to establish the local titanium environment. The corresponding spectra of the titanium-grafted samples are shown in Figure 5.4 b-d along with those for the parent PCH and TiO₂ anatase (Figure 5.4 a and e). All three Ti-PCH materials exhibit an absorption band in the range 210 - 220 nm whereas bulk titania (anatase) shows a band at 325 nm. The bands at 210 - 220 nm are attributed to ligand-to-metal charge transfer associated with isolated Ti(IV) framework sites in tetrahedral coordination.²⁵ The broad absorption band centered at 325 nm is typical for ligand-to-metal charge transfer occurring in bulk titania. The spectra for Ti-PCH's lack the 325 nm band characteristic for segregated titania. This suggests that most of the titanium atoms in our grafted PCH materials occupy site-isolated positions in the silica framework. No absorption arises from the parent PCH, which is transparent in this region (Figure 5.4 a). We notice that the spectra for the titanium modified PCH compounds change with increasing Ti loading. At low titanium content the main resonance is at 220 nm signifying that much of the titanium is in site-isolated form. With increasing titanium amount, this band is shifting towards 210 nm and a broader band at 240 nm is observed. The possibility of some Ti-O-Ti clustering in the framework cannot be unequivocally precluded as amorphous TiO₂/SiO₂ gels exhibit absorption bands in the intermediate range of 240 - 330 nm. 26,27 The increase in width of the 240

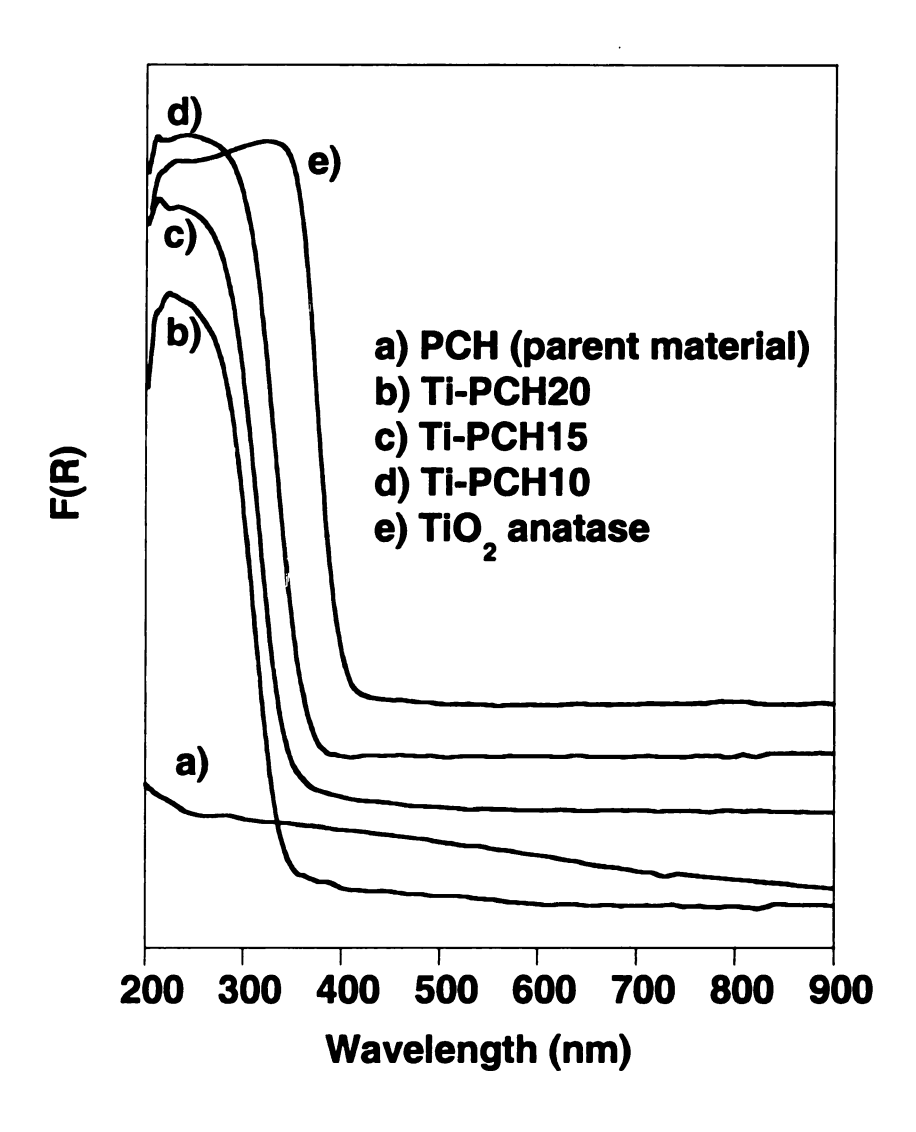


Figure 5.4: UV-Vis spectra of the calcined Ti-containing materials.

nm band may be also indicative of titanium in a distorted tetrahedral environment.^{28,29} We believe that this distorted environment is a direct consequence of the amorphous character of the intragallery nanostructures (i. e. a wide range of Ti-O-Si bond angles).

The catalytic performance of the Ti-PCH and mesostructured Ti-MCM-41 is illustrated in Table 5.2. The major product is cyclohexene oxide along with small amounts of cyclohexanediol. The pore structure of the catalyst plays an important role in the oxidation process especially when a bulky oxidant (TBHP) is used. Even though the titanium grafted PCH possesses pores in the supermicropore to small mesopore range most of the titanium centers are accessible to the reactants. Relative to Ti-MCM-41, Ti-PCH yields a slightly smaller cyclohexene conversion. The acidic character of the clay layer^{21,22} favors the epoxide ring opening, converting the cyclohexene oxide to cylohexanediol. However, our new Ti-PCH materials proved to be competitive catalysts for the cyclohexene epoxidation.

Table 5.2. Oxidation of cyclohexene with TBHP* in the presence of Ti-PCH and Ti-MCM-41.

	Cyclohexene	Selectivity(%)		
Catalyst	Conversion (%)	Epoxide	diol	ol + one
Ti-PCH10	11.2	88.3	9.3	2.4
2%Ti-MCM-41	15.8	92.3	6.8	0.9

^{*}Reaction condition: 100 mg catalyst, 10 mmol cyclohexene, 11 mmol TBHP, 10 mL CH₂Cl₂, 40 °C, 6 h.

5.5 Conclusion

Titanium grafted porous clay heterostructures derived from synthetic saponite clays can be prepared via grafting method. XRD and nitrogen adsorption analyses confirm that the resulting materials designated Ti-PCH retain almost all the structural integrity of the parent PCH even at high titanium loadings. The amount of incorporated titanium can be tuned by controlling the concentration of Ti in the initial reaction composition. UV-Vis spectroscopy indicates that all titanium, inserted into the interlayer silica framework is in the tetrahedral environment.

The acidity of the clay layer along with the titanium modified gallery nanostructures make these new Ti-PCH materials promising bifunctional acid catalysts for chemical conversions. They were effectively utilized as catalysts for cyclohexene oxidation, their catalytic activity being comparable to that of the titanium grafted MCM-41.

5.6 References

- (1) Perego, G.; Taramasso, M.; Notari, B. In *Belg.*; (SNAM Progetti S.p.A., Italy). Be, 1981, p 18 pp.
- (2) Serrano, D. P.; Li, H. X.; Davis, M. E. *J. Chem. Soc., Chem. Commun.* **1992**. 745-747.
- (3) Reddy, J. S.; Kumar, R. Zeolites 1992, 12, 95-100.
- (4) Tuel, A. Zeolites 1995, 15, 236-242.
- (5) Blasco, T.; Camblor, M. A.; Corma, A.; Perezpariente, J. *J. Am. Chem. Soc.* **1993**, *115*, 11806-11813.
- (6) Camblor, M. A.; Corma, A.; Martinez, A.; Perezpariente, J. *Journal of the Chemical Society-Chemical Communications* **1992**, 589-590.
- (7) Beck, J. S.; Vartuli, J. C.; Roth, W. J.; Leonowicz, M. E.; Kresge, C. T.; Schmitt, K. D.; Chu, C. T. W.; Olson, D. H.; Sheppard, E. W.; McCullen, S. B.; Higgins, J. B.; Schlenker, J. L. *J. Am. Chem. Soc.* **1992**, *114*, 10834-10843.
- (8) Kresge, C. T.; Leonowicz, M. E.; Roth, W. J.; Vartuli, J. C.; Beck, J. S. *Nature* **1992**, *359*, 710-712.
- (9) Tanev, P. T.; Chibwe, M.; Pinnavaia, T. J. *Nature (London)* **1994**, *368*, 321-323.
- (10) Tanev, P. T.; Pinnavaia, T. J. Science 1995, 267, 865-867.
- (11) Zhang, W. H.; Froba, M.; Wang, J. L.; Tanev, P. T.; Wong, J.; Pinnavaia,T. J. J. Am. Chem. Soc. 1996, 118, 9164-9171.
- (12) Morey, M.; Davidson, A.; Stucky, G. *Microporous Materials* 1996, 6, 99-104.

- (13) Bagshaw, S. A.; DiRenzo, F.; Fajula, F. *Chemical Communications* **1996**, 2209-2210.
- (14) Maschmeyer, T.; Rey, F.; Sankar, G.; Thomas, J. M. *Nature* **1995**, *378*, 159-162.
- (15) Reichmann, M. G.; Bell, A. T. Applied Catalysis 1987, 32, 315-326.
- (16) Wauthoz, P.; Ruwet, M.; Machej, T.; Grange, P. *Applied Catalysis* **1991**, *69*, 149-167.
- (17) Ollis, D. F.; Pelizzetti, E.; Serpone, N. Environmental Science & Technology 1991, 25, 1522-1529.
- (18) Fernandez, A.; Leyrer, J.; Gonzalezelipe, A. R.; Munuera, G.; Knozinger,H. J. Catal. 1988, 112, 489-494.
- (19) Castillo, R.; Koch, B.; Ruiz, P.; Delmon, B. J. Catal. 1996, 161, 524-529.
- (20) Corma, A.; Diaz, U.; Fornes, V.; Jorda, J. L.; Domine, M.; Rey, F. Chemical Communications 1999, 779-780.
- (21) Polverejan, M.; Pauly, T. R.; Pinnavaia, T. J. *Chem. Mat.* **2000**, *12*, 2698-2704.
- (22) Polverejan, M.; Liu, Y.; Pinnavaia, T. J. *Stud. Surf. Sci. Catal.* **2000**, *129*, 401-408.
- (23) Sing, K. S. W.; Everet, D. H.; Haul, R. A. W.; Moscou, L.; Pierotti, R. A.; Rouquerol, J.; Siemieniewska, T. *Pure Applied Chemistry* **1985**, *57*, 603.
- (24) Gregg, S. J.; Sing, K. S. W. Adsorption, Surface Area and Porosity. 2nd Ed London, 1982.

- (25) Boccuti, M. R.; Rao, K. M.; Zecchina, A.; Leofanti, G.; Petrini, G. *Stud. Surf. Sci. Catal.* **1989**, *48*, 133-144.
- (26) Anpo, M.; Nakaya, H.; Kodama, S.; Kubokawa, Y.; Domen, K.; Onishi, T. *J. Phys. Chem.* **1986**, *90*, 1633-1636.
- (27) Notari, B. Stud. Surf. Sci. Catal. 1988, 37, 413-425.
- (28) Reddy, J. S.; Dicko, A.; Sayari, A. Chem. Ind. (Dekker) 1997, 69, 405-415.
- (29) Blasco, T.; Corma, A.; Navarro, M. T.; Perez Pariente, J. *J. Catal.* **1995**, *156*, 65-74.

Chapter 6

Assembly of a Hexagonal Aluminosilicate Mesostucture (MSU-C) from Restructured Synthetic Saponite Clay

6.1 Abstract

Aluminosilicate mesophase denoted MSU-C has been prepared from synthetic saponite. The layered aluminosilicate was acid treated in order to selectively remove the octahedral Mg²⁺ ions from the clay structure. Restructuring the resulting aluminosilicate sheets around the surfactant micelles, forms the mesoporous material. Calcination at 550 °C afforded the hexagonal aluminosilicate mesostructure. Solid state ²⁷Al MAS NMR, in conjunction with elemental analysis, powder X-ray diffraction and transmission electron microscopy establish that high concentration of aluminum has been incorporated into the aluminosilicate MSU-C framework, with retention of mesoscopic order.

Hexagonal MSU-C has been prepared with a Si/Al molar ratio 8.5, while retaining three XRD indexable reflections before and after calcination. Its well-ordered structure and high aluminum content along with the high surface area and pore volume make this material especially attractive candidate for acid catalyzed conversions of organic molecules.

6.2 Introduction

Since the discovery of the M41S family of mesoporous molecular sieves with tailorable pore sizes ranging from 2.0 to 10.0 nm^{1,2}, a great deal of interest has been focused on increasing the acidity of the surfactant-organized silicate frameworks.³⁻¹¹ With surface areas often over 1000 m²/g and well-defined pore sizes that are substantially larger than in zeolites, these materials show promise for applications in catalysis or molecular separation. Heteroatom substituted mesoporous molecular sieves have also attracted much interest due to their potential use as adsorbents or catalysts. 12,13 Of particular interest are the aluminum containing compounds that may be employed as solid acid catalysts. Bronsted acid sites can be generated by isomorphous substitution of aluminum for silicon in the silica matrix. Two potential ways for improving the reaction properties of Al substituted M41S mesoporous materials focus on increasing the concentration of aluminum atoms in the aluminosilicate framework or altering the local coordination of these framework aluminum sites. Such adjustments are anticipated to have a direct effect on the concentration and charge density of exchangeable ions present. The cations are required to compensate the negative framework charges introduced by the incorporation of tetrahedrally coordinated trivalent aluminum atoms into the siliceous walls. Such cations, usually protons are the main interaction sites for guest molecules that diffuse, adsorb and react in the porous channels. While the control of the local aluminum structure and ordering in M41S materials remains a challenging goal, more effort has been directed toward increasing the aluminum content of the mesopore

frameworks. Such framework aluminum species are generally tetrahedrally coordinated to oxygen atoms that form covalent bridges to neighboring silica tetrahedra.

Previous attempts to synthesize ordered mesoporous aluminosilicates with aluminum contents high enough to increase appreciably their reactivities have been partially successful, but have tended to vield materials with reduced degrees of mesoscopic organization. For example, earlier studies have reported diminished ordering of MCM-41 mesostructures when molar Si/Al ratios of 13 or lower have been used in the synthesis gels. 6-8 XRD patterns of such materials often show only a single low-angle reflection, from which detailed conclusion regarding the structure cannot be made. In addition, examples with high aluminum concentration show the appearance of the six-coordinated alumina in solid-state ²⁷Al MAS NMR spectra, which is usually considered to represent undesirable extra-framework species. 3-5,7-9 More recently, important advances have been made in improving the structural integrity of Al-MCM-41 through direct assembly method¹⁴ or via various post-synthesis procedures¹⁵⁻¹⁸ by grafting Al onto MCM-41 walls using different aluminum sources, followed by calcination. Also previous studies have shown that aluminated mesostructures can be obtained from layered aluminosilicates. 19 They were formed by intercalation of surfactant ions between the silicate layers of kanemite²⁰⁻²³ and that inorganic layers were then folded to develop the mesostructures.

Unfortunately, at high aluminum content these aluminated mesostructures cannot preserve their long-range order. Overall, the low acidity of these materials still limits potential applications in the cracking of hydrocarbons.²⁴

In this chapter we report the assembly of a hexagonal aluminosilicate mesostructure from restructured synthetic saponite clay. Our new material denoted MSU-C retains its hexagonal structure even at silicon to aluminum (Si/AI) molar ratio 8.5.

6.3 Experimental

6.3.1 MSU-C Synthesis

A saponite PCH was prepared according to the previously described procedure (Chapter 2). The synthetically prepared saponite was subsequently leached with 0.5 M HCl aqueous solution (50 mL/g clay) at room temperature for 1 h. A 2-g quantity of the leached saponite clay was then digested in 50 mL 0.5 M NaOH solution for 6 h at 100 °C. The hexagonal mesostructure was obtained by adding cetyltrimethylammonium bromide (0.007 mol) to the precursor suspension at a SiO₂/surfactant molar ratio of ~4.0 and lowering the pH of the suspension to a value of ~ 9.0 with H₂SO₄ (0.008 mol). After an aging period of 40 h at 100 °C, the resulting product was recovered by filtration and air-dried. Sodium ions and part of the surfactant were exchanged with ammonium ions by treating the as-made mesostructure with 0.2 M NH₄NO₃ solution at 60 °C. Complete surfactant removal and conversion of NH₄+ ions to protons was

achieved by calcination in air at 550 °C for 4 h affording the hexagonal aluminosilicate mesostructure designated MSU-C.

6.3.2 Physical Measurements

Powder X-ray diffraction patterns were obtained on a Rigaku Rotaflex diffractometer equipped with a rotating anode (CuK_{α} radiation) operated at 45 kV and 100 mA. The scattering and receiving slits were 1/6 and 0.3 degrees, respectively.

N₂ adsorption-desorption isotherms were obtained at -196 °C on a Micromeritics ASAP 2010 Sorptometer using static adsorption procedures. Samples were outgassed at 175 °C and 10⁻⁶ Torr for a minimum of 12 h prior to analysis. BET surface areas were calculated from the linear part of the BET plot according to IUPAC recommendations.²⁵ The pore size distributions were calculated by Horvath-Kawazoe method.²⁶

²⁷Al MAS (magic angle spinning) NMR spectra were obtained on a Varian VXR 400 MHz spectrometer at 104.26 MHz using a 7 mm zirconia rotor and a sample spinning frequency of 4 kHz. A pulse duration of 9 μs and a delay time of 1 sec. allowed for a full relaxation of the Al nucleus. External Al(H₂O)₆³⁺ was used as a reference to determine the chemical shift values.

Elemental analyses were provided by inductively coupled plasma emission spectroscopy at the University of Illinois Elemental Analysis Laboratory.

TEM images were obtained on a JEOL JEM-100CX II microscope with a CeB₆ filament and an accelerating voltage of 120 kV, a beam diameter of

approximately 5 μ m and an objective lens aperture of 20 μ m. TEM samples were prepared by sonication of the powder in ethanol for 20 minutes and evaporating 1 drop onto a holey carbon film.

6.4 Results and Discussion

In the present work we prepared a saponite composition with the unit cell formula $Na_{1.1}[Mg_6](Si_{6.9}Al_{1.1})O_{20}(OH)_4$, (Si/Al = 5.8) by hydrothermal treatment at 175 °C. A detailed saponite synthesis procedure is provided in Chapter 2, Section 2.3.

As a member of the trioctahedral subgroup of 2:1 phyllosilicates, saponite contains primarily Mg²⁺ cations in each of the six octahedral positions of the O₂₀(OH)₄ unit cell, and a mixture of Si⁴⁺ and Al³⁺ ions in the eight tetrahedral positions of the cell. Consequently, the layer charge density is determined primarily by the Si/Al ratio in the tetrahedral sheet, and the layer charge is balanced by exchangeable cations in the gallery region between the 2:1 layers. Another important feature of the saponite is the instability of its octahedral Mg²⁺ ions towards acids. Mg²⁺ ions can be selectively leached out of the structure by treating the clay with concentrated HCl solutions. Figure 6.1 shows the X-ray diffraction patterns of the saponite before and after acid treatment. It is clear that after 2 hours reaction time no crystallinity is retained. Table 6.1 shows the depleted Mg % and the BET surface areas of the treated samples as a function of time. The surface area increases dramatically from the parent clay value upon acid treatment, whereas the octahedral magnesium is depleted up to 93%. This

behavior is in general agreement with other reported observations for acid treated smectic clays such as montmorillonite^{27,28} and vermiculite.²⁹

Figure 6.2 reveals the ²⁷Al MAS NMR spectra of the parent and acid treated saponite. The saponite pattern exhibits one resonance assigned to tetrahedral aluminum center in the 2:1 layer, where the metal is covalently bonded to three silicon atoms and one magnesium atom via oxygen bridges.³⁰ As expected, after HCl reaction the 65 ppm resonance shifted to 54 ppm due to the change in the aluminum environment upon Mg depletition. The resonance at 54 ppm can be assigned to tetrahedrally coordinated aluminum atoms that are bonded only to next-nearest-neighbor silicon atoms by bridging oxygen atoms in the aluminosilicate framework.³¹ Weak spinning sidebands appear symmetrically on either side of the main aluminum peak. Despite the high aluminum content, no spectral intensity is observed in the region of 30 ppm to 0 ppm, where signals corresponding to aluminum atoms in five- or six-coordinate environments, respectively, are typically observed.

We note that during the leaching process, along with magnesium, small amounts of aluminum reacted with the acid. As a result an increase in the Si/Al is observed (Table 6.1).

The leached clay was further used as a starting material for the synthesis of the aluminosilicate mesostructure denoted MSU-C. First the acid treated clay was digested in NaOH solution for 6 hours. The formation of the hexagonal mesostructure was achieved by lowering the pH of the precursor suspension to a value of ~ 9 and introducing the surfactant. Thus the addition of CTAB and

Table 6.1. BET surface area of acid hydrolyzed saponite.

Reaction time (h)	Mg depletition (%)	BET Surface Area (m²/g)	Si/Aiª
0.0	0	90	5.8
0.5	54	150	7.2
1.0	80	190	8.1
2.0	93	230	8.5

^aSi/Al ratios determined by elemental analysis.

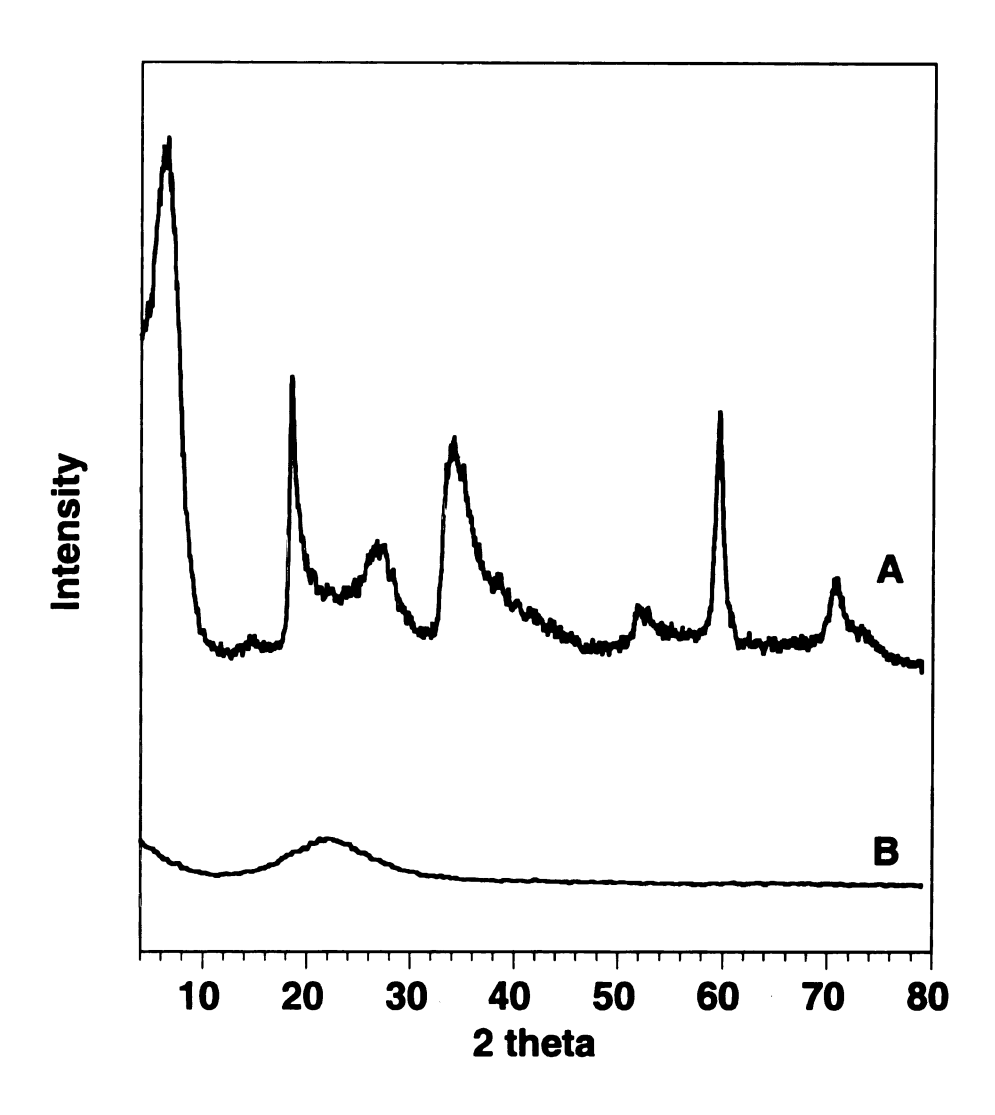


Figure 6.1: XRD patterns for the (A) parent and (B) acid hydrolyzed saponite (reaction time 2 h).

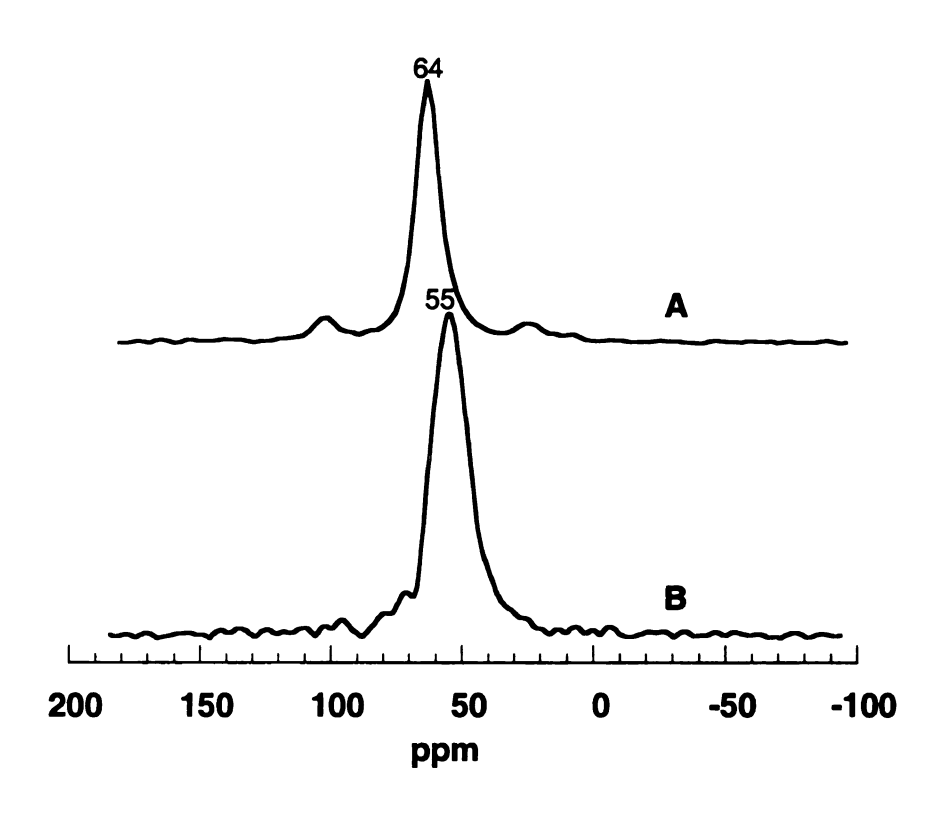


Figure 6.2: ²⁷Al MAS NMR spectra for the (A) starting saponite and (B) acid treated clay.

H₂SO₄ to the digested suspension afforded a hexagonal aluminosilicate mesostructure. The treatment of the as-made mesostructure with 0.2 M NH₄OH solution at 60 °C, displaced exchangeable sodium ions and part of the surfactant. The product then was calcined at 550 °C for 4 hours to remove the remaining surfactant and to convert ammonium ions at exchange sites to protons.

Mesoscopic ordering of the as-synthesized and calcined MSU-C materials was characterized using X-ray powder diffraction, which also permitted the structural stability of the materials to be examined. The well-resolved (100), (110) and (200) scattering reflections shown in Figure 6.3 A evidence the formation of hexagonally ordered aluminosilicate MSU-C. All the observed reflections for the as-synthesized material are preserved following calcination, albeit with an approximately 10 % reduction in the lattice parameters (Figure 6.3 B). Despite the high aluminum content, the structure of our MSU-C material retains the long-range mesoscopic ordering of hexagonal phases.

As shown in Figure 6.4, the MSU-C product exhibits type IV adsorption isotherm typical for the mesopores containing materials. The nitrogen isotherm of the calcined product has a sharp increase at P/Po = 0.3 indicating the formation of hexagonal MSU-C. However, the product possesses an uncommon type-H4 hysteresis at P/Po between 0.5 and 1. This hysteresis is defined as the difference in nitrogen adsorption volume between the adsorption and desorption branches in the range stated above. The existence of such hysteresis loop might indicate that some structural defects are formed in the MSU-C hexagonal

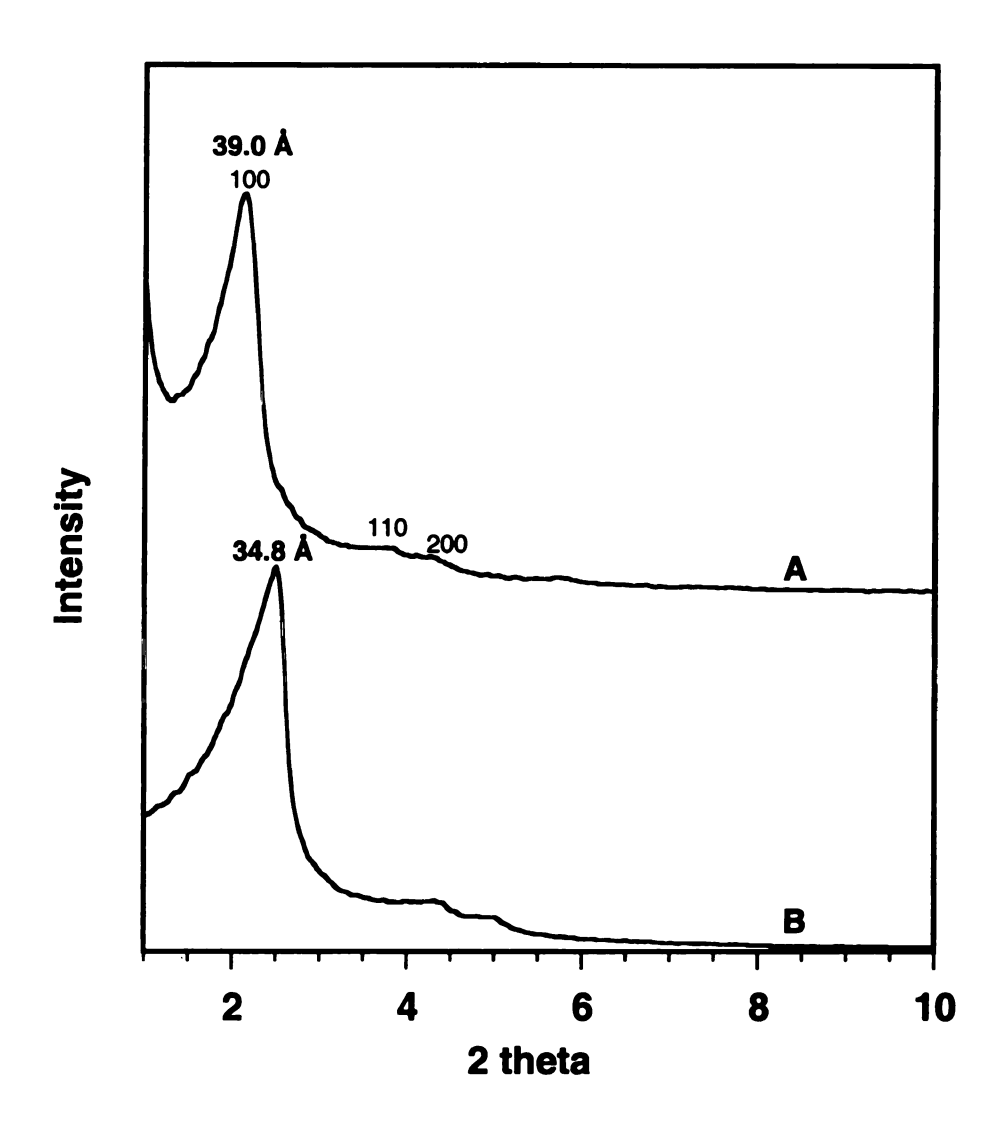


Figure 6.3: XRD spectra for the (A) as-synthesized and (B) calcined MSU-C samples.

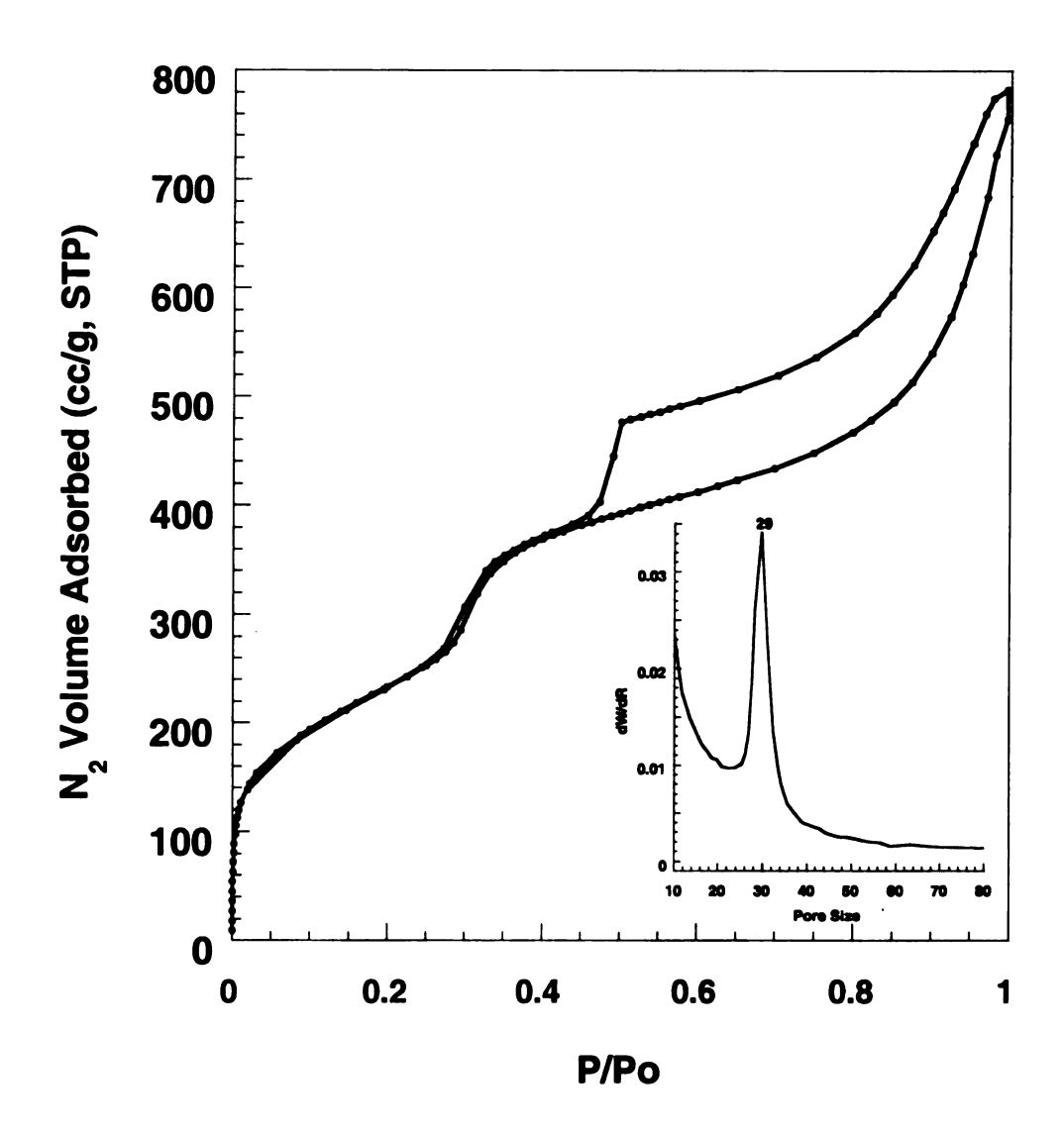
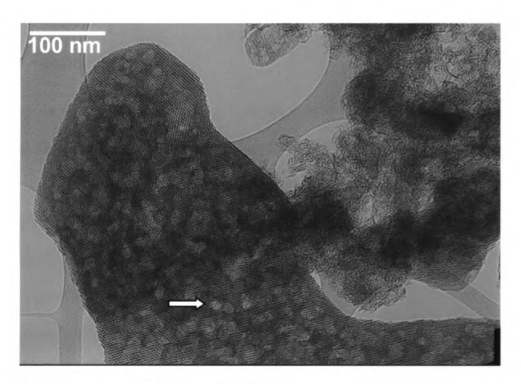


Figure 6.4: Nitrogen adsorption-desorption isotherm for the calcined MSU-C material. Insert: Horvath-Kawazoe pore size distribution curve.

channel matrix.³² The inset to Figure 6.4 provides a typical Horvath-Kawazoe pore size distribution. In spite of its high aluminum content, our new material owns high BET surface area (850 m²/g) and pore volume (0.60 cm³/g), which are within the range usually obtained for M41S materials.^{1,2}

The pore structure of MSU-C is directly visible by transmission electron microscopy. Our material possesses a regular hexagonal array of uniform channels of approximately 28 Å in diameter (Figure 6.5). We believe that the structure is defined by the organization of the surfactant molecules into micellar liquid crystals. The restructured saponite encases the surfactant micelles producing the desired hexagonal MSU-C in a similar way to M41S mesoporous molecular sieves formation. In addition to the honeycomblike pattern, the TEM micrographs show the presence of voids in the MSU-C structure (white areas indicated by arrows), which vary in size from 5 to 30 nm. These structural defects have the ability of making the nanochannels highly interconnected, and thus, improving the diffusion of large molecules in the MSU-C framework system. 33,34



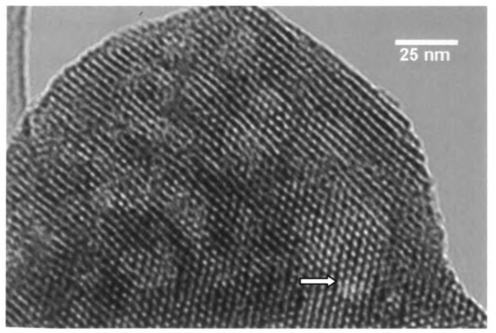


Figure 6.5: Representative TEM image of calcined MSU-C.

6.5 Conclusion

A new method for the preparation of a mesoporous aluminosilicate with high aluminum content in the tetrahedral framework sites, with a Si/Al molar ratio 8.5 has been presented. The mesoporous material was synthesized by acid treating saponite clay and restructuring the resulting aluminosilicate sheets around the surfactant micelles. Calcination at 550 °C afforded the porous product while retaining long-range mesoscopic order. X-ray diffraction, ²⁷Al MAS NMR and TEM techniques provide a self-consistent evidence for the preparation of mesoscopically ordered aluminosilicate framework structure. The hexagonal structure containing voids together with high aluminum content of this MSU-C material should make it promising acid catalyst for organic chemical conversions, including gas oil cracking.

6.6 References

- (1) Beck, J. S.; Vartuli, J. C.; Roth, W. J.; Leonowicz, M. E.; Kresge, C. T.; Schmitt, K. D.; Chu, C. T. W.; Olson, D. H.; Sheppard, E. W.; McCullen, S. B.; Higgins, J. B.; Schlenker, J. L. *J. Am. Chem. Soc.* **1992**, *114*, 10834-10843.
- (2) Kresge, C. T.; Leonowicz, M. E.; Roth, W. J.; Vartuli, J. C.; Beck, J. S. *Nature* **1992**, *359*, 710-712.
- (3) Kolodziejski, W.; Corma, A.; Navarro, M. T.; Perezpariente, J. *Solid State Nucl. Magn. Reson.* **1993**, *2*, 253-259.
- (4) Chen, C. Y.; Burkett, S. L.; Li, H. X.; Davis, M. E. *Microporous Materials* 1993, 2, 17.
- (5) Chen, C. Y.; Burkett, S. L.; Li, H. X.; Davis, M. E. *Microporous Materials* 1993, 2, 27.
- (6) Luan, Z. H.; He, H. Y.; Zhou, W. Z.; Cheng, C. F.; Klinowski, J. *J. Chem. Soc.-Faraday Trans.* **1995**, *91*, 2955-2959.
- (7) Luan, Z. H.; Cheng, C. F.; Zhou, W. Z.; Klinowski, J. *J. Phys. Chem.* **1995**, *99*, 1018-1024.
- (8) Luan, Z. H.; Cheng, C. F.; He, H. Y.; Klinowski, J. *J. Phys. Chem.* **1995**, *99*, 10590-10593.
- (9) Reddy, K. M.; Song, C. S. Catal. Lett. 1996, 36, 103-109.
- (10) Janicke, M.; Kumar, D.; Stucky, G. D.; Chmelka, B. F. *Stud. Surf. Sci. Catal.* **1994**, *84*, 243-250.

- (11) Kloetstra, K. R.; Zandbergen, H. W.; Vanbekkum, H. *Catal. Lett.* **1995**, *33*, 157-163.
- (12) Mokaya, R.; Jones, W. J. Catal. 1997, 172, 211-221.
- (13) Corma, A.; Grande, M. S.; GonzalezAlfaro, V.; Orchilles, A. V. *J. Catal.* **1996**, *159*, 375-382.
- (14) Janicke, M. T.; Landry, C. C.; Christiansen, S. C.; Birtalan, S.; Stucky, G.D.; Chmelka, B. F. *Chem. Mat.* 1999, *11*, 1342-1351.
- (15) Mokaya, R.; Jones, W. Chemical Communications 1997, 2185-2186.
- (16) Ryoo, R.; Ko, C. H.; Howe, R. F. *Chem. Mater.* **1997**, *9*, 1607-1613.
- (17) Ryoo, R.; Jun, S.; Kim, J. M.; Kim, M. J. *Chemical Communications* **1997**, 2225-2226.
- (18) Hamdan, H.; Endud, S.; He, H. Y.; Muhid, M. N. M.; Klinowski, J. *J. Chem. Soc.-Faraday Trans.* **1996**, *92*, 2311-2315.
- (19) Inagaki, S.; Yamada, Y.; Fukushima, Y. *Stud. Surf. Sci. Catal.* **1997**, *105A*, 109-116.
- (20) Kan, Q.; Fornes, V.; Rey, F.; Corma, A. J. Mater. Chem. 2000, 10, 993-1000.
- (21) Inagaki, S.; Yamada, Y.; Fukushima, Y.; Kuroda, K. *Stud. Surf. Sci. Catal.* **1995**, *92*, 143-148.
- (22) Inagaki, S.; Fukushima, Y.; Okada, A.; Kurauchi, T.; Kuroda, K.; Kato, C. *Proc. Int. Zeolite Conf., 9th* **1993**, *1*, 305-311.
- (23) Inagaki, S.; Fukushima, Y.; Kuroda, K. *J. Chem. Soc., Chem. Commun.* **1993**, 680-682.

- (24) Corma, A. Chemical Reviews 1997, 97, 2373-2419.
- (25) Sing, K. S. W.; Everet, D. H.; Haul, R. A. W.; Moscou, L.; Pierotti, R. A.; Rouquerol, J.; Siemieniewska, T. *Pure Applied Chemistry* **1985**, *57*, 603.
- (26) Horwath, G.; Kawazoe, K. J. Journal of Chemical Engineering of Japan 1983, 16, 470.
- (27) Mendioroz, S.; Pajares, J. A.; Benito, I.; Pesquera, C.; Gonzalez, F.; Blanco, C. Langmuir 1987, 3, 676-681.
- (28) Jovanovic, N.; Janackovic, J. Appl. Clay Sci. 1991, 6, 59-68.
- (29) Suquet, H.; Chevalier, S.; Marcilly, C.; Barthomeuf, D. *Clay Miner.* **1991**, *26*, 49-60.
- (30) Woessner, D. E. Am. Mineral. 1989, 74, 203-215.
- (31) Stocker, M. Microporous and Mesoporous Materials 1998, 22, 533-535.
- (32) Lin, H.-P.; Wong, S.-T.; Mou, C.-Y.; Tang, C.-Y. *J. Phys. Chem. B* **2000**, *104*, 8967-8975.
- (33) Lin, H.-P.; Wong, S.-T.; Liu, S.-B.; Mou, C.-Y.; Tang, C.-Y. *Stud. Surf. Sci. Catal.* **2000**, *129*, 15-22.
- (34) Wong, S. T.; Lin, H. P.; Mou, C. Y. Appl. Catal., A 2000, 198, 103-114.

